

Sediment Transport Measurements and Modelling  
in the Meldorf Bight Tidal Channels,  
German North Sea Coast

Dissertation

zur Erlangung des Doktorgrades  
der Mathematisch-Naturwissenschaftlichen Fakultät  
der Christian-Albrechts-Universität  
zu Kiel

vorgelegt von

**Poerbandono**

Kiel  
November 2003

Referent: Prof. Dr. Roberto Mayerle  
Korreferent: Prof. Dr. Franciscus Colijn  
Tag der mündlichen Prüfung: ...  
Zum Druck genehmigt Kiel, den ...

Der Dekan

gez. ...

# Abstract

Study of fine sand transport process in tidal channels of the Meldorf Bight, German North Sea coast based on field measurement and numerical modelling is the main concern of this work. The work comprises the description of main characteristics of sediment transport dynamics in the domain of investigation, the reliability of measuring technology for capturing site-specific sediment transport dynamics and an evaluation of the use of empirical formulae for sand transport prediction and their incorporation in a numerical modelling environment for simulating sediment transport dynamics.

Cross-sectional measurements of water current velocities using a 1200kHz Broad-band Direct Reading Acoustic Doppler Current Profiler (ADCP) and suspended sediment concentrations using an optical beam transmissometer calibrated with filtrated direct sampling concentrations for estimating sediment transport rates have been carried out in three main cross sections covering various tidal ranges. Information on bed and suspended sediment properties are collected. Field measurement results are used to develop and calibrate the numerical model for simulating the time-series concentration and total load transport dynamics. In this case, a two-dimensional horizontal type model developed by the Delft Hydraulics is used.

The calculation of sediment transport dynamics is carried out based on the locally measured velocity and numerical simulation of two-dimensional velocity field. In the latter case, equilibrium sand transport formulae and the solution of advection-diffusion equation are used. Besides, two empirical formulae for sand transport prediction are considered. The modelling performance is quantified using Relative Mean Absolute Error (RMAE) method. Equilibrium sand transport formulae is found to be unable to handling conditions with lag effects. Improvement is made by using the solution of advection-diffusion equation. Within the range of the accuracy of field measurement, the modelling result is found to be able to reproduce the principal characteristics of concentration and total load transport dynamics in the investigation area.





# Kurzfassung

Das Hauptinteresse dieses Vorhabens besteht in der Untersuchung des Transports von feinem Sand in Tiderinnen der Meldorfer-Bucht. Die Basis dieser Untersuchungen bilden dabei Feldmessungen und die Anwendung numerischer Modelle. Die Arbeit umfasst dabei die Beschreibung von Hauptmerkmalen des Sedimenttransports im Untersuchungsgebiet, die Beschreibung der Zuverlässigkeit der ortsspezifischen Sedimenttransport-Messungen und die Auswertung von empirischen Formeln zur Vorhersage des Sandtransport in Verbindung mit dem Einsatz in numerischen Modellen.

Messungen der Strömungsgeschwindigkeit mit einem 1200kHz BB ADCP (Broadband Direct Reading Acoustic Doppler Current Profiler) und der Schwebstoffe mittels optischer, kalibrierter Transmissiometer wurden an drei Querschnitten durchgeführt. Dabei wurden verschiedene Zeiträume einer Tide abgedeckt. Außerdem wurden Informationen über die Eigenschaften der Bodensedimente und Schwebstoffe gesammelt. Die Ergebnisse der Feldmessungen werden genutzt, um ein numerisches Model aufzubauen und zu kalibrieren und damit die zeitliche Änderung der Konzentration und des gesamten Sedimenttransports simulieren zu können. In diesem Fall wurde ein zwei-dimensionales tiefenintegriertes Model der Firma Delft Hydraulics eingesetzt.

Die Berechnung des Sedimenttransports wurde unter Berücksichtigung der örtlich auftretenden Geschwindigkeiten und eines numerisch berechneten zwei-dimensionalen Geschwindigkeitsfeldes durchgeführt. Im letzteren Fall wurden Gleichgewichts-Sandtransport-Formeln und die Lösung der Advektions-Diffusions-Gleichung verwendet. Außerdem wurden zwei empirische Formeln zur Berechnung des Sandtransports betrachtet. Die Modellgüte wird durch die RMAE-Methode (Relative Mean Absolute Error Method) quantifiziert. Herausgefunden wurde, dass mit der Gleichgewichts-Sandtransport-Formel keine Bedingungen mit Zeitversatz simuliert werden können. Eine Verbesserung konnte durch Verwendung der Advektions-Diffusions-Gleichung erzielt werden. Mit Rücksicht auf die Genauigkeit der Feldmessungen kann festgestellt werden, dass die Modelergebnisse die wesentlichen Merkmale des Gesamt-Sediment-Transports und der Konzentrationsverteilung im Untersuchungsgebiet wiedergeben.



# Notations

|           |  |
|-----------|--|
| $A$       | dimensionless reference level  |
| $a$       | reference level, slope of a regression line                                |
| $b$       | empirical coefficient, intercept of a regression line, cross section width |
| $C$       | Chézy coefficient  |
| $c$       | (suspended) sediment concentration   |
| $c(z)$    | sediment concentration at height $z$ above bed                             |
| $C'$      | grain-related Chézy coefficient  |
| $C'_{90}$ | Chézy coefficient related to $d_{90}$                                      |
| $c_0$     | maximum volumetric bed concentration = 0.65                                |
| $c_a$     | reference concentration  |
| $c_b$     | volumetric bed load concentration  |
| $c_d$     | concentration obtained from the trap sampler                               |
| $c_o$     | concentration measured by optical beam transmissometer                     |
| $c_r$     | reference concentration  |
| $c_s$     | computed actual depth-integrated concentration                             |
| $c_{se}$  | equilibrium suspended sediment concentration                               |
| $D$       | deposition rate  |
| $d$       | sediment grain diameter  |
| $D_*$     | dimensionless particle diameter  |
| $d_{16}$  | sediment grain diameter in which 16% of sample by mass is smaller          |
| $d_{50}$  | sediment grain diameter in which 50% of sample by mass is smaller          |
| $d_{84}$  | sediment grain diameter in which 84% of sample by mass is smaller          |
| $d_{90}$  | sediment grain diameter in which 90% of sample by mass is smaller          |
| $E$       | erosion rate   |
| $e$       | natural number   |
| $E_0$     | erosion rate at $\tau_b = \tau_{be}$                                       |
| $e_r$     | discrepancy between computed and measured independent variables            |
| $EI$      | acoustic echo intensity  |
| $EI_r$    | acoustic echo intensity reference  |
| $F$       | external driving forces  |
| $F_r$     | Froude number  |
| $F_s$     | shape factor   |

|                   |  |
|-------------------|--|
| $g$               | acceleration due to gravity  |
| $h$               | water depth  |
| $I$               | optical transmission received by transmissometer light detector                                |
| $i$               | bed inclination  |
| $I_0$             | optical transmission transmitted from transmissometer light source                             |
| $I_1$ and $I_2$   | Einstein's integrals   |
| $K$               | proportionality constant for converting acoustic intensity to suspended sediment concentration |
| $k_1$ and $k_2$   | transmissometer calibration constants  |
| $K_C$             | signal coefficient factor  |
| $k_s$             | effective bed roughness height   |
| $k_s''$           | form-related effective bed roughness   |
| $k_s'$            | grain-related effective bed roughness  |
| $k_x$ and $k_y$   | effective dispersion coefficients  |
| $k_{sd}''$        | form-related effective bed roughness due to sand dunes   |
| $k_{sr}''$        | form-related effective bed roughness due to ripples  |
| $L$               | transmissometer's path length  |
| $M$               | erosion rate constant  |
| $\bar{q}_s$       | depth-integrated suspended load transport  |
| $q_b$             | bed load transport rate  |
| $q_s$             | suspended load transport   |
| $q_s(z)$          | suspended load transport at height $z$ above bed   |
| $R$               | distance   |
| $r$               | correlation coefficient  |
| $r_f$             | discrepancy factor   |
| $r_r$             | distance of reference layer from the acoustical transducer                                     |
| $r_s$             | distance from the acoustical transducer  |
| $s$               | relative density   |
| $S_a$             | salinity   |
| $T$               | transport stage parameter  |
| $t$               | time   |
| $T_e$             | water temperature  |
| $T_{sd}$          | dimensionless adaptation time for vertical sediment concentration profile                      |
| $\bar{u}$         | depth-integrated velocity magnitude  |
| $\overline{u'w'}$ | time-averaged turbulent fluctuation of the flow in horizontal and vertical directions          |
| $u$ and $v$       | fluid velocities in $x$ and $y$ directions   |
| $u(z)$            | current velocity magnitude   |
| $u_*$             | bed shear velocity   |
| $u_b$             | velocity of near bed particle movement   |

---

|                 |   |
|-----------------|---|
| $u_o$           | maximum near bed wave orbital velocity  |
| $u_s$           | local total velocity  |
| $V_0$           | voltage measured by light detector with no suspended sediment concentration               |
| $V_T$           | voltage measured by light detector with suspended sediment concentration                  |
| $V_{rms}$       | recorded root-mean-squared voltage from the transducer                                    |
| $w_s$           | sediment settling velocity  |
| $X$             | dimensionless height  |
| $x$             | dependent variable used in regression analysis  |
| $y$             | independent variable used in regression analysis  |
| $y'$            | computed independent variable   |
| $Z$             | Rouse's or suspension number  |
| $z$             | height from bottom  |
| $Z'$            | modified suspension number  |
| $z_0$           | zero velocity level   |
| $z_b$           | model bed level   |
| $\alpha_e$      | coefficient used in erosion rate formula  |
| $\alpha_f$      | coefficient used in fluid mixing coefficient  |
| $\alpha_w$      | acoustical attenuation coefficient due to water absorption                                |
| $\bar{\alpha}$  | depth-integrated acoustical attenuation coefficient due to scatterers in suspension       |
| $\beta$ -factor | fluid-sediment mixing coefficient proportionality   |
| $\Delta$        | bedform height  |
| $\delta_b$      | height of bed load layer  |
| $\Delta_d$      | dune height   |
| $\Delta_r$      | ripple height   |
| $\kappa$        | von Karman constant   |
| $\lambda$       | bedform length  |
| $\lambda_d$     | dune length   |
| $\lambda_r$     | ripple length   |
| $\mu$           | ripple factor   |
| $\nu$           | kinematic viscosity   |
| $\Phi$          | optical attenuation constant  |
| $\phi$ -factor  | damping effect of sediment to the turbulent flow structure                                |
| $\Psi$          | overall correction factor for suspension number   |
| $\rho$          | density of water  |
| $\rho_s$        | density of sand   |
| $\sigma_e$      | standard deviation of the discrepancy between computed and measured independent variables |
| $\sigma_g$      | geometric standard deviation of a sediment sample   |

|                 |   |
|-----------------|---|
| $\tau_b$        | bed shear stress  |
| $\tau_{b,cr}$   | critical bed shear stress   |
| $\tau_{bd}$     | critical bed shear stress for deposition  |
| $\tau_{be}$     | critical bed shear stress for erosion   |
| $\tau_{br}$     | resultant bed shear stress due to wave and current  |
| $\tau_b'$       | grain-related bed shear stress  |
| $\theta$        | Shields parameter   |
| $\theta_{cr}$   | critical Shields parameter  |
| $\varepsilon_f$ | fluid mixing coefficient  |
| $\varepsilon_s$ | sediment mixing coefficient   |
| $\varsigma$     | suspended sediment acoustical attenuation constant  |
| $\xi$           | empirical coefficient used in the proportionality of current related and resultant bed shear stress |
| $\zeta$         | model water level   |

# Contents

|          |   |           |
|----------|---|-----------|
| <b>1</b> | <b>Introduction</b>                                   | <b>1</b>  |
| 1.1      | State-of-the-art . . . . .                            | 1         |
| 1.2      | Objectives . . . . .                                  | 2         |
| 1.3      | Investigation area . . . . .                          | 3         |
| 1.4      | Contents and structure . . . . .                      | 4         |
| 1.5      | Research materials . . . . .                          | 5         |
| <b>2</b> | <b>Sediment Transport: Process and Prediction</b>     | <b>7</b>  |
| 2.1      | Introduction . . . . .                                | 7         |
| 2.2      | Sediment transport process . . . . .                  | 7         |
| 2.2.1    | Sand transport . . . . .                              | 7         |
| 2.2.1.1  | Properties of sand . . . . .                          | 8         |
| 2.2.1.2  | Sand transport process . . . . .                      | 9         |
| 2.2.1.3  | Bed roughness . . . . .                               | 12        |
| 2.2.2    | Mud transport . . . . .                               | 15        |
| 2.2.2.1  | Properties of mud . . . . .                           | 15        |
| 2.2.2.2  | Process of mud transport . . . . .                    | 15        |
| 2.2.2.3  | Bedforms in muddy coasts . . . . .                    | 18        |
| 2.3      | Sediment transport prediction . . . . .               | 18        |
| 2.3.1    | Empirical equations . . . . .                         | 19        |
| 2.3.1.1  | Bed load transport . . . . .                          | 19        |
| 2.3.1.2  | Suspended load transport . . . . .                    | 21        |
| 2.3.1.3  | Reference concentration and reference level . . . . . | 24        |
| 2.3.1.4  | Erosion and deposition rate . . . . .                 | 25        |
| 2.3.2    | Sediment transport modelling . . . . .                | 26        |
| 2.3.2.1  | Flow model . . . . .                                  | 27        |
| 2.3.2.2  | Sediment transport model . . . . .                    | 28        |
| 2.3.3    | Evaluation of the model performance . . . . .         | 28        |
| 2.4      | Discussion . . . . .                                  | 30        |
| <b>3</b> | <b>Sediment Transport Measurement</b>                 | <b>31</b> |
| 3.1      | Introduction . . . . .                                | 31        |

|          |  |           |
|----------|--|-----------|
| 3.2      | Measuring devices . . . . .                              | 31        |
| 3.2.1    | Current measurement . . . . .                            | 31        |
| 3.2.1.1  | Acoustical current profiling . . . . .                   | 32        |
| 3.2.1.2  | Working principles . . . . .                             | 32        |
| 3.2.1.3  | Limitations and sources of error . . . . .               | 34        |
| 3.2.2    | Measurement of concentration . . . . .                   | 36        |
| 3.2.2.1  | Mechanical sampling . . . . .                            | 36        |
| 3.2.2.2  | Optical sampling . . . . .                               | 37        |
| 3.2.2.3  | Acoustical profiling . . . . .                           | 39        |
| 3.2.3    | Sediment grain size analysis . . . . .                   | 43        |
| 3.3      | Field measurements . . . . .                             | 44        |
| 3.3.1    | Measuring strategy . . . . .                             | 45        |
| 3.3.2    | Current velocity profiles . . . . .                      | 47        |
| 3.3.3    | Sediment concentration profiles . . . . .                | 47        |
| 3.3.3.1  | Trap sampling . . . . .                                  | 48        |
| 3.3.3.2  | Development of calibration curve . . . . .               | 48        |
| 3.3.3.3  | Estimation of near-bed sediment concentration . . . . .  | 52        |
| 3.3.4    | Estimation of suspended load transports . . . . .        | 53        |
| 3.4      | Assessment of measuring uncertainties . . . . .          | 54        |
| 3.4.1    | Accuracy of current measurement . . . . .                | 54        |
| 3.4.2    | Accuracy of sediment concentration measurement . . . . . | 55        |
| 3.5      | Discussion . . . . .                                     | 56        |
| <b>4</b> | <b>Sediment Properties and Transport Dynamics</b>        | <b>59</b> |
| 4.1      | Introduction . . . . .                                   | 59        |
| 4.2      | Bed and suspended sediment properties . . . . .          | 59        |
| 4.2.1    | Bed sediment sizes distribution . . . . .                | 61        |
| 4.2.2    | Mud fractions and bed sediment types . . . . .           | 62        |
| 4.2.3    | Suspended sediment sizes . . . . .                       | 63        |
| 4.2.3.1  | Ranges of grain sizes . . . . .                          | 64        |
| 4.2.3.2  | Materials moving in suspension . . . . .                 | 65        |
| 4.3      | Suspended sediment dynamics . . . . .                    | 66        |
| 4.3.1    | Suspended sediment concentrations . . . . .              | 67        |
| 4.3.2    | Suspended load transports . . . . .                      | 71        |
| 4.4      | Discussion . . . . .                                     | 73        |
| <b>5</b> | <b>Prediction of Sediment Transport Dynamics</b>         | <b>75</b> |
| 5.1      | Introduction . . . . .                                   | 75        |
| 5.2      | Prediction based on the measured velocity . . . . .      | 78        |
| 5.2.1    | Estimation of bed shear stress . . . . .                 | 78        |
| 5.2.2    | Sediment transport prediction . . . . .                  | 80        |



---

|          |  |            |
|----------|--|------------|
| 5.3      | Prediction based on model simulations . . . . .          | 85         |
| 5.3.1    | Flow simulation . . . . .                                | 86         |
| 5.3.2    | Sediment transport simulation . . . . .                  | 88         |
| 5.3.2.1  | Equilibrium transport formulae . . . . .                 | 89         |
| 5.3.2.2  | Advection-diffusion equation . . . . .                   | 93         |
| 5.4      | Discussion . . . . .                                     | 99         |
| <b>6</b> | <b>Evaluation of Prediction Results</b>                  | <b>105</b> |
| 6.1      | Introduction . . . . .                                   | 105        |
| 6.2      | Concentration and transport dynamics . . . . .           | 105        |
| 6.2.1    | Comparison of concentration predictions . . . . .        | 107        |
| 6.2.1.1  | Norderpiep channel . . . . .                             | 107        |
| 6.2.1.2  | Suederpiep channel . . . . .                             | 108        |
| 6.2.1.3  | Piep channel . . . . .                                   | 110        |
| 6.2.2    | Comparison of total load transport predictions . . . . . | 112        |
| 6.2.2.1  | Norderpiep channel . . . . .                             | 112        |
| 6.2.2.2  | Suederpiep channel . . . . .                             | 113        |
| 6.2.2.3  | Piep channel . . . . .                                   | 115        |
| 6.3      | Cross sectional and tide-integrated transports . . . . . | 117        |
| 6.3.1    | Cross sectional integrated transport . . . . .           | 117        |
| 6.3.2    | Tide-integrated transport . . . . .                      | 122        |
| 6.4      | Modelling applications . . . . .                         | 124        |
| 6.5      | Discussion . . . . .                                     | 129        |
| <b>7</b> | <b>Conclusions</b>                                       | <b>131</b> |
|          | <b>References</b>  | <b>145</b> |
|          | <b>Acknowledgement</b>                                   | <b>147</b> |



# List of Figures

|      |   |    |
|------|---|----|
| 1.1  | Investigation area . . . . .  | 3  |
| 1.2  | Schematisation of research scope and interrelationship between chapters   | 5  |
| 3.1  | ADCP time gating and transect . . . . .   | 33 |
| 3.2  | ADCP beam pattern [Simpson, 2001] . . . . .   | 34 |
| 3.3  | Trap sampler mounted with CTD sensors and an optical beam transmissometer . . . . .                             | 37 |
| 3.4  | Optical beam transmissometer . . . . .  | 38 |
| 3.5  | Working principle of a laser granulometer Störtenbecker [1992] . . . . .  | 43 |
| 3.6  | Measuring locations and their cross sectional profiles . . . . .  | 44 |
| 3.7  | Illustration of the measuring procedure in a cross section . . . . .  | 45 |
| 3.8  | Measuring operation from a moving vessel . . . . .  | 46 |
| 3.9  | Estimation of current velocity profiles over an entire water column . . . . .                                   | 47 |
| 3.10 | Regression line and current calibration curve developed based on measurement 2000 . . . . .                     | 50 |
| 3.11 | All data and those taken during low temperature with the calibration curve . . . . .                            | 51 |
| 3.12 | Estimation of current velocity and sediment concentration profiles over an entire water column . . . . .        | 52 |
| 3.13 | Estimation of suspended load transport rate . . . . .   | 53 |
| 3.14 | Schematisation of calculation of suspended sediment transport load in cross section . . . . .                   | 54 |
| 3.15 | Optical profiling uncertainty assessment . . . . .  | 56 |
| 4.1  | Bed sediment composition and bedform measurement in Norderpiep and Suederpiep channels [Kesper, 1992] . . . . . | 60 |
| 4.2  | Grab sampling locations . . . . .   | 61 |
| 4.3  | Bed sediment types [Mayerle et al., 2002] . . . . .   | 63 |
| 4.4  | Relationship of mud fraction in bed sediment sample with water depth and median grain diameter . . . . .        | 63 |
| 4.5  | Median grain size of suspended sediment samples . . . . .   | 64 |
| 4.6  | Photos of material moving in suspension without pre-treatment . . . . .   | 65 |

|      |   |    |
|------|---|----|
| 4.7  | Variation of maximum depth-integrated suspended sediment concentration and suspended load transport with tidal range . . . . .                                  | 67 |
| 4.8  | Vertical distributions of velocity, suspended sediment concentration and suspended load transport at station 4 of cross-section T3 on March 23, 2000 . . . . .  | 68 |
| 4.9  | Cross-sectional distribution of suspended sediment concentration . . . . .  | 69 |
| 4.10 | Depth-integrated velocity, suspended sediment concentration and suspended load transport variation over tidal cycle in Norderpiep . . . . .                     | 70 |
| 4.11 | Depth-integrated velocity, suspended sediment concentration and suspended load transport variation over tidal cycle in Suederpiep . . . . .                     | 70 |
| 4.12 | Depth-integrated velocity, suspended sediment concentration and suspended load transport variation over tidal cycle in Piep . . . . .                           | 71 |
| 4.13 | Variation of the maximum suspended load transport in cross section (left) and tide-integrated suspended load transport (right) with tidal range                 | 71 |
| 4.14 | Variation of flow discharges and suspended load transport in cross section along T1, T2 and T3 on March 21 to 23, 2000 . . . . .                                | 72 |
| 4.15 | Variation of the tide-integrated suspended load transport along cross sections T1, T2 and T3 on March 21 to 23, 2000 . . . . .                                  | 72 |
| 5.1  | Validity of the selected representative bed sediment sizes ( $d_{50}$ and $d_{90}$ ) and settling velocity ( $w_s$ ) of sediment moving in suspension . . . . . | 78 |
| 5.2  | Typical example of bed shear velocity estimation taken from measurement in cross section T3 (Piep channel) on March 23, 2000 . . . . .                          | 79 |
| 5.3  | Sensitivity of total load transport prediction using Bijker's empirical formulae . . . . .  | 81 |
| 5.4  | Sensitivity of total load transport prediction using van Rijn's empirical formulae . . . . .  | 81 |
| 5.5  | Comparison between measured and predicted total load transport using empirical formulae . . . . .   | 83 |
| 5.6  | Comparison between measured and predicted depth-integrated concentration using empirical formulae . . . . .   | 84 |
| 5.7  | Nesting scheme of the Meldorf Bight Model . . . . .   | 86 |
| 5.8  | Comparison between measured and simulated depth-integrated velocity magnitudes . . . . .  | 87 |
| 5.9  | Sensitivity of total load transport prediction using Bijker's equilibrium formulae . . . . .  | 89 |
| 5.10 | Sensitivity of total load transport prediction using van Rijn's equilibrium formulae . . . . .  | 90 |
| 5.11 | Comparison between measured and predicted total load transport using equilibrium formulae . . . . .   | 91 |

|      |  |     |
|------|--|-----|
| 5.12 | Comparison between measured and predicted depth-integrated concentration using equilibrium formulae . . . . .                                  | 92  |
| 5.13 | Sensitivity of depth-integrated concentration prediction using Bijker's advection-diffusion equation . . . . .                                 | 95  |
| 5.14 | Sensitivity of depth-integrated concentration prediction using van Rijn's advection-diffusion equation . . . . .                               | 95  |
| 5.15 | Comparison between measured and predicted depth-integrated concentration using advection-diffusion equation . . . . .                          | 97  |
| 5.16 | Comparison between measured and predicted total load transport using advection-diffusion equation . . . . .                                    | 98  |
| 5.17 | Spatial $k_s$ distribution in the flow model simulation . . . . .  | 102 |
| 5.18 | Time-dependent effective bed roughness height ( $k_s$ ) development in conjunction with simulated and measured time series concentration . . . | 103 |
| 5.19 | Relationship between $k_s$ value and tidal range . . . . .   | 103 |
| 6.1  | Comparison between measured and predicted depth-integrated concentration in cross section T1 . . . . .   | 108 |
| 6.2  | Comparison between measured and predicted depth-integrated concentration in cross section T2 . . . . .   | 109 |
| 6.3  | Comparison between measured and predicted depth-integrated concentration in cross section T3 . . . . .   | 111 |
| 6.4  | Comparison between measured and predicted total load transport in cross section T1 . . . . .   | 113 |
| 6.5  | Comparison between measured and predicted total load transport in cross section T2 . . . . .   | 114 |
| 6.6  | Comparison between measured and predicted total load transport in cross section T3 . . . . .   | 116 |
| 6.7  | Comparison of measured and predicted total load transport in cross sections T1, T2 and T3 using empirical formulae . . . . .                   | 118 |
| 6.8  | Comparison of measured and predicted total load transport in cross sections T1, T2 and T3 using equilibrium formulae . . . . .                 | 120 |
| 6.9  | Comparison of measured and predicted total load transport in cross sections T1, T2 and T3 using advection-diffusion equation . . . . .         | 121 |
| 6.10 | Comparison of measured and estimated balance of total transported sediment in cross section over a tidal cycle . . . . .                       | 123 |
| 6.11 | Predicted concentration dynamics during a spring tide . . . . .  | 125 |
| 6.12 | Predicted concentration dynamics during a neap tide . . . . .  | 126 |
| 6.13 | Predicted total load transport dynamics during a spring tide . . . . .   | 127 |
| 6.14 | Predicted total load transport dynamics during a neap tide . . . . .   | 128 |
| 6.15 | Contribution of suspended load to the total load transport . . . . .   | 129 |



# List of Tables

|      |   |    |
|------|---|----|
| 2.1  | Suspended sediment distribution over the depth [van Rijn, 1993] . . . . .   | 11 |
| 2.2  | Bedform classification [van Rijn, 1993] . . . . .   | 14 |
| 2.3  | Qualification of modelling performance based on RMAE values [van Rijn et al., 2002b] . . . . .                      | 30 |
| 3.1  | Performance of conversion approaches . . . . .  | 42 |
| 3.2  | Evaluation of calibration curve constants based on different sets of data . . . . .                                 | 51 |
| 4.1  | Bed sediment samples analysis result . . . . .  | 62 |
| 4.2  | Ranges of median values of suspended sediment samples . . . . .   | 65 |
| 4.3  | Resume of field measurement data [Poerbandono et al., 2003] . . . . .   | 66 |
| 5.1  | Measurement data sets . . . . .   | 77 |
| 5.2  | Input parameter settings for total load transport prediction using empirical formulae . . . . .                     | 82 |
| 5.3  | Performance of total load transport prediction using empirical formulae . . . . .                                   | 83 |
| 5.4  | Performance of depth-integrated concentration prediction using empirical formulae . . . . .                         | 85 |
| 5.5  | Absolute error of flow simulation and the corresponding unit discharge . . . . .                                    | 88 |
| 5.6  | Input parameter settings for total load transport prediction using equilibrium formulae . . . . .                   | 90 |
| 5.7  | Performance of total load transport prediction using equilibrium formulae . . . . .                                 | 91 |
| 5.8  | Performance of depth-integrated concentration prediction using equilibrium formulae . . . . .                       | 92 |
| 5.9  | Input parameter settings based on data set 1 [Winter & Mayerle, 2003] . . . . .                                     | 94 |
| 5.10 | Input parameter settings for depth-integrated concentration prediction using advection-diffusion equation . . . . . | 96 |
| 5.11 | Performance of depth-integrated concentration prediction using advection-diffusion equation . . . . .               | 96 |
| 5.12 | Performance of total load transport prediction using advection-diffusion equation . . . . .                         | 98 |

6.1 Performance comparison of depth-integrated concentration prediction . 106  
6.2 Performance comparison of total load transport prediction . . . . . 106



# Chapter 1

## Introduction

Within coastal zone, major movements of sediments powered by waves, tides and currents shape the coastal profile and produce erosional and depositional landform [Komar, 1998; Villes & Spencer, 1999]. Transport of sediment is therefore the governing process responsible for the changing levels of seabed and, hence, coastal morphology. The development in sediment transport research has changed from simple phenomenological descriptions to sophisticated empirical and numerical models in which the flow and the sediment dynamics are described in detail [Fredsoe & Deigaard, 1992]. Accordingly, increasing reliability of measuring instruments has led to further understanding of detailed physical processes of sediment transport in natural coastal environment. In addition to laboratory experiments, theoretical works and field observations [King, 1959], such a development has led to a new form of research in coastal study termed as modelling [Cowell & Thom, 1997]. In the modelling, the physical processes that occurs in the nature are reproduced and simulated using a numerical model employing mathematical expressions which are calibrated and validated against field measurement data.

### 1.1 State-of-the-art

Approaches for describing sediment transport processes can be classified into: sand (non-cohesive sediment) transport in which its behaviour can be related to particle characteristics and mud (cohesive sediment) transport in which the process is less dependent on the particle characteristics. The latter includes the description of mixed sediment (sand with presence of mud). Predictive models (either empirical or numerical) describing the nature of sand transport as a function of several adequately known parameters (i.e. flow and sediment characteristics) are available in the literature and have been the main concern in sediment transport studies. In case of mixed sediment and mud transports, the information on their general processes is very limited due to the complex interdependency between various properties of sediment and flow. Although the general behaviour of the process is fairly known, most of the methods can

only give non-specific description on the transport process using calibration parameter determined by *in-situ* (site specific) measurements or laboratory experiments.

Most of coastal sediment transport models have been derived from theoretical works and verified with laboratory experiments under isolated conditions (i.e. steady-uniform flow in an artificial stream) with controlled influencing parameters (i.e. known sediment characteristics) [van Rijn, 1993]. Many of them have been derived from methods used in river flows [Soulsby, 1997]. The applicability of existing methods for sediment transport prediction is restrained to the condition at which they were derived and verified. Application for wider uses in the natural coastal environments are conceivable with some limitations.

## 1.2 Objectives

Study of fine sand transport based on field measurements and numerical modelling will be the main concern in this work and formulated into several main objectives:

1. To investigate the reliability of measuring technology for capturing site specific sediment transport dynamics;
2. To describe the main characters of sediment transport dynamics in tide dominated shallow coastal area; and
3. To evaluate the use of empirical sand transport formulae for simulating sediment transport dynamics and their incorporation in a numerical model.

Field measurements are expected to give representative features and processes in a tide-dominated shallow coastal area that are difficult to be achieved by theoretical works or laboratory experiments. Limitations appear on the time covering the period at which all the distinctive processes occur and the reliability of the measuring instrument to precisely capture the natural condition. Field data considered here was obtained during calm weather. Therefore the sediment transport dynamics being characterised do not represent conditions typical to rough and stormy weathers.

Sand transport models (in which many influencing parameters can be described in detail) might be the promising option to be applied. Unique behaviour of the sediment and mud mixture transport will be carefully considered. Due to the limited coverage of measurement, field data does not represent condition where the combination of tidal currents and wave action initiate erosion and resuspension. As current velocities are the dominant processes in sediment transport during calm weather, the influences of wave in the modelling were excluded.

### 1.3 Investigation area

The study area covers the Meldorf Bight and the adjacent tidal regions on the German North Sea coast (Figure 1.1). The morphology is dominated by tidal flats and a tidal channel system with two tidal inlets; Norderpiep in the North West of the domain and Suederpiep in the South West that intersect within the area to form the Piep tidal channel. The tidal flats are exposed during low water. No dredging activities take place and the study area is subjected to moderate traffic of mainly fishing boats from and to the Buesum port.

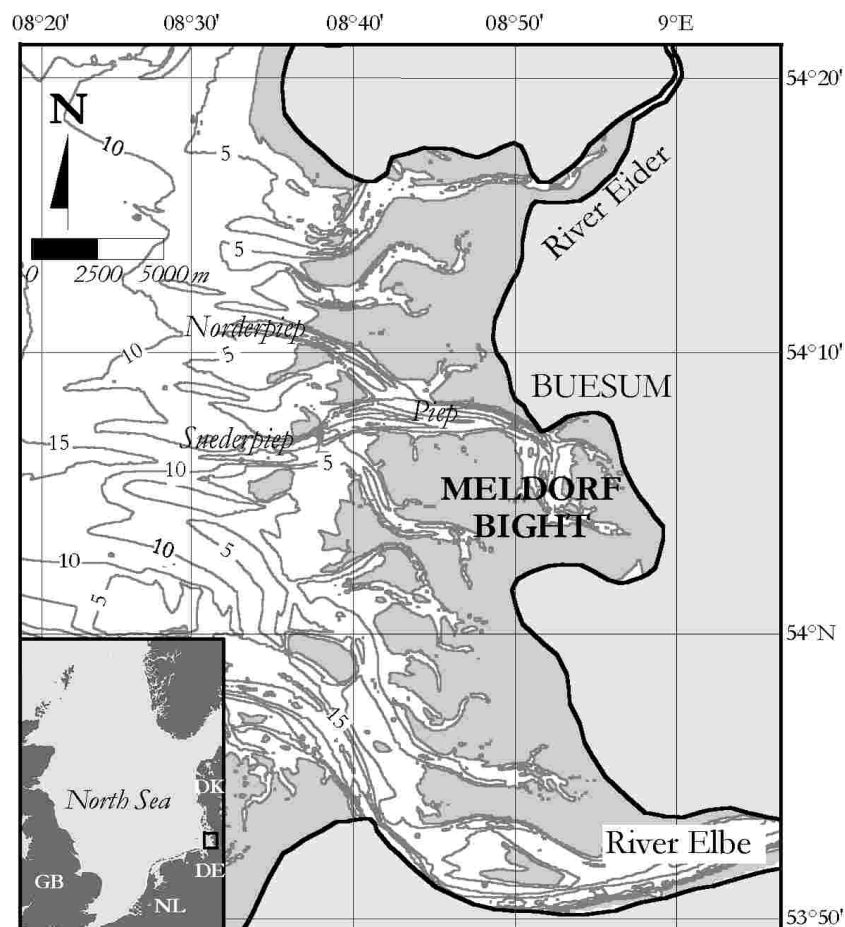


Figure 1.1: Investigation area

The area is characterised by a meso-tide regime with a mean tidal range of 3.2m (neap: 2.8m, spring: 3.5m) leading to an open tidal flat without barrier islands. Westerly winds prevail in the area. Wave heights in the outer region are up to 3 to 4m but break at the outer margin of the area of interest. Even in the absence of barrier islands, inter tidal sandbanks in the outer parts hinder the entrance of waves into the tidal flat. Small waves up to about 0.5m height generated locally by wind are observed. The influence of local waves on the currents is moderate on the tidal flats and negligible in the tidal channels. Storm surges can result in water level setups of up to 5m favouring

the propagation of waves in the shallow parts. However, even under such conditions the wave effects are more distinctive in the outer sandbanks.

The composition of the surface sediments is mainly very fine to fine sands with varying proportions of silt and clay. The bed sediment size varies from 80 to 170 $\mu\text{m}$ . The sediment sizes transported in suspension are much finer ranging from 6 to 86 $\mu\text{m}$  [Mayerle et al., 2002]. The water temperatures vary from 4 to 8°C in winter and from 14 to 18°C in summer. The salinity varies from 20 to 29ppt in winter and from 25 to 33ppt in summer. No significant salinity gradients over the vertical and across the channels could be observed.

The water depths of the main channels vary from 5 to 25m. Plane bed, mega ripples and sand dunes were observed. In the deeper area where consolidated mud exists, generally no bedforms are found. Mega ripples with lengths less than 10m and sand dunes with lengths of up to about 20m are found mainly in the Norderpiep channel. In Suederpiep channel mega ripples and sand dunes with lengths of up to about 20m can be found. Mega ripples of 10 to 12m length and 0.2 to 0.4m height are found in Piep channel [Mayerle et al., 2002].

## 1.4 Contents and structure

Three important subjects are included in this research: (1) measurement of suspended sediment transport, (2) site specific description of the nature of sediment transport dynamics and (3) the use of empirical formulae and their incorporation in a numerical model for simulating the sediment transport process. The first subject concerns the reliability of existing technology on current and suspended sediment concentration measurement. The use of various methods for measuring suspended sediment concentration are discussed. The second subject concentrates on the description of temporal and spatial variations of sediment concentration and transport in the main channels with respect to the tidal action. Finally, the verification and evaluation of empirical formulae and their incorporation in a numerical model for predicting the concentration sediment transport dynamics in the investigation area are discussed.

This dissertation is organised in 7 chapters. In Chapter 1, introductory notes containing research state-of-the-art, objectives and a brief description of the investigation area are given. Chapter 2 presents a brief review of concepts and approaches used in sediment transport studies. Discussion and evaluation of the techniques used in this study for measuring current velocity and suspended sediment concentration are presented in Chapter 3. Additionally the description of the field measuring operation is also given. In Chapter 4, site specific description of bed and suspended sediment properties and the nature of sediment transport processes in the investigation area are analysed and discussed. Evaluation of concentration and total load transport predictions using empirical sand transport formulae is presented in Chapter 5. The use of numerical model with equilibrium and non-equilibrium equations for simulating

sediment transport in the domain of investigation is also discussed. In Chapter 6 the evaluation to the prediction results is carried out. Application of the modelling results representing various tidal conditions is also given. Finally, Chapter 7 summarises the main findings and concludes the final outcome of the research work. Figure 1.2 shows the schematisation of the research scope and the interrelationship between the main chapters in this dissertation.

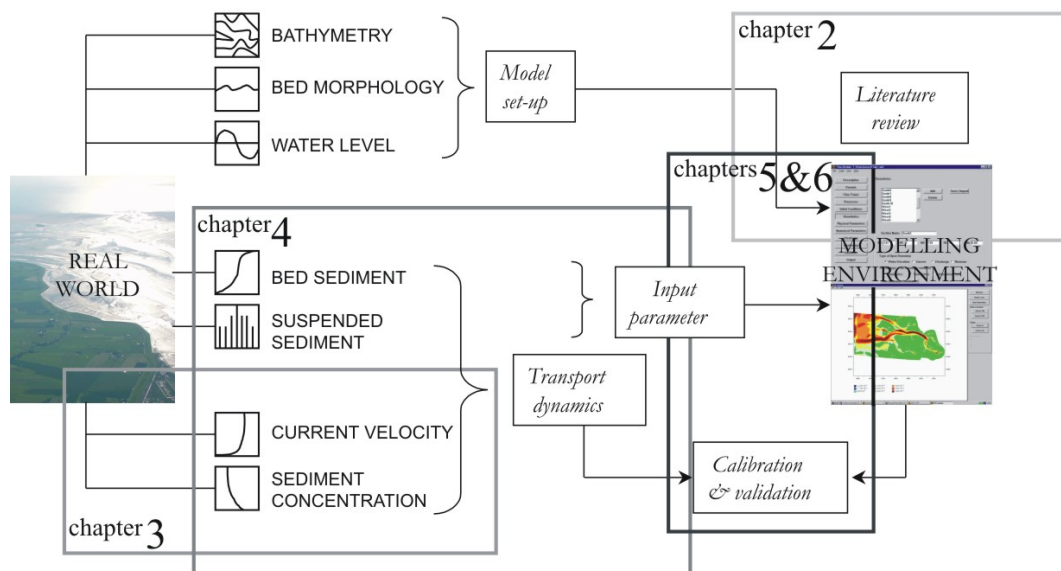


Figure 1.2: Schematisation of research scope and interrelationship between chapters

## 1.5 Research materials

Most of data used in this research were obtained from regular measuring campaigns in the years 2000 to 2002 in the domain of investigation using the research facilities of the Research and Technology Centre Westcoast (*Forschungs- und Technologiezentrum - FTZ Westküste*) in BÜsum. The campaigns were carried out as a part of a research project Predictions of Medium-term Coastal Morphodynamics (*Prognose mittelfristiger Küstenmorphologieänderungen - PROMORPH*) funded by the German Ministry of Education and Research (*Bundesministerium für Bildung und Forschung - BMBF*) [PROMORPH, 2003].



## Chapter 2

# Sediment Transport: Process and Prediction

### 2.1 Introduction

In this chapter, concepts and approaches used in sediment transport studies are briefly discussed. The corresponding discussion is organised into two main parts: the process and the prediction of sediment transport. The first part consists of the description of sand (non-cohesive sediment) and mud (cohesive sediment) transport processes. The latter part presents the empirical and numerical modelling for predicting the dynamics of sediment transport in a natural coastal environment. Additionally, available methods for evaluating the performance of sediment transport prediction are discussed.

### 2.2 Sediment transport process

Fundamental parameters and processes governing the transport of sediment are summarised here. The properties of sediment and the process for entraining it are discussed. In addition, the discussion of bedform and its potential equivalent effect to the flow and transport of sediment is presented.

#### 2.2.1 Sand transport

Sediments originate from fragmentation of rocks by weathering process. Among several sediment properties, the sediment grain size (sediment particle diameter) and settling velocity are of particular importance in sediment transport study. In non-cohesive sediment studies the behaviour of the transport of sediment can be related to the particle characteristics. Based upon adequate information of sediment particle characteristics and hydraulics, the process of sand transport can be quantitatively described.

### 2.2.1.1 Properties of sand

Conventionally according to their diameters ( $d$ ) measured in micrometres ( $\mu\text{m}$ ), sediment grains are classified into muds (clays and silts), sands, gravels (granules, pebbles and cobbles) and boulders. Muds, sands and gravels are commonly found sediment material in natural coastal environment and distinguished according to their sizes with less than  $63\mu\text{m}$  being muds, between  $63$  and  $2000\mu\text{m}$  being sands and coarser than  $2000\mu\text{m}$  being gravels.

Sediments from natural coastal environment are rarely homogeneous. Sieve analysis is a convenient way to characterise sediment samples according to their grain size. A frequency distribution can be obtained from such an analysis giving median grain diameter ( $d_{50}$ ) of which 50% of mass of sediment samples being finer. Median grain diameter is widely used as representative size of sediment samples. A sediment sample with narrow range of grain sizes is classified into well-sorted ( $d_{84}/d_{16} < 2.4$ ) whereas wide range is classified into well-mixed ( $d_{84}/d_{16} > 16$ ) and the value in between is termed as intermediate sorting [Dyer, 1986].

Most of sediment grains in coastal area contain quartz material having an approximate density ( $\rho_s$ ) of  $2650\text{kg/m}^3$ . With the approximate water density ( $\rho$ ) of  $1000\text{kg/m}^3$ , the relative density ( $s$ ) of sediment grain becomes approximately 2.65. The settling velocity ( $w_s$ ) of natural sediment grain in still water can be approximated as [van Rijn, 1993; Soulsby, 1997]:

$$\begin{aligned} w_s &= \frac{(s-1)gd^2}{18\nu} && \text{for } 1 < d \leq 100\mu\text{m} \\ w_s &= \frac{10\nu}{d} \left[ \left[ 1 + \frac{0.01(s-1)gd^3}{\nu^2} \right]^{0.5} - 1 \right] && \text{for } 100 < d < 1000\mu\text{m} \\ w_s &= 1.1 [(s-1)gd]^{0.5} && \text{for } d \geq 1000\mu\text{m} \end{aligned} \quad (2.1)$$

with,

$$s = \frac{\rho_s}{\rho}$$

$$\nu = (1.14 - 0.031(T_e - 15) + 0.00068(T_e - 15)^2)10^{-6}$$

in which  $w_s$  = sediment settling velocity in m/s,  $g$  = acceleration due to gravity in  $\text{m/s}^2$ ,  $d$  = diameter of sediment particle in m,  $s$  = relative density,  $\rho_s$  = density of sand in  $\text{kg/m}^3$ ,  $\rho$  = density of water in  $\text{kg/m}^3$ ,  $\nu$  = kinematic viscosity in  $\text{m}^2/\text{s}$  and  $T_e$  = water temperature in  $^\circ\text{C}$ . For many practical purposes, sediment grain size is usually transformed into dimensionless form termed as dimensionless particle diameter ( $D_*$ ) and reads as:

$$D_* = d_{50} \left[ \frac{g(s-1)}{\nu^2} \right]^{\frac{1}{3}} \quad (2.2)$$



### 2.2.1.2 Sand transport process

A moving fluid exerts friction in each adjacent layer of the water column resulting in velocity gradient where exchange of momentum occurs between parcels of moving water. The friction known as shear stress is responsible as flow forcing agent on the sediment movement.

#### Bed shear stress

According to Reynolds' procedure, the shear stress is made up by a contribution of turbulent and viscous shear stress. Turbulent shear stress is dominant in the major part of flow depth. Viscous shear stress occurs in a thin layer close to bed, since the turbulent flow fluctuation die out close to bottom. In this layer, the flow is laminar.

In the natural coastal environment with shallow water depth and sandy bed sediment, the thin layer of laminar flow close to bed can be neglected since the bed is rarely smooth. The turbulent shear stress over the column is assumed to be constant and equal to the bed shear stress ( $\tau_b$ ) in  $\text{N/m}^2$  and is defined as:

$$\tau_b = \rho u_*^2 \quad (2.3)$$

in which  $u_*$  = bed shear velocity in m/s representing the turbulent fluctuation of the flow in horizontal and vertical directions ( $\overline{u'w'}$ ), thus, dependent on the magnitude of the flow (current velocity) and the roughness of the bed.

In a steady-uniform flow, with water depth of  $h$  in m and bed slope of  $i$ , the overall time-averaged shear stress acting on the bed is given by:

$$\tau_b = \rho g h i \quad (2.4)$$

In turbulent logarithmic layer, the current velocity distribution over the water column is generally expressed as:

$$u(z) = \frac{u_*}{\kappa} \ln \left[ \frac{z}{z_0} \right] \quad (2.5)$$

in which  $u(z)$  = current velocity magnitude in m/s at height  $z$  in m from bottom,  $\kappa$  = von Karman constant (for clear water,  $\kappa = 0.4$ ) and  $z_0$  = zero velocity level in m.

Averaging Equation 2.5 over the depth and incorporating Equation 2.4, Chézy found empirically:

$$\bar{u} = C \sqrt{h i} \quad (2.6)$$

in which  $\bar{u}$  = depth-integrated velocity magnitude in m/s and  $C$  = Chézy coefficient in  $\text{m}^{0.5}/\text{s}$ .

Considering Equations 2.6 and 2.4 the bed shear stress can be calculated by:

$$\tau_b = \rho g \left[ \frac{\bar{u}}{C} \right]^2 \quad (2.7)$$

For hydraulically rough flow, the Chézy coefficient can be estimated using:

$$C = 18 \log \left[ \frac{12h}{k_s} \right] \quad (2.8)$$

in which  $k_s$  = effective bed roughness height in m.

### Initiation of motion

For many practical purposes the dimensionless form of bed shear stress and its relationship with sediment is usually used [Soulsby, 1997]. The factor  $g(\rho_s - \rho)d$  which represents the weight of a sediment layer with diameter  $d$  is used to produce the dimensionless form of bed shear stress known as Shields parameter ( $\theta$ ) and reads as:

$$\theta = \frac{\tau_b}{g(\rho_s - \rho)d} \quad (2.9)$$

Shields [1936] had conducted an experimental work on the initiation of motion of sediment grains resting on a plane bed. He measured the transport rate at a given shear stress for a given sediment size and extrapolated the scatter relating both magnitudes to get the bed shear stress value at which the transport rate is zero. It gives the critical bed shear stress for movement ( $\tau_{b,cr}$ ) in  $\text{N/m}^2$  and transformed into dimensionless form termed as critical Shields parameter ( $\theta_{cr}$ ). Bonnefille [1963] and Yalin [1972] have further related the critical Shields parameter with the dimensionless particle diameter giving:

$$\begin{aligned} \theta_{cr} &= 0.24D_*^{-1} & \text{for } 1 < D_* \leq 4 \\ \theta_{cr} &= 0.14D_*^{-0.64} & \text{for } 4 < D_* \leq 10 \\ \theta_{cr} &= 0.04D_*^{-0.1} & \text{for } 10 < D_* \leq 20 \\ \theta_{cr} &= 0.013D_*^{0.29} & \text{for } 20 < D_* \leq 150 \\ \theta_{cr} &= 0.055 & \text{for } D_* > 150 \end{aligned} \quad (2.10)$$

### Modes of transport

Different modes of sediment transport can be distinguished as bed load and suspended load. For current speeds significantly above the threshold of motion, sediment is entrained off the bed. If the sediment particles move with continuous contact with seabed (by sliding, rolling or saltation) bed load transport occurs. For increasing current speeds sediment loses continuous contact with seabed and transported as

suspension termed as suspended load and it is carried at the same speed as the current. The proportion of sediment carried in suspension is generally much larger than that being carried simultaneously as bed load especially for fine sediment particles. Suspended load is an important contribution to the total sediment transport rate.

For grains to remain in suspension, their settling velocity ( $w_s$ ) must be smaller than the upward turbulent component of velocity, which is related to  $u_*$ . This leads to an approximate criterion for the threshold of suspension of sediment given by the relationship [Soulsby, 1997]:

$$u_* = w_s \quad (2.11)$$

Equation 2.11 can be applied to each grain-size fraction for mixed sediment. If the bed material is widely graded, only the finer fractions are suspended, with the coarser ones moving as bed load. The sediment can also be divided into a number of grain-size classes, each comprising a narrow band of grain diameters, and treat each class separately. A simpler approach is favoured by selecting a single grain size which is representative of the whole sample [Soulsby, 1997]. The importance of suspended load can be determined using the proportionality of  $u_*$  and  $w_s$  giving different types of sediment distribution over the depth (Table 2.1).

**Table 2.1: Suspended sediment distribution over the depth [van Rijn, 1993]**

| $u_*/w_s$ | Distribution of suspended sediment      |
|-----------|---|
| 0.5       | In near-bed layer                       |
| 1.25      | Up to mid depth                         |
| 2.5       | Up to water depth                       |
| 25        | Almost uniformly distributed over depth |

The criteria presented in Table 2.1 is developed based on concentration profile model assuming parabolic mixing coefficient, reference level (margin between bed and suspended load) of  $0.05h$ ,  $\kappa = 0.4$  and  $\beta$ -factor = fluid-sediment mixing coefficient proportionality = 1 [van Rijn, 1993].

The margin between bed and suspended load known as reference level (being the height from seabed to the edge of bed load layer) is not clearly defined. Einstein [1950] defined that the reference level is as thin as a few of sediment grain diameters. Since the typical motion of particle transported as bed load is saltation (hopping), Bagnold [1956] considered the height of saltating particle as the bed load layer thickness being about 10 particle diameter [Francis, 1973; Abott & Francis, 1977]. For accurate prediction of suspended load transport van Rijn [1984b] proposed a minimum reference level of  $0.01h$  for smooth bed. For rough bed, van Rijn [1984b] recommended to use half of the average sand dune height or equivalent bed roughness height ( $k_s$ ).

### 2.2.1.3 Bed roughness

Bedform (or bed feature) is a feature (e.g. ripple, dune, sandwave, etc.) developed at the bed of sandy sediment environment. The type of bedform depends on the strength and nature of the flow [Soulsby, 1997]. Different types of current (i.e. tidal current, wave-induced current) develop different types of bedform. Tidal current may form small ripples, large dunes and ripples on the back of the dunes. The corresponding dimension can be up to some decimetres in height and some metres in length.

The presence of bedform influences the frictional characteristics and turbulent flow structure near the bed and affects the sediment transport by introducing bed roughness or bottom friction being the flow resistance agent. The best predictor for the bed roughness coefficient and the effect of bedform in sediment transport are not adequately known and recommended as future research [van Rijn et al., 2001]. An arbitrary height had been conceptually introduced by Nikuradse [1932] to simulate the bottom roughness known as effective (or equivalent) bed roughness height ( $k_s$ ).

#### Approximation of bed roughness based on the application of logarithmic current boundary layer theory

Approach for estimating effective bed roughness height is usually based on the law of the wall or logarithmic current boundary layer theory (Equation 2.5). Towards seabed, current velocity profile decreases logarithmically and dies out or turns zero at a finite distance very close above the seabed. This zero velocity level ( $z_0$ ) is termed as roughness length and usually used to interpret the effective bed roughness height ( $k_s$ ). When the seabed is rough the effective bed roughness height can commonly be approximated using [Yalin, 1977]:

$$k_s = 30z_0 \quad (2.12)$$

Recent works on the estimation of effective bed roughness heights based on the measured current velocity profiles have been carried out in the field by, for example, Cheng et al. [1999], Whitehouse et al. [2000] and Feddersen et al. [2003] as well as in the flume by Aberle & Smart [2003]. In the corresponding works theoretical assumption of logarithmic current boundary layer is applied. In bidirectional flow (i.e. tidal flow) environments the appliance of law of the wall should be carried out with a great care as the current velocity profiles are not logarithmic during accelerating and decelerating phases. Sufficient number of measurement should be taken to reduce errors. An independent measurement to verify the estimation results may also be required.

Cheng et al. [1999] demonstrated the estimation of roughness length from stationary measurement of high resolution current velocity profiles over a long period (45 days) in a tide dominated bay. In the corresponding work only current profile measurements with good correlation (between theoretical and observed profiles;  $r^2 \geq 0.8$ )

are considered. The boundary layer is assumed to be fully rough. The roughness lengths are assumed to remain constant within a short period (5-25 hours). It is found that the daily averaged roughness lengths vary between 0.03 to 3cm. It is also found that the roughness length varies with the spring and neap tidal cycles. Additionally, a tendency of decreasing roughness length with increasing velocity is observed.

### Approximation of bed roughness based on the prediction of bedform dimensions

Another approach for estimating the effective bed roughness height can be based on the bed sediment grain size and bedform dimension. In this particular case, the effective bed roughness height ( $k_s$ ) is commonly considered to be the accumulation of grain-related ( $k'_s$ ) generated by skin friction forces and form-related ( $k''_s$ ) generated by pressure forces acting on the bedforms giving:

$$k_s = k'_s + k''_s \quad (2.13)$$

The grain-related effective bed roughness height ( $k'_s$ ) is proposed to be [van Rijn, 1993]:

$$k'_s = 3d_{90} \quad (2.14)$$

The form-related effective bed roughness height ( $k''_s$ ) is proposed to be the summation of individual case of bedform [van Rijn, 1993]:

$$k''_s = k''_{sr} + k''_{sd} \quad (2.15)$$

in which  $k''_{sr}$  = form-related effective bed roughness height due to ripples in m and  $k''_{sd}$  = form-related effective bed roughness height due to sand dunes in m. Empirical formulae for estimating form-related effective bed roughness height for lower transport regime are proposed by van Rijn [1993] as:

$$k''_{sr} = 20\gamma_r\Delta_r \left[ \frac{\Delta_r}{\lambda_r} \right] \quad (2.16)$$

$$k''_{sd} = 1.1\gamma_d\Delta_d \left[ 1 - e^{-\frac{25\Delta_d}{\lambda_d}} \right] \quad (2.17)$$

in which  $\gamma_r = 1$  for ripples alone,  $\gamma_r = 0.7$  for ripples superimposed on dunes and  $\gamma_d = 0.7$  for field condition.

Prediction and field observation for determining the average height and length of bedform and, hence, the estimation of effective bed roughness in natural coastal environment are very difficult. Scientific investigations for determining bedform dimension have been therefore carried out mainly using flume experiment data. The investigation is usually focused on the classification and development of bedform based on known hydraulic and sediment parameters.

Several classifications of equilibrium bedform dimension based on an investiga-

tion of bedform development in flume have been proposed by, for example, Liu [1957], Simons & Richardson [1966] and van den Berg & van Gelder [1989]. Recent classification based on flume and field data had been proposed by van Rijn [1984c, 1993]. The corresponding classification is related to an uni-directional current with sandy bed environment. van Rijn [1993] classified bedform dimension based on dimensionless particle diameter ( $D_*$ ), transport stage parameter ( $T$ ) and occasionally Froude number ( $F_r$ ) as shown in Table 2.2.

**Table 2.2: Bedform classification [van Rijn, 1993]**

|            | Transport regime          | Particle size                |            |
|------------|---------------------------|------------------------------|------------|
|            |                           | $1 \leq D_* \leq 10$         | $D_* > 10$ |
| Lower      | $0 \leq T \leq 3$         | Mini-ripples                 | Dunes      |
|            | $3 < T \leq 10$           | Mega-ripples and dunes       | Dunes      |
|            | $10 < T \leq 15$          | Dunes                        | Dunes      |
| Transition | $15 < T \leq 25$          | Washed out dunes, sand waves |            |
| Upper      | $T \geq 25, F_r < 0.8$    | Symmetrical sand waves       |            |
|            | $T \geq 25, F_r \geq 0.8$ | Plane bed and/or anti-dunes  |            |

In addition to bedform classification, formulae for predicting bedform height ( $\Delta$ ) and length ( $\lambda$ ) in a lower transport regime ( $T \leq 15$ ) have been proposed by Yalin [1985] for mini-ripples and van Rijn [1993] for mega-ripples and dunes and read respectively as:

$$\Delta_r = 50 \text{ to } 200d_{50} \qquad \lambda_r = 500 \text{ to } 1000d_{50} \text{ (mini-ripples)} \quad (2.18)$$

$$\frac{\Delta_r}{h} = 0.02(1 - e^{-0.1T})(10 - T) \qquad \lambda_r = 0.5h \text{ (mega-ripples)} \quad (2.19)$$

$$\frac{\Delta_d}{h} = 0.11 \left[ \frac{d_{50}}{h} \right]^{0.3} (1 - e^{-0.5T})(25 - T) \qquad \lambda_d = 7.3h \text{ (dunes)} \quad (2.20)$$

in which  $\Delta_r$  = ripple height in m,  $\lambda_r$  = ripple length in m,  $\Delta_d$  = dune height in m,  $\lambda_d$  = dune length in m and  $T$  = transport stage parameter expressed as:

$$T = \frac{\tau'_b - \tau_{b,cr}}{\tau_{b,cr}} \quad \text{for } \tau'_b > \tau_{b,cr} \quad (2.21)$$

$$T = 0 \qquad \text{for } \tau'_b \leq \tau_{b,cr}$$

in which  $\tau'_b$  = grain-related bed shear stress in  $\text{N/m}^2$  obtained from:

$$\tau'_b = \rho g \left[ \frac{\bar{u}}{C'} \right]^2 \quad (2.22)$$

in which  $C'$  = grain-related Chézy coefficient in  $\text{m}^{0.5}/\text{s}$  calculated using:

$$C' = 18 \log \left[ \frac{12h}{3d_{90}} \right] \quad (2.23)$$

in which  $d_{90}$  = sediment grain diameter at which 90% of sample by mass is smaller in m.

### 2.2.2 Mud transport

Mud is defined as a fluid-sediment mixture consisting of saltwater, sands, silts, clays and organic materials. Such materials are classified as cohesive sediments because the electro-statical forces acting between the particles are comparable to or higher than the gravity force [Partheniades, 1986]. Brief discussion on the important aspects of mud transport from a theoretical point of view is given here considering erosional and settling behaviour of sediment with the presence of silt and clay particles.

#### 2.2.2.1 Properties of mud

Partheniades [1986] stated that plasticity and cohesion are the most important properties of cohesive sediments. Plasticity is a nature of cohesive material to undergo substantial permanent deformation without breaking. Cohesion is the ability of sediment sample to withstand a finite shear stress without deformation [van Rijn, 1993]. A high shear stress is required to overpower the mechanical resistance to deformation by friction and interlocking of the individual particles.

Cohesive properties become important as the mud fraction in the sediment mixtures is larger than critical value of about 13% [Torfs, 1997]. It leads to increasing resistance of bed sediment to be eroded. In suspension, mud sediments do not behave as individual particles but tend to stick together due to mutual forces experienced by two or more clay particles in close proximity forming aggregates known as flocs. Such a process is termed as flocculation. Flocculation is dominant in tide driven environments with concentration smaller than  $10\text{kg}/\text{m}^3$  [van Rijn, 1993].

#### 2.2.2.2 Process of mud transport

In natural coastal environment with non-steady flow (e.g. tidal flow) there is a cyclic process of erosion (and resuspension), transport, settling (flocculation), deposition and consolidation of cohesive sediment. In low concentration domain detectable by optical methods or mechanical sampling, cohesive sediments are transported as dilute suspension. Specific erosional and depositional behaviour and flocculation are important processes distinguishing mud and sand transport.

Flocculation may occur intensively in still water and due to higher salinity, presence of organic material, higher temperature, increasing concentration and low shear-

ing force. Flocs and fine sediment particles remain in suspension supported by turbulence induced fluid forces and transported by tide driven currents. Accelerating and decelerating flows govern the destruction of flocs due to increasing and decreasing turbulent shear stresses. Large shearing forces in the fluid may break-up the flocs into smaller flocs or particles. The destruction is minimum around slack water (high or low water level) leading to deposition. It will be again introduced to the water column by large shearing forces near the bed.

As results of the continuing process of flocculation and break-up, suspended sediment concentrations vary in time. It decreases around slack water and increase towards maximum flow [Nichols, 1986; van Rijn, 1993]. Maximum concentrations generally occur at a certain period of time after maximum flow because it takes time to transport the particles or flocs to the water column [van Rijn, 1993]. This effect is termed as scour lag [Postma, 1967]. The lag period is relatively small near the bottom and relatively large near the water surface [van Rijn, 1993]. On the other hand, a certain time termed as settling lag [Postma, 1967] is needed by the flocs and particles to settle in bed at decelerating flow due to small settling velocity. Thus, the concentration remains always larger than zero even during slack water known as background concentration [van Rijn, 1993].

### **Erosional behaviour**

Erosion occurs as the shear stress exceeds the critical value. In cohesive sediment, unlike those happened with the coarser sediment grains, the critical value of shear stress for erosion is less dependent on the particle size. The resistance for erosion is mainly controlled by [Nichols, 1986]:

- Sediment composition (grain size and silt/clay percentage, organic content, clay mineralogy, cation exchange capacity);
- Pore water character (temperature, pH, cation/anion composition, sodium adsorption ratio);
- Eroding fluid character (salinity, temperature, pH, chemical composition);
- Bed structure (age of sedimentation/consolidation rate, stress history, sediment density with depth).

The deposition of cohesive sediment to settle in bed is mainly governed by decreasing shear stress. Flocculation is the prerequisite and is the first stage of the deposition of cohesive sediment [Partheniades, 1993]. During settling, sediment particles and flocs are moving continuously through zones of high and low turbulence intensity [van Leussen, 1997]. Dependent on the properties of the flocs and the physical conditions in the water, the flocs will grow (and settled) or be broken up into smaller



parts (and introduced to suspension) due to higher shear stress near the bottom during these movements. When the bed shear stress is smaller than the critical bed shear stress for full deposition flocs and sediment particles will be fully deposited. Partial deposition relates to a case at which a group of relatively strong flocs are deposited whereas another group of relatively weak flocs (with shear strength equal or smaller than the bed shear stress) remain in suspension.

Deposited muds may lead to a consolidation of bed sediment. Consolidation is a continuing steps of increasing points of contact and decreasing inter-particles distances due to increasing pressure on the lower deposits of bed, thus increasing sediment densities [Partheniades, 1986]. Increasing pressure may occur due to continuous process of deposition. Initial stage of consolidation occurs within a couple of days indicated by grouping of freshly deposited layer in an open structure with a large pore volume. During consolidation, the flocs are compacted under the influence of gravity forces with a simultaneous expulsion of pore water and a gain in strength of bed material [van Rijn, 1993].

### **Flocculation and settling behaviour**

Factors affecting flocculation are: size, concentration, salinity, temperature and organic material. Flocculation requires particles collision mechanism that may occur due to Brownian motion, turbulent mixing and settling velocity difference [Krone, 1986; Partheniades, 1993].

Analysis of under-water photographs shows the presence of macroflocs (100 to 1000 $\mu\text{m}$ ), miniflocs (10 to 100 $\mu\text{m}$ ) and single mineral particles smaller than about 10 $\mu\text{m}$  [van Rijn, 1993]. Experiment showed that in 0.1 $\text{kg}/\text{m}^3$  sediment concentration, the grains were flocculated in 5 to 10 minutes and had a steady state diameter of 30 $\mu\text{m}$  [Lick & Huang, 1993]. When the floc grows larger the density become smaller. Individual clay particles will have a density of about 2600 $\text{kg}/\text{m}^3$ . Large flocs of about 1000 $\mu\text{m}$  may have a density of 1001 to 1010 $\text{kg}/\text{m}^3$  since most of the flocs consists of pore [van Rijn, 1993]. An approximation to the actual density of a floc can be determined from Stokes Law, once the settling velocities have been determined [Lick & Huang, 1993].

The settling velocity of flocs is strongly related to the salinity, concentration, water depth and flow velocity. For concentration less than 1 $\text{kg}/\text{m}^3$  at salinity up to 10ppt, an effect of salinity to the settling velocity can be seen. An increase of the settling velocity with concentration has been observed as a result of the flocculation effect. Linear increase of settling velocity can be observed for concentration larger than 1 $\text{kg}/\text{m}^3$ . When sediment concentrations are larger than about 10 $\text{kg}/\text{m}^3$  the settling velocities decrease with increasing concentrations due to hindered settling effect (reduction due to an upward flow of fluid displaced by the flocs).

### 2.2.2.3 Bedforms in muddy coasts

In muddy coastal environments (i.e. intertidal flats) bedforms may be developed by a moving fluid over a cohesive substrate. A broad classification of bedforms in the intertidal flats with cohesive sediments is summarised in Whitehouse et al. [2000] as:

- Channels, creeks and gullies;
- Ridge-runnel systems;
- Cliffs; and
- Ripples and other micro topography.

The first three types of bedforms are mainly found in a muddy coastal environment and formed by the wave and tidally induced current over a tidal flats. The latter is formed in a muddy coastal area where non-cohesive sediment is predominant.

Whitehouse et al. [2000] discussed the influence of bedforms in muddy coastal environment on the vertical current velocity distribution. In the discussion, vertical current velocity distribution is described in terms of the standard semi-logarithmic boundary layer equation. At locations where bedforms are presents the friction due to bedforms is expressed as [Ke et al., 1994]:

$$z_0 = \alpha_z \frac{\Delta^2}{\lambda} \quad (2.24)$$

in which  $\alpha_z$  = constant in the order of 1 and  $\Delta$  = bedform height in m and  $\lambda$  = bedform length in m. It is summarised that typical values of  $z_0$  found in the sea are 0.2mm for mud substrate, 0.7mm for muds and sands and 6mm for rippled sand [Soulsby, 1997]. Larger value of  $z_0$  of 16.5mm was found in the lower part of an intertidal area with bedforms height and length of respectively 0.15 and 0.7m [Ke et al., 1994]. For a relatively flat topography with small ripples and biological roughness element,  $z_0$  value of between 0.7 to 1mm is found [van der Lee, 1998].

## 2.3 Sediment transport prediction

Empirical or numerical models have been widely used to predict and simulate sediment transport in natural coastal environment. Results of sediment transport prediction and simulation should give quantification of total sediment transport rates (or total load transport) as a key element in the prediction of seabed changes, coastline evolution and the morphological impacts of human interference [van Rijn et al., 2001].

The bed load ( $q_b$ ) and suspended load ( $q_s$ ) contributions to the total load transport ( $q_{tot}$ ) may be calculated separately and added (in which the two contributions must be

compatible and matched at a well defined height) as:

$$q_{tot} = q_b + q_s \quad (2.25)$$

The depth-integrated sediment concentration ( $\bar{c}$ ) can be calculated based on the predicted total load transports ( $q_{tot}$ ) and the locally measured or simulated depth-integrated velocity magnitude ( $\bar{u}$ ):

$$\bar{c} = \frac{q_{tot}}{\bar{u}h} \quad (2.26)$$

Formulae for predicting bed, suspended and total load transports based on different approaches and concepts exist. The use of appropriate formulae for a certain domain should consider mainly the suitability of the problem being solved with the conditions at which the formulae were derived.

### 2.3.1 Empirical equations

Empirical formulae for predicting total load transports have been derived for application in steady (or quasi-steady) flow conditions under current or wave only and under wave plus current. Some of them separate the contribution of bed and suspended loads to the total load transports. The derivations were based on theoretical works and validated with laboratory experiment and field measurement data. Further use of such formulae for wider application have been based on individual cases and tested against flume (artificial channel), river and coastal measurement data sets.

Several empirical equations for sediment transport predictions have been proposed by many authors. Among them, empirical formulae separating the contribution of bed and suspended load to the total load transport proposed by Bijker [1971] and van Rijn [1984a,b] have been widely used and will be discussed herein.

#### 2.3.1.1 Bed load transport

Bijker [1971] proposed a wave and current related bed load transport rate formula as:

$$q_b = b d_{50} u_* e^{-0.27 \frac{\mu}{\theta}} \quad (2.27)$$

with,

$$\mu = \left[ \frac{C}{C'_{90}} \right]^{1.5} \quad (2.28)$$

$$C'_{90} = 18 \log \left[ \frac{12h}{d_{90}} \right] \quad (2.29)$$

in which  $q_b$  = (volumetric) bed load transport rate per unit width in  $\text{m}^2/\text{s}$ ,  $b$  = empirical coefficient ranging from 1 to 5,  $\mu$  = ripple factor and  $C'_{90}$  = Chézy coefficient related to

$d_{90}$  in  $\text{m}^{0.5}/\text{s}$ .

Equation 2.27 is originated from an empirical formulation developed by Frijlink [1952]:

$$q_b = 5d_{50} \left[ \frac{\mu\tau_b}{\rho} \right] e^{\left[ -0.27(s-1)d_{50} \frac{\rho g}{\mu\tau_b} \right]} \quad (2.30)$$

The exponential factor  $e^{\left[ -0.27(s-1)d_{50} \frac{\rho g}{\mu\tau_b} \right]}$  is termed as "stirring-up factor" and the factor  $5d_{50} \left[ \frac{\mu\tau_b}{\rho} \right]$  is termed as "transport factor". The bed shear stress is expressed as a resultant value due to wave and current as:

$$\tau_{br} = \left[ 1 + 0.5 \left[ \xi \frac{u_o}{\bar{u}} \right]^2 \right] \tau_b \quad (2.31)$$

in which  $\tau_{br}$  = resultant bed shear stress due to wave and current in  $\text{N}/\text{m}^2$ ,  $u_o$  = maximum wave orbital velocity near the bed in  $\text{m}/\text{s}$  and  $\xi$  = empirical coefficient given by:

$$\xi = 0.45 \frac{\kappa C}{g^{0.5}} = 0.0575C \quad (2.32)$$

For representing the transport of material due to current, Equation 2.7 is substituted to Equation 2.30 for the value  $\tau_b$  in the transport factor. For representing the stirring up of sediment by wave and current, Equation 2.31 is substituted to Equation 2.30 for the value  $\tau_b$  in the stirring up factor. Finally, the ripple factor ( $\mu$ ) is omitted from the transport factor and the final expression (Equation 2.27) is obtained.

A current related bed load transport rate formulae for sand grains is proposed by van Rijn [1984a] as:

$$\begin{aligned} q_b &= 0.053(s-1)^{0.5} g^{0.5} d_{50}^{1.5} D_*^{-0.3} T^{2.1} & \text{for } T < 3 \\ q_b &= 0.1(s-1)^{0.5} g^{0.5} d_{50}^{1.5} D_*^{-0.3} T^{1.5} & \text{for } T \geq 3 \end{aligned} \quad (2.33)$$

The derivation of Equation 2.33 was based on a conceptual definition of bed load transport rate as:

$$q_b = u_b \delta_b c_b \quad (2.34)$$

in  $u_b$  = velocity of bed load particle movement in  $\text{m}/\text{s}$ ,  $\delta_b$  = height of bed load layer in  $\text{m}$  and  $c_b$  = volumetric bed load concentration.

In the derivation of Equation 2.33, the height of bed load layer ( $\delta_b$ ) is assumed to be equal to the saltation height and computed using equations of motion proposed by White & Schultz [1977]. The computational results are related to the transport stage parameter ( $T$ ) and the dimensionless particle diameter ( $D_*$ ). In the computations, sediment grain diameters ranging from 100 to 2000  $\mu\text{m}$  with bed shear velocities ranging from 0.02 to 0.14  $\text{m}/\text{s}$  were considered. As a result, a set of curves relating dimension-

less saltation heights ( $\delta_b/d$ ) and  $T$  for several  $D_*$  values were obtained. The curves are approximated by the equation:

$$\frac{\delta_b}{d} = 0.3D_*^{0.7}T^{0.5} \quad (2.35)$$

The particle velocity ( $u_b$ ) is described by adapting a concept proposed by Bagnold [1973] and is represented by the proportionality between the dimensionless particle velocity ( $u_b/u_*$ ) and the Shields parameters ( $\theta_{cr}/\theta$ ). Sets of curves relating  $u_b/u_*$  and  $\theta_{cr}/\theta$  are calculated for several dimensionless particle diameter values. The curves are approximated by relating the term  $u_b/u_*$  with  $T$  giving:

$$\frac{u_b}{[(s-1)gd]^{0.5}} = 1.5T^{0.6} \quad (2.36)$$

Having determined the height of the bed load layer ( $\delta_b$ ) and the bed load particle velocity, the bed load concentration ( $c_b$ ) is calculated using Equation 2.34 considering measured bed load transport rates ( $q_b$ ). The results are related to the transport stage parameter ( $T$ ) and the dimensionless particle diameter ( $D_*$ ). The relationship gives:

$$\frac{c_b}{c_0} = 0.18 \frac{T}{D_*} \quad (2.37)$$

in which  $c_0$  = maximum volumetric bed concentration = 0.65.

The final equation (Equation 2.33) is obtained by substituting Equations 2.37, 2.36 and 2.35 to Equation 2.34.

### 2.3.1.2 Suspended load transport

Approaches used in the derivation of the equation for predicting suspended load transports are generally originated from convection-diffusion equation under steady-uniform turbulent flow. It considers a uniform sediment grain size ( $d$ ) with settling velocity of  $w_s$ . In steady uniform flow, the time-averaged upward and downward transport rates are equal. The downward transport rate term due to gravity is represented by  $cw_s$  and adopting Fick's law (diffusion model) the upward transport is proportional to the concentration gradient  $\partial c/\partial z$ . The proportionality factor is called sediment mixing or diffusion coefficient ( $\varepsilon_s$ ) giving:

$$w_s c + \varepsilon_s \frac{\partial c}{\partial z} = 0 \quad (2.38)$$

in which  $c$  = sediment concentration.

The sediment mixing coefficient is usually related to the fluid mixing coefficient

( $\varepsilon_f$ ) which can be assumed to be parabolic, constant or linear as:

$$\varepsilon_f = \kappa u_* h \left[ \frac{z}{h} \right] \left[ \left( 1 - \frac{z}{h} \right) \right] \quad (2.39)$$

$$\varepsilon_f = \left[ \frac{1}{\alpha_f} \right] \kappa u_* h \quad (2.40)$$

$$\varepsilon_f = \left[ \frac{1}{\alpha_f} \right] \kappa u_* h \left[ \frac{z}{h} \right] \quad (2.41)$$

in which  $\alpha_f$  = coefficient.

Equation 2.38 can be solved for obtaining the vertical suspended sediment concentration distribution subject to several certain assumptions (i.e. sediment mixing coefficients). Rouse [1937] has proposed an integration of it by assuming the sediment mixing coefficient ( $\varepsilon_s$ ) equal to the fluid mixing coefficient ( $\varepsilon_f$ ) which varies parabolically with the depth and substituting Boussinesq equation of shear stress in turbulent flow ( $\tau_b = \rho \varepsilon \frac{\partial u}{\partial z}$ ) in order to obtain the sediment distribution over a vertical as:

$$\frac{c(z)}{c_a} = \left[ \frac{h-z}{z} \frac{a}{h-a} \right]^Z \quad (2.42)$$

in which  $c(z)$  = concentration at height  $z$  above bed,  $c_a$  = reference concentration,  $a$  = reference level, and  $Z = w_s/\kappa u_*$ , known as Rouse's or suspension number and had been widely used for application of sediment transport studies in rivers [Soulsby, 1997].

For deriving the suspended load transport rate formulae, Bijker [1971] followed the procedure developed by Einstein [1950] and gives:

$$q_s = 1.83 q_b \left[ I_1 \ln \left[ 33 \frac{h}{a} \right] + I_2 \right] \quad (2.43)$$

with,

$$I_1 = 0.216 \frac{A^{Z-1}}{(1-A)^Z} \int_A^1 \left[ \frac{1-X}{X} \right]^Z dX$$

$$I_2 = 0.216 \frac{A^{Z-1}}{(1-A)^Z} \int_A^1 \left[ \frac{1-X}{X} \right]^Z \ln(X) dX$$

in which  $q_s$  = suspended load transport rate in  $m^2/s$ ,  $I_1$  and  $I_2$  = Einstein's integrals,  $A$  = dimensionless reference level =  $a/h$  and  $X$  = dimensionless height =  $z/h$ . Alternatively, the suspended load transport ( $q_s$ ) can also be estimated by numerical integration of a product of current velocity and suspended sediment concentration profiles. The current velocity profile is assumed to have logarithmic distribution over the water column (Equation 2.5) and the suspended sediment concentration profile is calculated using Equation 2.42 having firstly determined the reference concentration ( $c_a$ ), the reference level ( $a$ ) and the suspension number ( $Z$ ).

Bijker formulae was initially verified in a laboratory basin for computing littoral drift using sediment sizes having mean diameter of  $220\mu\text{m}$  and further validated for longshore transport measurement along a sandy coastal area with grain diameter of  $400\mu\text{m}$  [Bijker, 1971].

For deriving the suspended load transport rate formulae, van Rijn [1984b] assumed a parabolic-constant mixing coefficient (parabolic for  $\frac{z}{h} < 0.5$  and constant for  $\frac{z}{h} \geq 0.5$ ) giving the concentration distribution over the vertical as:

$$\begin{aligned} \frac{c(z)}{c_a} &= \left[ \frac{a(h-z)}{z(h-a)} \right]^Z & \text{for } \frac{z}{h} < 0.5 \\ \frac{c(z)}{c_a} &= \left[ \frac{a}{h-a} \right] e^{-4Z[\frac{z}{h}-0.5]} & \text{for } \frac{z}{h} \geq 0.5 \end{aligned} \quad (2.44)$$

The sediment mixing coefficient ( $\varepsilon_s$ ) is related to the fluid mixing coefficient ( $\varepsilon_f$ ) by:

$$\varepsilon_s = \beta\phi\varepsilon_f \quad (2.45)$$

with,

$$\begin{aligned} \beta &= 1 + 2 \left[ \frac{w_s}{u_*} \right] \\ \phi &= 1 + \left[ \frac{c}{c_0} \right]^{0.8} - 2 \left[ \frac{c}{c_0} \right]^{0.4} \end{aligned}$$

in which  $\beta$ -factor = a coefficient for describing the turbulence of sediment particles and the  $\phi$ -factor represents the damping effect of sediment to the turbulent flow structure. The  $\beta$ -factor is taken into account and included in the suspension number giving  $Z = w_s/\beta\kappa u_*$ . The  $\phi$ -factor should be considered in environments where the concentration is higher than about  $10\text{kg}/\text{m}^3$  [van Rijn, 1993].

For solving the advection-diffusion equation (Equation 2.38) numerical computations are required and the concentration distribution over the depth should be calculated using numerical integrations. A simplified method is proposed by an analytical approximation and to correct all additional effects due to the approximation of the numerical computation, a modified form of suspension number is given as [van Rijn, 1984b]:

$$Z' = Z + \Psi \quad (2.46)$$

with,

$$\Psi = 2.5 \left[ \frac{w_s}{u_*} \right] 0.8 \left[ \frac{c_a}{c_0} \right]^{0.4} \quad (2.47)$$

in which  $Z'$  = modified suspension number and  $\Psi$  = overall correction factor representing all additional effects due to analytical approximation of the numerical compu-

tation.

Considering Equations 2.44, 2.46, 2.47 and assuming logarithmic distribution of current velocity (Equation 2.5), van Rijn [1984b] derived the suspended sediment transport rate distribution over the depth as:

$$q_s = \int_a^h u(z)c(z)dz \quad (2.48)$$

The solution of the integration of Equation 2.48 is approximated using [van Rijn, 1984b]:

$$q_s = F_s \bar{u} h c_a \quad (2.49)$$

with,

$$F_s = \frac{A^{Z'} - A^{0.5}}{(1 - A)^{Z'}(1.2 - Z')}$$

in which  $F_s$  = shape factor.

### 2.3.1.3 Reference concentration and reference level

The prediction of suspended sediment concentration profile for calculating suspended load transport requires the determination of reference concentration ( $c_a$ ) at a certain height near the seabed termed as reference level ( $a$ ). Bijker [1971] uses bed load transport formulation for the reference concentration assumed at the height equal to the effective bed roughness height ( $k_s$ ) being the reference level ( $a$ ):

$$c_a = \frac{q_b}{6.34u_*a} \quad (2.50)$$

An empirical equation assuming reference concentration ( $c_a$ ) equal to the bed load concentration ( $c_b$ ) at the edge of the bed load layer ( $\delta_b$ ) equal to the reference level ( $a$ ) is proposed by van Rijn [1984b]:

$$q_b = c_b u_b \delta_b = c_a u_a a \quad (2.51)$$

in which  $u_a$  = particle velocity at the reference level and is assumed to be:

$$u_a = \alpha_a u_b \quad (2.52)$$

Substituting Equations 2.35, 2.37 and 2.52 to Equation 2.51 gives:

$$c_a = 0.035 \frac{d_{50}}{\alpha_a a} \frac{T^{1.5}}{D_*^{0.3}} \quad (2.53)$$

The actual value for the  $\alpha_a$  factor was determined by fitting of measured and com-



puted concentration profiles assuming  $a = k_s$  using twenty flume and field data with flow depth ranging from 0.1 to 25m, mean velocity ranging from 0.4 to 1.4m/s and sediment sizes varying from 180 to 700 $\mu$ m resulting in [van Rijn, 1984b]:

$$c_a = 0.015 \frac{d_{50}}{a} \frac{T^{1.5}}{D_*^{0.3}} \quad (2.54)$$

For flat bed, van Rijn [1993] proposed  $a = 2$  to  $10d_{50}$ . Since the seabed is rarely flat, estimation of reference level for rough bed is proposed to be equal to the half of the bedform height ( $a = \frac{1}{2}\Delta$ ) or equal to the effective bed roughness ( $a = k_s$ ).

### 2.3.1.4 Erosion and deposition rate

Basic processes of cohesive sediment transport particularly in the erosional and depositional behaviour and flocculation are not very well recognised. As a result of the complexity and lack of fundamental knowledge, the description of the various processes is largely empirical. Most information is based on laboratory experiments which are often not representative because of small water depths and the missing biogenic mechanisms and the organic materials. The deposition and consolidation history of the bed is different from the nature and therefore more *in-situ* research should be carried out [van Rijn, 1993]. For describing erosion and deposition, time dependent formulations are usually used giving increases (for erosion) and decreases (for deposition) of the rates of concentration.

Partheniades [1965] proposed a general expression for erosion of cohesive material as:

$$E = M \left[ \frac{\tau_b - \tau_{be}}{\tau_{be}} \right] \quad (2.55)$$

in which  $E$  = erosion rate in kg/m<sup>2</sup>s,  $M$  = erosion rate constant in kg/m<sup>2</sup>s, and  $\tau_{be}$  = critical bed shear stress for erosion in N/m<sup>2</sup>.

Erosion rate is a measure of increasing concentration per unit area in a certain period of time. Several laboratory experiments confirmed a linear relationship between erosion rate ( $E$ ) and excess shear stress ( $\tau_b - \tau_{be}$ ) [Torfs, 1997; Krishnappan & Engel, 1997]. The erosion rate constant ( $M$ ) is an empirical constant obtained by fitting the measured data and can be related to the composition of the sediment (e.g. silt and clay fraction in the sediment mixture) [van Rijn, 1993].

For increasing (non constant) bed density, an expression for the erosion rate shows a non linear pattern. Such a relationship was found to be [Parchure & Mehta, 1985]:

$$E = E_0 e^{(\alpha_e \sqrt{\tau_b - \tau_{be}})} \quad (2.56)$$

in which  $E_0$  = erosion rate at  $\tau_b = \tau_{be}$  in N/m<sup>2</sup> and  $\alpha_e$  = coefficient in the range of 5 to 30m/N<sup>0.5</sup>.

The critical shear stress for erosion is less dependent on the particle size distribution and therefore site specific. Field measurements and laboratory experiments (using site samples) are usually conducted to obtain such a value. An average critical value for erosion of  $0.13\text{N/m}^2$  was observed in a field measurement [Black, 1997].

Deposition models based on field measurements and extensive laboratory experiments suggested a relationship between decreasing concentration in a unit square of area during a certain period of time (known as deposition rate) and decreasing excess shear stress [Einstein & Krone, 1962] as:

$$D = \left[ \frac{\tau_{bd} - \tau_b}{\tau_{bd}} \right] w_s c_a \quad (2.57)$$

in which  $D$  = deposition rate in  $\text{kg/m}^2\text{s}$  and  $\tau_{bd}$  = critical shear stress for deposition in  $\text{N/m}^2$ .

### 2.3.2 Sediment transport modelling

Near bed sediment (bed load) transport process adjusts rapidly with changes in hydraulic conditions. Such a phenomena can be modelled by formulae-typed models. On the other hand, the sediment in suspension experiences convection over vertical space and diffusive process over horizontal space and consequently certain time and space is required to adjust with changes in hydraulic conditions. A numerical model solving sets of equations representing convection and diffusion process (continuum model) is therefore recommended particularly for simulating suspended sediment transport.

The type of model depends on the scale of process being solved. For modelling sediment transport process in river a one-dimensional model of continuity equation describing the corresponding motion using mathematical equations formulated in terms of one independent space variable can be used. A two-dimensional type of model is usually used to simulate sediment transport in shallow water area where the water density can be considered to be constant. For modelling complex physical process in an estuary with vertical stratification a three-dimensional type model might be required.

Numerical equations for modelling flow and sediment transport are derived considering discretion of changes of flow and sediment transport along an independent space variable and time ( $dt$ ) into a unit volume (control volume) with dimensions of  $dx$ ,  $dy$  and  $dz$  respectively along the axis  $x$ ,  $y$  and  $z$ . It is assumed that the sum of masses flowing into the unit volume must equal that flowing out, thus, to conserve the mass current flow or suspended sediment concentration magnitude should change. Appropriate initial values and boundary conditions must be given to solve the equation. Optimal time step and discretisation length must also be considered to ensure computational stabilisation. Estimation of the corresponding magnitude in the

centre of the control volume to give calculated value at a given position or time is generally solved by iteration.

### 2.3.2.1 Flow model

For sediment transport to be modelled, the flow field due to current and/or wave must be a priori known. In non-steady flows (e.g. tidal flows) an assumption of a quasi-steady flows using analytical approach of steady flow can be applied. However, for better description the mass-balance equations for fluid (and sediment) and momentum-balance equations for fluid (or fluid-sediment mixture) are commonly used. In the present study 2-dimensional flow and sediment transport models were used. The continuity equation in 2-dimensional numerical model for fluid may be expressed as follows:

$$\frac{\partial h}{\partial t} + \frac{\partial}{\partial x}(h\bar{u}) + \frac{\partial}{\partial y}(h\bar{v}) = 0 \quad (2.58)$$

in which  $\bar{u}$  and  $\bar{v}$  = depth-integrated fluid velocities in  $x$  and  $y$  directions respectively and  $t$  = time. The momentum-balance equation in 2-dimensional numerical model for fluid may be expressed as follows:

$$\begin{aligned} x : \frac{\partial}{\partial t}(h\bar{u}) + \frac{\partial}{\partial x}(h\bar{u}\bar{u}) + \frac{\partial}{\partial y}(h\bar{u}\bar{v}) + gh\frac{\partial}{\partial x}(h + z_b) \\ - k_x h \left[ \frac{\partial^2 \bar{u}}{\partial x^2} + \frac{\partial^2 \bar{v}}{\partial y^2} \right] - \frac{\tau_{bx}}{\rho} - \Sigma \frac{F_x}{\rho} = 0 \end{aligned} \quad (2.59)$$

$$\begin{aligned} y : \frac{\partial}{\partial t}(h\bar{v}) + \frac{\partial}{\partial x}(h\bar{v}\bar{v}) + \frac{\partial}{\partial y}(h\bar{v}\bar{u}) + gh\frac{\partial}{\partial y}(h + z_b) \\ - k_y h \left[ \frac{\partial^2 \bar{v}}{\partial x^2} + \frac{\partial^2 \bar{u}}{\partial y^2} \right] - \frac{\tau_{by}}{\rho} - \Sigma \frac{F_y}{\rho} = 0 \end{aligned} \quad (2.60)$$

in which  $z_b$  = bed level above reference datum,  $k_x$  and  $k_y$  = effective dispersion coefficients representing the integration effects and  $F$  = external driving forces (e.g. wind, waves, Coriolis effect).

The bed shear stresses usually are related to the depth-integrated velocities:

$$\begin{aligned} \tau_{bx} &= \rho g \frac{\bar{u}\bar{v}_r}{C^2} \\ \tau_{by} &= \rho g \frac{\bar{v}\bar{v}_r}{C^2} \end{aligned} \quad (2.61)$$

with  $\bar{v}_r$  being the velocity vector magnitude defined as follow:

$$\bar{v}_r = \sqrt{\bar{u}^2 + \bar{v}^2}$$

### 2.3.2.2 Sediment transport model

In this study, a depth-integrated approach for sediment transport modelling is applied. The actual depth-integrated sediment concentration ( $c_s$ ) is computed from an advection-diffusion equation:

$$\frac{\partial hc_s}{\partial t} + \frac{\partial h\bar{u}c_s}{\partial x} + \frac{\partial h\bar{v}c_s}{\partial y} - \frac{\partial}{\partial x} \left[ \varepsilon h \frac{\partial c_s}{\partial x} \right] - \frac{\partial}{\partial y} \left[ \varepsilon h \frac{\partial c_s}{\partial y} \right] = h \frac{(c_{se} - c_s)}{T_s} \quad (2.62)$$

with,

$$\begin{aligned} T_s &= \left[ \frac{h}{w_s} \right] T_{sd} \\ T_{sd} &= w_* e^{[a_0 + a_1 w_* + a_2 w_*^2 + a_3 w_*^3]} \\ w_* &= \frac{w_s}{u_*} \\ a_0 &= 2.1963 + 0.5467 \frac{u_*}{u_s} \\ a_1 &= -6.4061 + 0.1385 \ln \left[ \frac{u_*}{u_s} \right] \\ a_2 &= -0.2 + 326.832 \left[ \frac{u_*}{u_s} \right]^{2.2047} \\ a_3 &= 1.547 + 20.12 \left[ \frac{u_*}{u_s} \right] \end{aligned}$$

in which  $c_{se}$  = equilibrium concentration for suspended sediment,  $\varepsilon$  = horizontal dispersion coefficient,  $u_s$  = local total velocity,  $T_{sd}$  = dimensionless adaptation time for vertical sediment concentration profile [Galappatti, 1983]. The factor  $(c_{se} - c_s)$  represents the source or sink term. The equilibrium concentration for suspended sediment ( $c_{se}$ ) is calculated as:

$$c_{se} = \frac{q_s}{u_s h} \quad (2.63)$$

The local total velocity is obtained from the simulated flow field and the corresponding water depth. The suspended load transport is calculated using an empirical sand transport formulae.

### 2.3.3 Evaluation of the model performance

The ability of empirical or numerical models to quantitatively predict sediment transport or concentration magnitudes in natural coastal environments is usually evaluated by comparing the computed (or simulated) value with those obtained from field measurements. The corresponding evaluation is termed as discrepancy factor ( $r_f$ ) given

by [van Rijn, 1984a]:

$$r_f = \frac{q_{s,computed}}{q_{s,measured}} \quad (2.64)$$

The discrepancy factor is applied to each pair of computed and measured data and classified by separating it into a factor of 1.5 for  $\frac{1}{1.5} < r_f < 1.5$ , 2 for  $\frac{1}{2} < r_f < 2$  and 3 for  $\frac{1}{3} < r_f < 3$ . For qualifying the quality of sand transport (or concentration) prediction, the number of data pairs within the given factors (i.e. 0.75-1.5, 0.50-2, 0.33-3 or 0.2-5) is counted and presented in percentage relative to the total amount of data. Such an evaluation can be applied in many cases of comparison between various magnitudes of computed and measured values and is usually used for evaluating the performance of instantaneous sediment transport rate or concentration prediction.

On the basis of recent literature study, it can be concluded that the best accuracy that can be achieved by sand transport formulae presently is of about 70% of predictions within a factor of 2 of observations and in case of concentration prediction, the modelling results demonstrated larger inaccuracy in which only up to 50% of predictions are within a factor of 2 of observations [Damgaard et al., 2001; Davies et al., 2002]. The corresponding study considered only non-cohesive sediment material with  $d_{50}$  of varying from 100 to 450  $\mu\text{m}$ . Various modelling approaches were applied. This includes mainly the hydrodynamics process to be considered, the approach for estimating effective bed roughness height, the assumption of sediment grain sorting and the modes of transport.

For evaluating the performance of time-dependent prediction of sediment transport rate or concentration dynamics for a given observation point, a quantitative criteria termed as Relative Mean Absolute Error (RMAE) has been proposed and reads as [van Rijn et al., 2002b]:

$$\text{RMAE} = \frac{\langle |c_c - c_m| - \Delta c_m \rangle}{\langle c_m \rangle} \quad (2.65)$$

in which  $c_c$  = computed concentration,  $c_m$  = measured concentration,  $\Delta c_m$  = measuring accuracy,  $|\dots|$  gives absolute value,  $\langle \dots \rangle$  gives time averaging. The term  $\langle |c_c - c_m| - \Delta c_m \rangle$  is set to zero for  $|c_c - c_m| < \Delta c_m$ .

Such a quantification was originally developed to evaluate results from current and wave numerical modelling by comparing it with field measurement data. The inaccuracy of measuring instruments is taken into account by introducing the relative error of measurement data. A qualification for wave and current modelling based on RMAE criteria is given in Table 2.3. Currently no qualification was found in the literature for evaluating the performance of sediment transport modelling.

**Table 2.3: Qualification of modelling performance based on RMAE values [van Rijn et al., 2002b]**

| Qualification | Wave       | Current   |
|---------------|------------|-----------|
| Excellence    | <0.05      | <0.1      |
| Good          | 0.05 - 0.1 | 0.1 - 0.3 |
| Reasonable    | 0.1 - 0.2  | 0.3 - 0.5 |
| Poor          | 0.2 - 0.3  | 0.5 - 0.7 |
| Bad           | >0.3       | >0.7      |

## 2.4 Discussion

How should sediment transport dynamics be properly predicted?

The nature of local sediments and the governing forces are the main factors for determining the most proper method in predicting the sediment transport dynamics. Cohesive model should work well in predicting sediment transport in muddy coastal environment, whereas sand transport formulae should be applicable for sandy coastal environment. Scientific works of an application of cohesive sediment transport model have been carried out by, for example, Toorman & Berlamount [1993], Le Hir et al. [1993], Willis & Crookshank [1997], and, recently, Teeter et al. [2001]. The sand transport formulae have been longer and widely applied. Recent scientific works of an application of sand transport formulae can be found in, for example, Green & Black [1999] and Bayram et al. [2001].

The sizes of sediment in this study lie between the area of applications of cohesive and non-cohesive sediment transport approaches. With respect to those given by cohesive sediment transport models, sand or non-cohesive sediment transport models offer a circumstantially description of physical processes occur in sediment transportation. Sediment properties (i.e. particle size and settling velocity) can be used for characterising what process should occur in sand transportation due to the strong dependency between particle characteristics and the nature of sand transport. The corresponding erosional and settling behaviour can be acceptably predicted using Shields parameter. Therefore, sand transport formulae is applied here to study the dynamic of sediment transport in the domain of investigation in question.

The performance of predictive sediment transport formulae is usually qualified by comparing the modelling results with measurement. Good qualification is obtained if the model is able to reproduce the dynamic of the measured values or, at least, to show the same tendency of those shown by the measurement. The quality of field measurement data should be considered and is usually represented by the accuracy of the measuring method in the field. The RMAE method, recently proposed by van Rijn et al. [2002b], takes the quality of the field measurement data into account for quantifying the modelling performance and is used in this study.

## Chapter 3

# Sediment Transport Measurement

### 3.1 Introduction

This chapter presents an assessment of measuring methods and instruments (devices) used in this study to obtain reliable field data of current velocity, suspended sediment concentration and the corresponding suspended load transport. Theoretical background of measuring principles are also summarised. Field measurement data will be used to validate and evaluate the performance of empirical formulae as well as numerical model for predicting time-series sediment transport. Evaluation of measuring uncertainty is therefore important to assess the quality of modelling results.

Devices for suspended sediment transport measurement can be classified as direct and indirect according to the measuring principles. Direct measurements are based on measuring the time-averaged sediment transport in a certain point (point integrating) or over a certain depth range (depth integrating). Indirect measurements rely on the simultaneous but separate measurements of time-averaged fluid velocities and time-averaged sediment concentrations, which are multiplied to obtain the time-averaged sediment transport. This particular measuring principal is being considered in this study. The method assumes that the fluctuations in velocity and sediment concentration are zero and that the fluid and sediment particle velocities are equal.

### 3.2 Measuring devices

#### 3.2.1 Current measurement

In many practical applications, water current measurement is used to estimate mainly the discharging water through a channel or river. To some extents, current measurements are of importance for scientific study of the nature of water current itself (e.g. degree of turbulence, three dimensional magnitude and direction, oscillatory behaviour, etc.). Since sediment in suspension is usually assumed to move in the same speed of water current, in conjunction with concentration measurement, current ve-

Locality measurements are also useful for estimating the sediment transport rate.

Direct method of current measurement in a fixed position (point) and observing the current magnitude and direction have been conventionally applied accomplishing the Eulerian method. Such a measurement is usually done using a conventional current meter and enables observation over an adequately long period of current magnitude and direction at a point (a fixed position relative to the free surface or seabed). Current velocity profile can also be obtained employing several current meters at different layer of water column. In many applications, those techniques are less practical.

Advancing research and development in underwater acoustics has introduced a high resolution indirect current measurement techniques using Acoustic Doppler Current Profiler (ADCP) based on Doppler principles. Although such instruments are still in a development stage, their encouraging performance has led to the use of ADCPs and similar products employing Doppler principles (e.g. Acoustic Doppler Profiler, Acoustic Doppler Velocimeter, Aquadopp, etc.) as standard equipment for measuring water current velocity.

### 3.2.1.1 Acoustical current profiling

The use of Doppler principle in ADCP measurement enables indirect and non-intrusive current velocity measurement. The so-called 'time gating' method provides a measurement over an entire vertical range of water column. Utilisation of internal gyro compass and three or four beams configuration gives a possibility to obtain three dimensional velocity components. Additionally, the ability of ADCP to detect the sea bottom provides a correction for measurement from a moving vessel and, at the same time, a good estimate of water depth.

Application of ADCP for measuring current velocity is restrained by several limitations and sources of error. The limitations arise mainly from the design and technology used by the device and the nature of acoustic wave propagation in the water. Errors may appear from the uncertainty of the calculation due to noise presence from transmitted echo and pulse, frequency of sound wave and beam angle. Mishandling in the operation of the equipment may also lead to big errors.

### 3.2.1.2 Working principles

ADCPs use Doppler principles by transmitting short pulse ( $10\mu s$ ) or ping of high frequency (1 to 5 MHz) sound from a transducer and listening to echoes returning from sound scatterers (suspended small particles) in the water [Gordon, 1996]. When the scatterers move towards or away from the ADCP, the sound heard by the transducer is Doppler shifted. The amount of this shift is proportional to the relative velocity between the ADCP and the scatterers and enables an estimation of relative velocity with respect to the ADCP. Since the suspended particles move with the same speed of water then the velocity of water is measured.



ADCPs have four beams pointing to four different directions with an inclination of  $20^\circ$  to the vertical axes and an internal gyro compass. The first two beams are used to estimate North and vertical velocity components and the others are used to estimate East and vertical velocity components. Such a configuration provides velocity components along North and East directions. The redundant data from the two vertical measurements is defined as error velocity and can be used to observe the homogeneity of water velocity in the layer being measured.

As the acoustical wave is emitted to the water column, the received echo (backscattered acoustical wave) approaches the transducer at a time proportional to the distance from the scattering layer to the transducer. A time-gating recording process enables ADCP to calculate the velocity component from the received echo sequentially to provide velocity measurement at each depth cell giving a velocity profile measurement from the entire water column (see: Figure 3.1(a)).

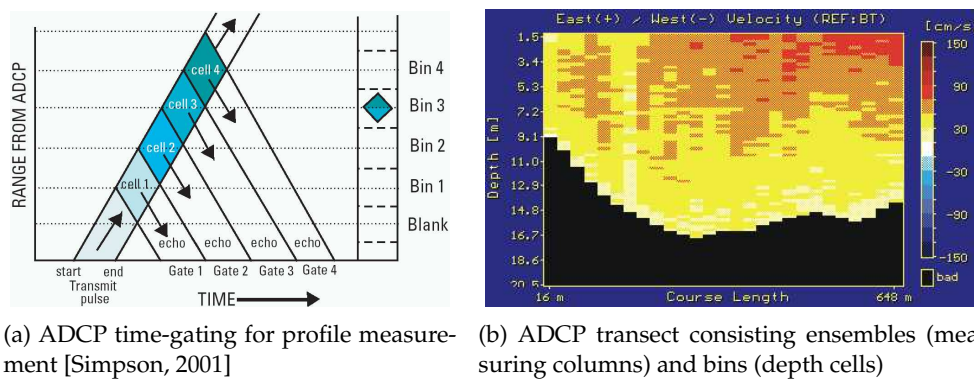


Figure 3.1: ADCP time gating and transect

ADCPs employ longer sound wave pulses to detect the bottom known as bottom-tracking. A long pulse is used for bottom-tracking measurements to properly ensonify the bottom so that the return echoes are stronger than echoes from material suspended in the water column [Griffin & Mueller, 1998]. Since the echo reflected back from the bottom will be Doppler shifted, the relative movement of ADCP with respect to the bottom can be estimated to give approximate vessel speed. Thus a correction to the current velocity measurement relative to the ADCP can be given. Alternatively, the GPS can also be used. At the same time the bottom tracking also provides an estimate of water depth.

As an ADCP is used for current velocity measurement from a moving vessel, vertical profiles along the ship path or cross sectional measurement data termed as transects are obtained. A transect is composed of ensembles that are the columns of data along the ship path and that is formed by bins that are the unit depth cells (see: Figure 3.1(b)) for which the ADCP measures the velocity (magnitude and direction). The recording is controlled by a configuration file that also stores all the settings used by the ADCP to make the measurements.

The data of each transect is stored in one file in binary or ASCII format. Each tran-

sect data consists mainly of velocity magnitude and direction at each bin and the corresponding North and East velocity components as well as the error velocity. ADCP also provides echo intensity data obtained from each transducer resulted from the measurement of backscattered sound and indicates the strength of energy received by the transducers. Additionally, information of water depth, position, time and data quality are also provided.

### 3.2.1.3 Limitations and sources of error

The echo reflected back to ADCP transducers is contaminated by noise due to different properties of water and scattering particles. A significantly high signal to noise ratio is required to enable accurate estimation of current velocity from each bin. However, due to the nature of acoustic wave propagation from a transducer in a water column (i.e. absorption and beam spreading) the signal to noise ratio of the echo decreases within distance from the transducer leading to an increasing uncertainty.

Current underwater acoustic technology provides a transducer that produces parasitic side lobes that are emitted about 30 to 40° from the axis of the main beam (see: Figure 3.2). When the side lobe strikes the bottom, it usually swamps the receivers with an increased amplitude signal that smears the velocity information that is being gathered from the main beam echo. On a 1200kHz ADCP system, the loss of vertical profiling range because of this effect is approximately 15% with 30 beam angles and 6% with 20° angles [Simpson, 2001].

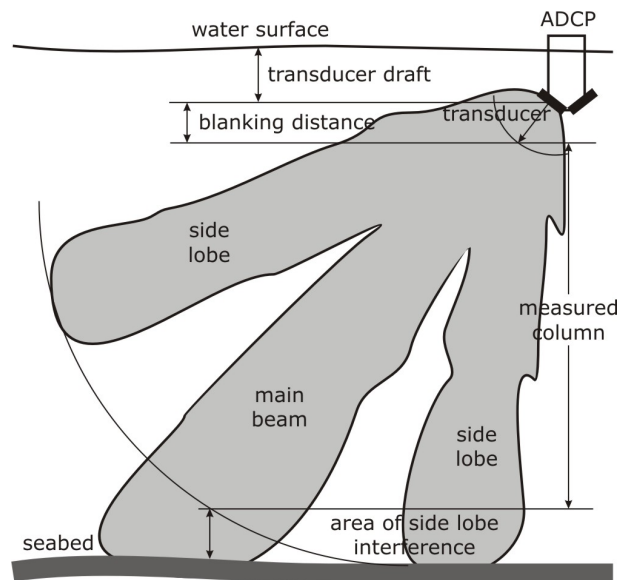


Figure 3.2: ADCP beam pattern [Simpson, 2001]

The use of small beam angle may increase the percentage of profiling range over the water column, however the precision of current velocity measurement is reduced because of decreased coupling with the horizontal [Simpson, 2001]. ADCP uses a

processing algorithm that incorporates the beam angle to predict the deviation of the measured current velocity magnitude in each beam. The data processing algorithm gives an increasing standard deviation of single ping measurement as the beam angle decreases. Additionally, an uncorrected error in the alignment of beam pointing angle may lead to a large uncertainty which can only be reduced by factory calibration.

After transmitting acoustic pulses, ADCP transducers and associated electronics must rest a short time before receiving the reflected acoustic signals. A ceramic transducer vibrated at 1200kHz resonant frequency must be allowed to die out before it is used as a listening device. During that time, the acoustic pulse has travelled about several decimetres. Measurements cannot be made within that distance termed as blanking distance and limits the coverage of the measured profile. Thus, the actual distance to the first measured bin depends on several factors: blanking distance, speed of sound, operating mode, bin size, transmitting frequency and transducer beam angles [Simpson, 2001].

The accuracy of ADCP measurement is affected by mainly two sources of error: (1) random error and (2) bias or systematic error. Statistical treatment to the data may reduce the uncertainty due to random error, whereas, measuring procedures (e.g. measurement under calm weather condition, accurate estimate of transducer depth, etc.) should be able to handle bias errors which may occur from the application of ADCP measurements in field condition. Furthermore, a rough water surface condition may reduce the accuracy of the measurement since the pendulum-type sensor used by ADCP can not properly compensate the pitch and roll. In this case additional or external pitch and roll sensors should be used.

A random velocity-vector error is composed of a random magnitude and a random direction which mainly caused by the noise. Random error is reduced by the square root of the number of samples. Various sources of random error are as follows [Simpson, 2001]:

- pulse length; the shorter the pulse length for a given frequency in a narrow-band ADCP, the greater the random error,
- transmit frequency; the lower the frequency at a given pulse length (or lag distance), the greater the random error,
- signal-to-noise ratio; the lower the signal-to-noise ratio, the greater the random error, and
- beam angle; as the beam angle approaches vertical, random error approaches infinity.

Bias errors are non-random and, therefore, cannot be reduced by data averaging. Fortunately, in most cases, bias error in ADCP measured velocities is relatively small. Possible sources of bias errors may arise from the limitations of device. Additionally, inaccurate estimation of underwater sound velocity may also cause bias errors. Accurate measurement of salinity and temperature which affect the speed of acoustical

propagation in the water is required. Furthermore, human factor (operator-caused) can also be important sources of bias errors due to incorrect setting of measurement configurations (e.g. transducer draft, mounting, choice of cross section, etc.).

### 3.2.2 Measurement of concentration

In addition to the reliable current velocity measurement over the water column, an accurate measurement of sediment concentration moving in suspension is also required for the prediction of suspended load transport. Many options exist for the measurement techniques of suspended sediment concentration. The decision of what technique to use must be based on budget constraints, manpower and desired quality. Comprehensive discussion on field techniques for suspended sediment concentration measurement is discussed in Wren et al. [2000].

Devices for measuring sediment concentration in suspension can be based on mechanical, optical or acoustical principles. In this study, devices for measuring suspended sediment concentration based on these three different principles are used and discussed.

#### 3.2.2.1 Mechanical sampling

Mechanical sampling has been considered as the most reliable method in measuring suspended sediment concentration. It consists of direct collection of water-sediment samples over a certain period. A variety of mechanical samplers with different designs based on different operation principles are available. They can be classified into two main categories, i.e. trap (and bottle) samplers and pump samplers. Trap-type instruments can only be used under (quasi) steady flow conditions since they can only be used to make instantaneous measurements. The other samplers can also be used in oscillatory flow conditions since they are able to make continuous measurements.

Suspended sediment concentration measurements using a trap sampler giving an instantaneous measured value at a point is considered in this study. The main objective of the use of such a device is to calibrate the simultaneously measured optical sampling data by developing a calibration curve for estimating suspended sediment concentration. Furthermore, the water samples are analysed to give the estimated representative sizes of sediment moving in suspension.

The trap sampler consists of a cylinder-shaped (or funnel-shaped box) with sampling volume of about 2 litres. It has shutters on top and bottom controlled mechanically by means of a balance of weight and a steel spring system. The weight must be adequate to allow the spring system to lock and keep the shutters opened. During deployment, the shutters are initially open. The sampler is placed vertically and lowered to the sampling point. Once the weight reaches the bottom the shutters are immediately closed. The rope connecting the weight and the sampler determines the position at which the sampler is located.

In this study, a trap sampler was deployed to obtain water samples at about 1m above seabed at several vertical stations along measured cross sections. Water depth from the free surface is measured using pressure sensor mounted as part of Conductivity, Temperature and Depth (CTD) sensors (see: Figure 3.3).

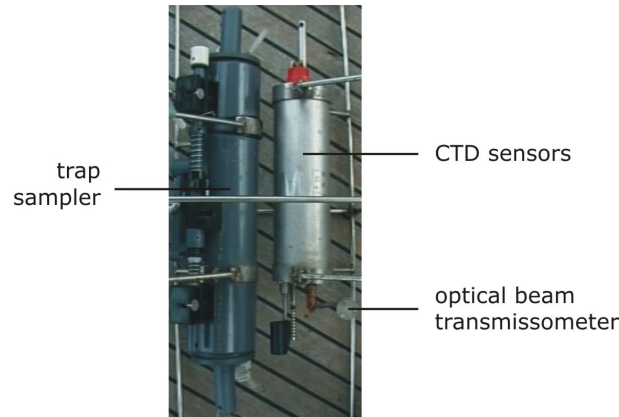


**Figure 3.3: Trap sampler mounted with CTD sensors and an optical beam transmissometer**

### 3.2.2.2 Optical sampling

In this study, the amount of suspended sediment concentration has been estimated based on optical measurement using an optical beam transmissometer. It gives relative measure of suspended sediment concentration in terms of optical transmission. An absolute measurement can only be obtained by calibration using direct samples. The use of optical beam transmissometer for measuring suspended sediment concentration is discussed herein.

An optical beam transmissometer comprises light transmitter and detector devices. A red light beam with  $660 \pm 12 \text{ nm}$  wavelength from the light transmitter is transmitted through a measuring volume. The integrated reference diode in the light detector measures voltages proportional to temperature compensation due to light transmission. The received optical transmission will correspond to the scattering and absorption of light beam due to the existence of material in the measuring volume (Figure 3.4(a)). Thus, low optical transmission will associate with large concentration of material in suspension and *vice versa*.

Transmissometer light sensor records a voltage  $V_T$  proportional to the light intensity at a distance  $L$  from the light source, and the relation with the suspended sediment concentration ( $c$ ) is given by [Holdaway et al., 1999]:

$$c = \frac{1}{\Phi L} \ln \left[ \frac{V_0}{V_T} \right] \quad (3.1)$$

in which  $\Phi$  = optical attenuation constant obtained by mean of direct sampling cali-

bration,  $L$  = path length (distance separating light transmitter and detector),  $V_0$  = voltage measured with no suspended sediment concentration and  $V_T$  = voltage measured with suspended sediment concentration.

In this study an optical beam transmissometer with path length of 2cm is used (Figure 3.4(b)). It is mounted in conjunction with CTD sensors and a trap sampler (see: Figure 3.3) enabling simultaneous measurement of optical transmission, depth, water properties and directly sampled sediment concentration.

Since  $V_0/V_T$  is proportional to the light intensity  $I_0/I$  and with  $I_0 = 100\% = 1$ , then:

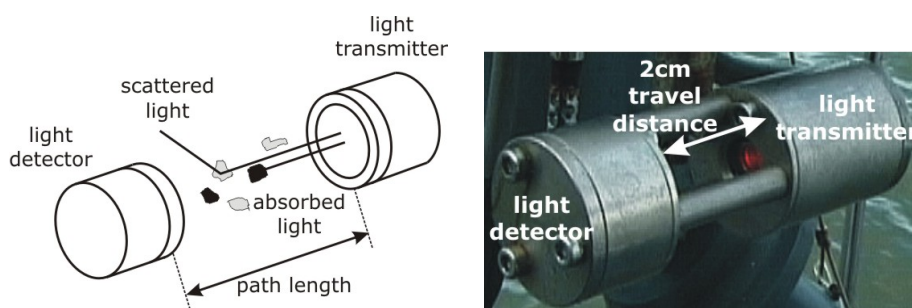
$$\frac{V_0}{V_T} = k_1 \frac{I_0}{I} = \frac{k_1}{I} \quad (3.2)$$

in which  $I_0$  = light (optical) transmission transmitted from the light source,  $I$  = optical transmission measured in the light detector and  $k_1$  = proportionality factor. Considering Equation 3.2 and  $k_2 = \Phi L$ , Equation 3.1 can be rewritten as [van Rijn, 1993]:

$$c = \frac{1}{k_2} \ln \left[ \frac{k_1}{I} \right] \quad (3.3)$$

in which  $k_2$  = calibration constant. The constants  $k_1$  and  $k_2$  can be obtained by means of statistical analysis.

The constant  $k_1$  is dependent on the characteristics of the instrument, fluid properties and travel distance (distance separating light source and detector) whereas  $k_2$  is dependent on particle properties (size and shape), wave length and travel distance [van Rijn, 1993]. If an optical instrument (with known characteristics, light wave length and travel distance) is used for field measurement under different conditions the remaining main influencing factor would be the fluid properties and the particle characteristics. Light transmission is scattered to all directions and attenuated (decreased) by water molecules. The fluid properties (e.g. density) correspond to the attenuation of light in the water column. Fluid with higher density will attenuate more light since the light beam will be scattered and absorbed by more water molecules.



(a) Scattering and absorption experienced by transmitted light due to presence of materials in suspension (b) Optical beam transmissometer with 2cm length of path

Figure 3.4: Optical beam transmissometer

The particle characteristics (i.e. size) have been found to be important in influencing light attenuation (optical transmission) in the water [Campbell & Spinrad, 1987; Moody et al., 1987]. The particle characteristics (size, colour and shape) affect the intensity of scattered light. Small particles (assumed to be spherical) with particle diameter ( $d$ ) smaller than  $1/10$  the wavelength of the light will give a symmetric scattering in backward and forward directions. Larger particle ( $d \approx 1/4$  wave length) will give a concentrated scattering in forward direction. Particle larger than the wavelength of the light will give a concentrated scattering in forward direction and develop minimum and maximum scatterings at wider angles.

Particle colour determines the ability to absorb or reflect the incident light beam. For example sand with light colour reflects the incident beam very well. Conversely, the black carbon has a tendency to absorb the incident beam. With all else being constant (particle size, shape, etc.), the fines from carbon filters have lower scattered light intensity. Particle shape determines the ability of the suspended solids to provide a constant spatial distribution pattern. A smooth, spherical-shaped particle will provide predictable results, whereas an irregularly-shaped particle can produce widely varying responses depending on the side that the incident light beam strikes. The difference between the refractive indexes of the particle and the sample fluid allows light scattering to occur. The intensity of the scattered light increases as the difference increases.

### 3.2.2.3 Acoustical profiling

Acoustical profilers bring several advantages among other suspended sediment measurement techniques (i.e. mechanical and optical samplers) since they are less susceptible to biological fouling, non-intrusive and are able to provide high spatial and temporal resolutions. Number of researches and tests of the use of acoustical backscatter signals (acoustic echo intensity) from acoustical profilers (i.e. ADCP) to estimate suspended sediment concentration have been increased within past decade. Such a method is nowadays still in a development stage.

Concentrations in water column can be related to the magnitudes of the acoustic echo intensity of the returned signal from the scatterers (suspended material). The strength of acoustic echo intensity is considered to be proportional to the concentration of suspended material. For converting the acoustic echo intensity to suspended sediment concentration, several corrections are required. The corrections account for sound attenuations due to water masses and scattering particles in the water column. The loss of acoustical energy proportional to the inverse function of the distance from the transducer should also be accounted. Due to the interdependency between acoustical propagations and water properties (i.e. salinity and temperature), sophisticated calculations and data processing algorithms as well as reliable additional measurements are needed.

References about the practical use of acoustical methods for estimating suspended sediment concentrations available in the literature are still very limited. However reports discussing laboratory and field tests conducted for application of such methods are available. Various approaches based on different levels of simplifications and assumptions are proposed. Most of them deal with the searching of the most effective approach for converting echo intensity to suspended sediment concentration.

In this study, a summary of available conversion approaches are presented. Accordingly, some field experiments have been carried out to confirm the effectiveness of the available conversion approaches. The results are also summarised here to document current achievement in the investigation of the use of acoustical profiler for estimating suspended sediment concentration.

Initial study of the use of acoustic backscatter for estimating suspended sediment concentration with qualitative evaluation has been previously done by, for example, Schott & Johns [1987], Flagg & Smith [1989] and Heywood et al. [1991]. Review on backscatter theory has been discussed by, for example, Libicki et al. [1989] and Thorne & Hardcastle [1991]. Conversion approaches based on empirical technique which are often time consuming were proposed [Young et al., 1982; Vincent et al., 1986; Hanes et al., 1988]. Applicable methods based on theoretical description of backscatter from sediment in suspension were also offered [Thorne et al., 1991]. Recently, some methods based on empirical techniques and simplified theoretical background are also being tested [Poerbandono & Mayerle, 2003; Lu, 2003].

Holdaway et al. [1999] has comprehensively reviewed and applied the conversion of echo intensity to suspended sediment concentration based on the development of backscatter theory using heuristic approach. The conversion approach was applied in a field experiment using a 1MHz ADCP system. Results comparable with an independent optical beam transmissometer were obtained. In the conversion approach the suspended sediment concentration ( $c$ ) is estimated using [Holdaway et al., 1999]:

$$c = KV_{rms}^2 r_s^2 e^{4(r_s \alpha_w + R\bar{\alpha})} \quad (3.4)$$

in which  $K$  = constant obtained by calibration with direct sampling being the proportionality of water sample concentration  $c$  with the factor  $V_{rms}^2 r_s^2 e^{4r_s \alpha_w}$  at a distance of  $r_r$  from the transducer,  $V_{rms}$  = recorded root-mean-squared voltage from the transducer,  $\alpha_w$  = attenuation coefficient due to water absorption,  $r_s$  = distance of layer being estimated from the transducer,  $R = r_s - r_r$  and  $\bar{\alpha}$  = depth-integrated attenuation coefficient due to scatterers in suspension estimated using:

$$\bar{\alpha} = \frac{\zeta}{R} \int_{r_r}^{r_s} c(r_s) dr_s \quad (3.5)$$

in which  $\zeta$  = sediment attenuation constant proportional to viscous and scattering properties of materials in suspension following an empirical equation proposed by



Urlick [1948].

To solve Equation 3.4, an iteration procedure is required. Some other parameters (e.g. water and sediment properties) must be adequately known. Additionally, accurate measurement for attenuation coefficient due to water absorption is needed. Furthermore, special setting should be developed to obtain directly the measured voltage from the transducer. Such a complication makes the application of the conversion approach less practical.

Study of the use of acoustical profiler for estimating suspended sediment concentration based on an empirical approach proposed by Deines [1999] had been done by Poerbandono & Mayerle [2003]. In the corresponding work the derivation of the approach was simplified assuming constant acoustical attenuation coefficient, transmit power and pulse length. The correction due to beam spreading and loss is assumed to have been accounted during the conversion of signal strength in count unit to dB unit. Hence the concentration ratio between two measuring layers was assumed to be proportional to the echo intensity increment.

Later on it was empirically found that to fit the measurement the regression line relating concentration ratio and echo intensity increment requires a coefficient of approximately 0.45. Incorporating this coefficient in the regression line provides comparable results with those measured using an optical device (optical beam transmissometer). It was found that 97% of the comparison data lied within a factor of 2 [Poerbandono & Mayerle, 2003].

Further works considering several other conversion approaches are summarised here. Conversion approaches developed based on empirical techniques proposed by SonTek [2002], Deines [1999], Patino & Byrne [2001] and Gartner [2002] have also been selected and tested in this study. Two different types of conversion approaches can be distinguished. The first type is based on the proportionality of echo intensity increment ( $\Delta EI = EI - EI_r$ ) with the logarithm of the concentration ratio ( $10\log(c/c_r)$ ) and the second type is based on a linear relationship between the logarithm of the echo intensity ( $10\log(EI)$ ) and concentration ( $c$ ). Equations for the conversion from SonTek [2002], Deines [1999], Patino & Byrne [2001] and Gartner [2002] read respectively as:

$$c = 10^{10 \log c_r + (EI - EI_r)} \quad (3.6)$$

$$c = 10^{10 \log c_r + K_C (EI - EI_r)} \quad (3.7)$$

$$c = 10^{(0.07462 + 0.00084 \log(S_a) - 0.02957 \log(T_e)) EI + 1.4615} \quad (3.8)$$

$$c = 10^{0.0378 (EI) + 1.338} \quad (3.9)$$

in which  $c_r$  = reference concentration for calibrating the acoustic measurement in  $\text{kg}/\text{m}^3$ ,  $EI$  = echo intensity from ADCP at the estimated layer in dB,  $EI_r$  = echo intensity at the reference level in dB,  $K_C$  = signal coefficient factor = 0.45 and  $S_a$  = salinity in ppt. The constants in Equation 3.9 have been derived using calibration with direct

sample measurement [Lu, 2003].

The performance of the empirical approaches for converting echo intensity to suspended sediment concentration proposed by SonTek [2002], Deines [1999], Patino & Byrne [2001] and Gartner [2002] have been validated. Simultaneous measurements of concentration using optical beam transmissometer and trap sampler and the corresponding echo intensity measured by ADCP have been made in several different locations in the investigation area (i.e. Outer Eider estuary and tidal channels of the Meldorf Bight) having similar ranges of particle sizes moving in suspension. A 1200kHz ADCP was used with 0.5m bin size and 12 seconds averaging ensemble. The echo intensity (acoustic backscatter) obtained from the ADCP has been corrected for beam spreading and attenuation assuming absorption coefficient of 0.618dB/m.

The concentration obtained by converting the echo intensity to concentration is compared with the concentration obtained by the optical beam transmissometer at each measured layer. In case of the approaches proposed by SonTek [2002] and Deines [1999], the reference level is chosen at mid depth. In case of the approach proposed by Patino & Byrne [2001], a temperature of 16°C and salinity of 25ppt were considered. In case of the approach proposed by Gartner [2002], a calibration curve was developed by comparing measured echo intensity and direct sampling to obtain the regression constants (i.e. regression slope and intercept).

The results are evaluated according to score (in percentage) of data lying within a factor of 2, relative error in percentage (RE) and root mean square error in kg/m<sup>3</sup> (RMS) [Lu, 2003]. The corresponding results are presented in Table 3.1. It is confirmed that acoustical measurements employing empirical conversion approaches are able to perform a good agreement with respect to those measured using an optical beam transmissometer.

**Table 3.1: Performance of conversion approaches**

| Approaches            | Equation | Data sets       |                    |                                |                 |                    |                                |
|-----------------------|----------|-----------------|--------------------|--------------------------------|-----------------|--------------------|--------------------------------|
|                       |          | 1 (Piep)        |                    |                                | 2 (Eider)       |                    |                                |
|                       |          | Factor of 2 (%) | Relative Error (%) | RMS Error (kg/m <sup>3</sup> ) | Factor of 2 (%) | Relative Error (%) | RMS Error (kg/m <sup>3</sup> ) |
| SonTek [2002]         | 3.6      | 76              | 159±976            | 0.91                           | 99              | 19±27              | 0.09                           |
| Deines [1999]         | 3.7      | 93              | 31±88              | 0.09                           | 100             | 10±10              | 0.04                           |
| Patino & Byrne [2001] | 3.8      | 91              | 39±77              | 0.09                           | 92              | 37±37              | 0.14                           |
| Gartner [2002]        | 3.9      | 88              | 35±44              | 0.07                           | 100             | 21±21              | 0.08                           |

Note:

Data set 1 = Piep channel, September 2001

Data set 2 = Outer Eider estuary, April 2002

It should be noted that the evaluation procedures presented here only give performance comparison between conversion approaches relative to each other. The results

from all conversion approaches show a reasonable agreement with the data measured using the optical beam transmissometer. Influences from other parameters such as range of velocity, suspended sediment concentration and water depth, variations of different measuring cross sections, salinity and temperature were investigated with no significant influences. Among all the approaches, the one proposed by Gartner [2002] offers an advantage since no reference values are required. Further tests to confirm the performance of the approaches for different field conditions including larger sizes of sediment moving in suspensions should be conducted.

### 3.2.3 Sediment grain size analysis

Sieve analysis is a common method for characterising sand (coarse) sediment samples. In the analysis, the proportion of sediment grain of each range of diameter in the sample is determined. Dry sediment sample is passed through several sieve apparatus of various size of opening. The proportion of each range of sediment diameter is given by weight of the sieved sample. Based on this analysis, a frequency histogram and a cumulative probability curve of the grain diameters of the sediment sample can be obtained. The representative size of sediment sample can be determined from the cumulative probability curve.

As the standard sieve apparatus has the smallest opening of about 0.074mm, different method should be used for analysing fine sediment samples. In this case several instruments of different working principles, for example Hydrometer, Coulter Counter or Laser Granulometer, can be used. Hydrometer analysis is based on Stokes law, which relates the terminal velocity of a sphere falling freely through a fluid to the diameter [U. S. Army, 1986]. The hydrometer is used to determine the percentage of dispersed sediment particles remaining in suspension at a given time. Coulter counter analysis is based on electro-resistivity in an electrolyte [Jantschik et al., 1992]. In this study a Galai CIS 1 laser granulometer (Figure 3.5) is used to analyse the suspended sediment sample.

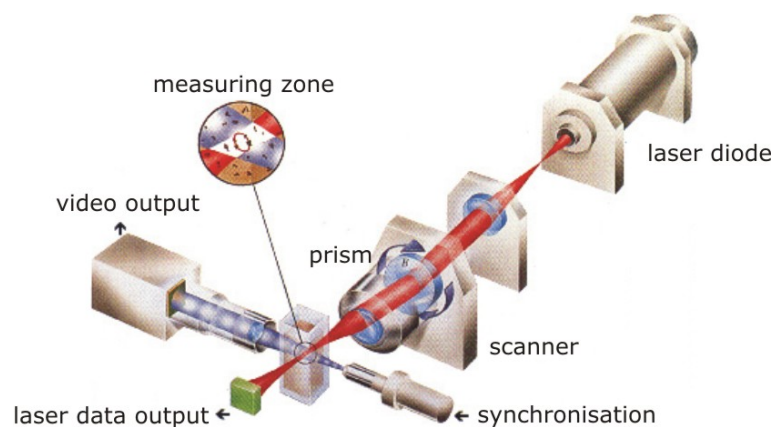


Figure 3.5: Working principle of a laser granulometer Störtenbecker [1992]

The working principles of the instrument is described in, for example, Jantschik et al. [1992] and Störtenbecker [1992]. The water sample contained in a spectrophotometer-type cell is scanned with a focused He-Ne laser beam using a rotating wedge prism. Knowing precisely the angular velocity, the size of each particle scanned at focus can be calculated from the duration of the obscuring of the beam. The standard measuring range extend from 5 and 150 $\mu\text{m}$  in steps of 0.5 $\mu\text{m}$ .

### 3.3 Field measurements

Within the framework of PROMORPH project, measuring campaigns in the investigation area were regularly carried out during the years 1999 to 2002. Among the objectives of the campaigns are to estimate the water discharges, the rate of transported material in suspension (suspended load transport) and the suspended load transport in the measured cross section over a tidal cycle. Along with, the results are also used to develop and validate a numerical model for simulating flow field, sediment transport and the dynamics of local morphology.

The measurements have been carried out mostly from moving vessels under calm weather conditions covering various seasons, measuring cross sections and tidal conditions. The astronomical tidal range during the experiments varied between 2.3m during neap tide and 4.2m during spring tide. Detailed discussion of the measured current velocity over vertical and along the cross section and its conjunction with suspended sediment concentration measurements is given herein. Attention is paid to the measurements carried out along two cross-sections on the main tidal inlets T1 and T2, and T3 near the coast (Figure 3.6).

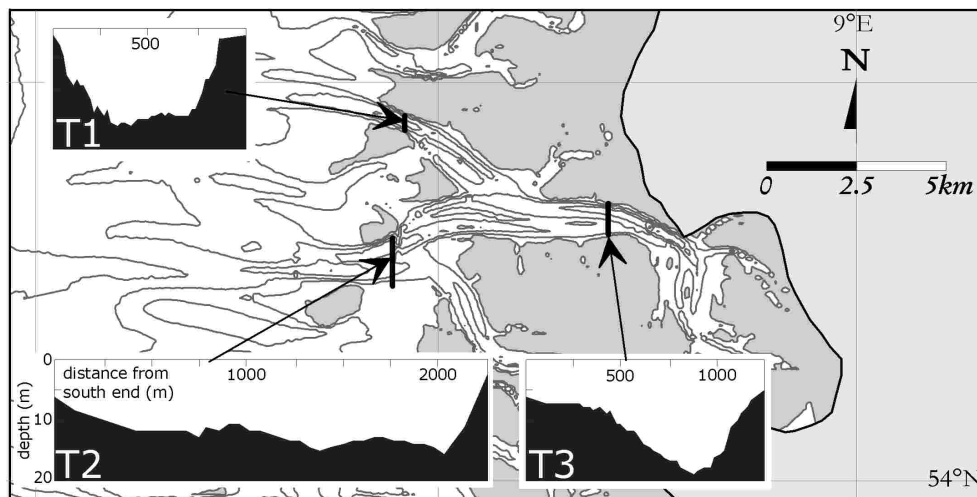


Figure 3.6: Measuring locations and their cross sectional profiles

The cross-sectional profiles suggest that T1 is about 770m wide with water depths varying from 2.8 to 16.1m in the Norderpiep tidal channel, T2 about 2040m wide with

water depths varying from 7.3 to 15.6m in the Suederpiep tidal channel and T3 about 1200m wide with water depths varying from 6.2 to 17.9m in the Piep tidal channel. To obtain a coverage over the entire tidal cycle about 20 to 75 transects (cross-sectional measurements) were made per measuring campaign.

A transect consists of several measuring stations along the cross section with approximately 180m intervals. The exact number of measuring stations vary within different measuring period. Cross section T1 consists of 4 measuring stations. Cross section T2 consists of 9 to 12 measuring stations and cross section T3 has 6 to 7 measuring stations. In each measuring station, the simultaneous measurement of current velocity and suspended sediment concentration profiles were carried out. Occasionally, water samples are also taken.

### 3.3.1 Measuring strategy

The measurements were done along a cross section (transect) with the measuring vessel moved back and forth over an entire tidal cycle. Along its path, measurements of current velocity and suspended sediment concentration profiles were carried out. Figure 3.7 illustrates the measuring procedure. A 1200kHz Broadband Direct Reading ADCP was used for continuously measuring current velocity profile along the cross section. The ADCP was configured with 12 seconds averaging ensemble and 0.5m depth of cell. Assuming vessel speed of about 1 Knot, it corresponds with an averaging ensemble of approximately 6m along the ship path. Due to the height of side lobe interferences and the vertical measuring resolution (bin size), the vertical measurements covered the water column from up to about 0.5m above the seabed. Below the free surface the vertical profile measurement is started at about 1.6m depth due to the blanking distance and transducer draft.

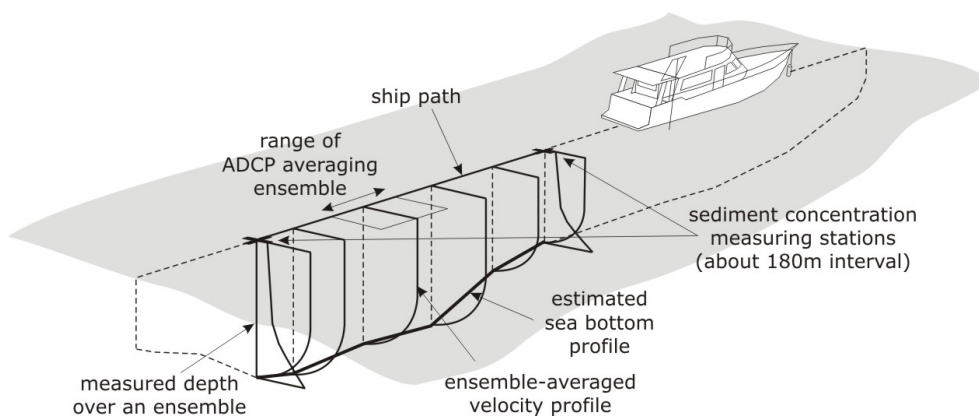


**Figure 3.7: Illustration of the measuring procedure in a cross section**

Instantaneous suspended sediment concentration over a vertical with about 0.2m resolution at specified locations (measuring stations) along the cross-section were measured simultaneously with the current velocity measurements. Depth and water prop-

erties measurements were also executed using CTD (Conductivity, Temperature and Depth) sensors. Simultaneously, water samples were taken at about 1m above seabed. The measurement covers the water column from the free surface down to about 0.25m from the bottom. This is due to the distance separating the optical transmissometer and the protecting frame at the bottom of the device.

The ADCP was mounted in the bow of the ship and faced down during measurement (Figure 3.8(b)). The optical beam transmissometer mounted in CTD sensors and trap sampler were deployed from the right amidships of the vessel (Figure 3.8(a)) and lowered by a winch (3.8(c)).



(a) Research vessel Südfall; ADCP mounted in the bow of the vessel is faced down during deployment; CTD is deployed from a winch in the right amidships of the vessel



(b) Deployment of ADCP from the bow of the vessel



(c) Deployment of CTD from the right amidships of the vessel

**Figure 3.8: Measuring operation from a moving vessel**



### 3.3.2 Current velocity profiles

Due to several limiting factors, water current measurements using ADCP cannot cover the entire water column (see: section 3.2.1.3). The measurements close to the free surface are limited by the transducer depth and the blank after transmit. In this case the corresponding distance can be up to about 1.6m. Close to the seabed, the measuring coverage over the water column is limited by the vertical resolution (bin size) defined in the device configuration setting. To cover the entire water column (from the free surface up to the seabed), the current velocity from the top most layer to the free surface is assumed to be constant and the current velocity close to the bottom is estimated using [van Rijn, 1993]:

$$u_a = u_{last} \left[ \frac{a}{z_{last}} \right]^{0.25} \quad (3.10)$$

in which  $u_a$  = estimated velocity in m/s at height  $a$  (in m) above seabed,  $u_{last}$  = measured current velocity at the layer closest to the seabed in m/s,  $z_{last}$  = height of the last measuring layer in m and  $a$  = reference level in m (assumed to be 0.01 times water depth). The corresponding illustration is shown in Figure 3.9.

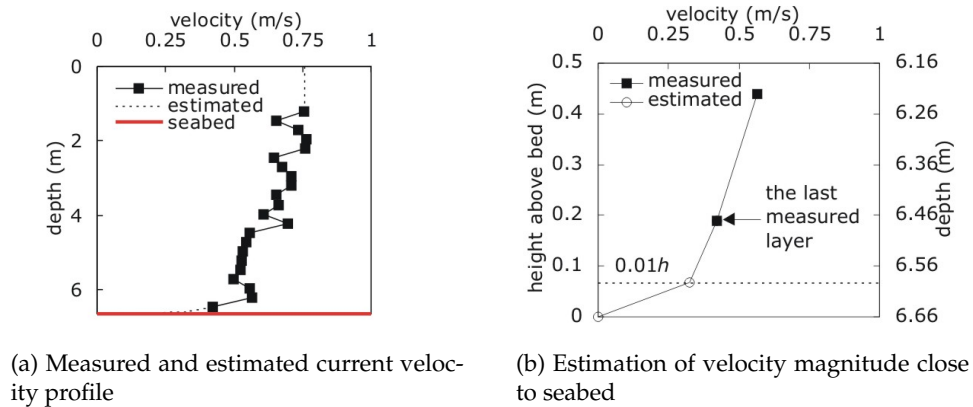


Figure 3.9: Estimation of current velocity profiles over an entire water column

### 3.3.3 Sediment concentration profiles

Suspended sediment concentration over a vertical is obtained using an optical beam transmissometer. Since the device gives a relative measure in percentage of optical transmission, a calibration against simultaneously measured water sample concentration is required for converting optical transmission measurement to suspended sediment concentration. Based on this calibration, a curve relating optical transmission and suspended sediment concentration is developed.

### 3.3.3.1 Trap sampling

Within regular measuring campaigns from the year 2000 to 2002, 479 water samples have been collected from different locations covering various conditions (i.e. water depth, tidal range, current velocity, etc.). During the data collection, various magnitudes of tidal ranges (neap and spring) and phases (ebb and flood) were covered. The water depth of the sampling locations varied from 3.8 to 20.6m and the instantaneous depth-integrated current velocity magnitudes from effectively zero to 1.6m/s with an average velocity of 0.58m/s. 225 samples collected from the year 2000 are used for the development of calibration curve for optical sampling.

The sediment content from the trap sampling is determined by filtering the water sample and through gravimetric analysis following a standard protocol resumed by van der Linde [1998]. Around 250ml of water sample was re-sampled to reduce time-consuming processing operation. For the filtration, a GF/F type filter was used. Before sampling, the filters are washed with distilled water, dried and weighed and after filtration, they are dried and weighed again. The suspended sediment concentration in the sample is defined by the difference in weight of the filter after and before filtration divided by the sample volume. The range of measured concentrations obtained from this study varies from 0.024 to 1.616kg/m<sup>3</sup>.

Uncertainties may occur due to the scale reading during volume and weight measurement, filter used stability and re-sampling process. The sampling volume scale reading is limited by 5ml resolution whereas filter weighing may lead to about 0.1mg inaccuracy. The filter used in the filtration is relatively stable. A test has been carried out with 37 filters. The average absolute weight discrepancies has been found to be 0.7mg with 1.5mg standard deviation. The re-sampling may lead to underestimated measurement due to the loss of sampling materials (water and suspended sediment) during filtration.

However, trap sampling combined with filtration methods provide reliable measurement data with limitations in spatial and temporal resolutions. The reliability of trap sampling may reduce due to the limited amount of sampling volume and deployment difficulties especially for high flow velocities. Such a sampling method can not obtain distributions of the suspended sediment concentration over the vertical (water column) or cross-sectional coverage since a large number of samplers need to be deployed. Therefore, a combination with another sampling device (in this case an optical beam transmissometer) is also used.

### 3.3.3.2 Development of calibration curve

A calibration curve used for converting optical transmission to concentration has been developed based on 225 simultaneous measurement of optical transmissions and direct sampling. The measurement was carried out along cross sections T1, T2 and T3 in the domain of investigation covering representative moon period and tidal cycle from



the year 2000. Simple regression analysis has been applied to obtain the calibration constants  $k_1$  and  $k_2$  with the following discussion.

Considering Equation 3.3 algebraic manipulation has been done by putting  $I$  at the left hand side giving [van Rijn, 1993]:

$$I = k_1 e^{-k_2 c} \quad (3.11)$$

Applying normal logarithmic on both sides gives:

$$\ln(I) = \ln(k_1) - k_2 c \quad (3.12)$$

Supposing  $\ln(I) = y$ ,  $\ln(k_1) = b$ ,  $-k_2 = a$  and  $c = x$ , a well known simple regression analysis equation  $y = a + bx$  is obtained, with  $y$  and  $x$  being respectively the dependent and independent variables.

225 data pairs of simultaneously measured concentration ( $c$ ) and optical transmission ( $I$ ) are considered here to determine the calibration constants ( $k_1$  and  $k_2$ ). Outliers were firstly removed visually and after the application of regression analysis, outliers appear from the discrepancy of measured ( $y$ ) and computed ( $y'$ ) independent variable ( $e_r = y' - y$ ) were removed using  $z$ -scores method. Using this method,  $|e_r| > 3\sigma_e$  is considered as outlier; in which  $\sigma_e$  = standard deviation of the discrepancies. The corresponding calibration constants have been found to be 110 and 2.86 for  $k_1$  and  $k_2$  respectively giving a correlation coefficient ( $r$ ) of 0.9 ( $r^2 = 0.8$ ). Hence, the formula for the conversion of optical transmission in % to suspended sediment concentration in  $\text{kg}/\text{m}^3$  is found to be:

$$c = \frac{1}{2.86} \ln \left[ \frac{110}{I} \right] \quad (3.13)$$

Equation 3.13 has been used as standard calibration curve for all suspended sediment concentration measurements considered in this study.

Figure 3.10(a) shows the regression line based on a simple regression analysis of  $y = \ln(I)$  and  $x = c$  after removal of outliers. Figure 3.10(b) shows the comparison of optical transmission and concentration for the corresponding calibration curve. Comparison between direct sampled and optical sampling concentration based on the conversion using Equation 3.13 shows 93% of data are within a factor of 2.

Sensitivity analysis of the calibration curve for suspended sediment concentration estimation due to the calibration constants confirmed that a variation of  $k_1$  by about 20% leads to an estimation deviation by a factor of 2 in lower concentration range (higher optical transmission range). On the other side, a variation of  $k_2$  by about 33% might correspond to a shift of the estimation over all ranges of optical transmission by a factor of 1.5.

As the measuring campaign continues, additional data have been obtained from

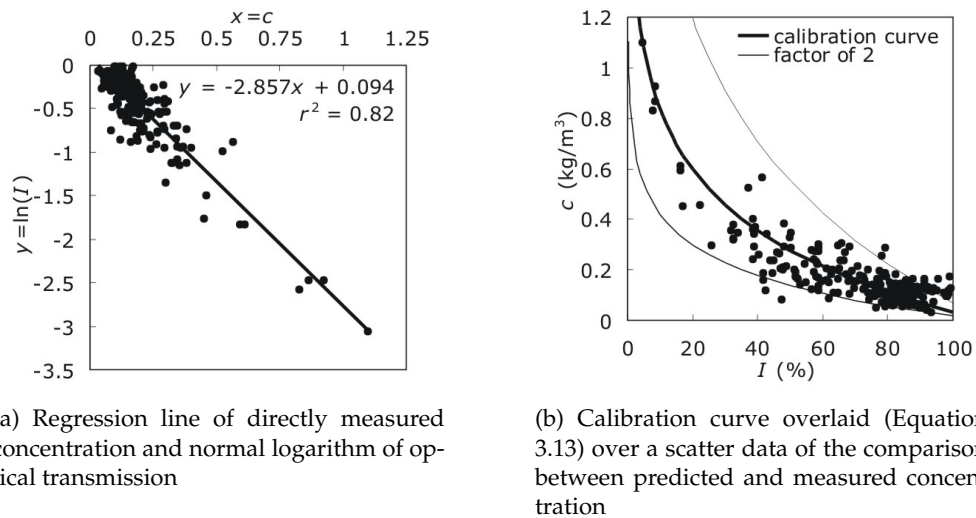


**Figure 3.10: Regression line and current calibration curve developed based on measurement 2000**

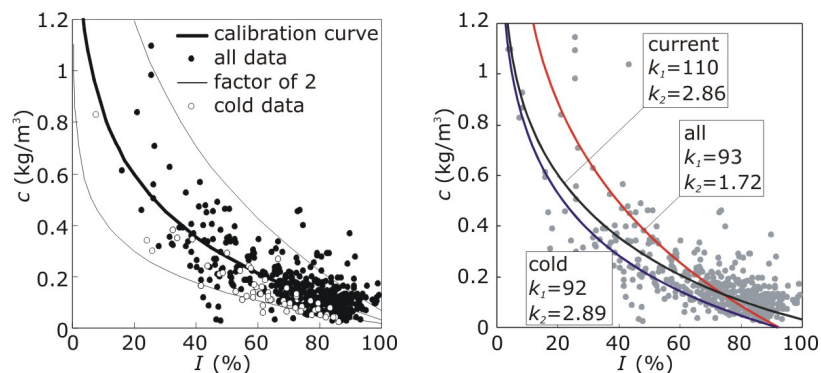
the following two years (2001 and 2002). Based on all direct sampling and optical transmission measurement data (479 data), new calibration constants have been found to be 93 and 1.72 for  $k_1$  and  $k_2$  respectively. The corresponding regression line gives a correlation coefficient of 0.75.

Devices used in this study are of the same type, thus, the beam properties remaining the same, the travel distances remaining constant and if the particle properties are assumed to be homogeneous, the remaining factors influencing the calibration constants are the fluid properties (which depend on temperature and salinity) and some other additional factors which are unknown. Investigation had been conducted by separating the comparison of optical transmission and suspended sediment concentration according to several different conditions: i.e. mean velocity, measuring depth, location (cross section), tidal phase (flow direction), salinity, season (measuring campaign) and water temperature. No clear dependency of the pattern relating the concentration and optical transmission for all those conditions could be drawn except for temperature ( $T_e$ ).

Such a phenomena can be seen in the measuring campaign carried out during winter time. During low temperatures or colder time ( $T_e < 7^\circ\text{C}$ ), the current calibration curve (Equation 3.13) tends to overestimate the prediction, whereas during warmer times it seems to work reasonably well. In low water temperatures, the optical beam transmission tends to correlate with less absorption and scattering, thus, underestimates the estimation of suspended sediment concentrations.

Under low temperature the calibration constants have been found to be 92 and 2.89 for  $k_1$  and  $k_2$  respectively. Such values were obtained from two selected measuring campaign (March 2000 and March-April 2001) representing fluid properties during low temperatures with average measured water temperatures of about  $5^\circ\text{C}$ . The

number of data used in the development of the calibration curve for low temperature measurements are 58, which covers 12% of all measurements of direct sampling concentration. Figure 3.11(a) shows the distribution of all measurement data and those taken during low temperatures.



(a) Calibration curve with ranges of factor of 2 plotted over all data and data collected during cold period (b) Calibration curves developed based on different conditions

**Figure 3.11: All data and those taken during low temperature with the calibration curve**

Assessing calibration curves developed based on different conditions, an evaluation showing the performance of each calibration curve is presented in Table 3.2. The corresponding curves are plotted in Figure 3.11(b).

**Table 3.2: Evaluation of calibration curve constants based on different sets of data**

| Calibration curve                         | Equation 3.13          | All data                | Cold data                       |
|---|------------------------|-------------------------|---------------------------------|
| Data set                                  | March to December 2000 | March 2000 to June 2002 | March 2000 and March-April 2001 |
| Calibration constants:                    |                        |                         |                                 |
| $k_1$                                     | 110                    | 93                      | 92                              |
| $k_2$                                     | 2.86                   | 1.72                    | 2.89                            |
| Correlation coefficient                   | 0.91                   | 0.75                    | 0.93                            |
| Prediction agreement to its own data set: |                        |                         |                                 |
| Factor of 1.5                             | 60%                    | 46%                     | 78%                             |
| Factor of 2                               | 88%                    | 70%                     | 95%                             |
| Factor of 3                               | 97%                    | 84%                     | 100%                            |
| Agreement to all data:                    |                        |                         |                                 |
| Factor of 1.5                             | 61%                    | 46%                     | 30%                             |
| Factor of 2                               | 84%                    | 70%                     | 49%                             |
| Factor of 3                               | 95%                    | 84%                     | 68%                             |

No significant discrepancy can be found in the calibration constants. However, current calibration curve performs better agreement for all data sets. For simplicity reasons, current calibration curve (Equation 3.13) is considered and used for converting optical transmissions to concentrations for all optical measurements executed in

this study.

### 3.3.3.3 Estimation of near-bed sediment concentration

Vertical concentration measurements are limited mainly by the measurement close to the bottom. This is due to the distance separating the device (optical beam transmissometer) with the bottom frame. Such a construction limits the lowest measurement to about 0.25m from the seabed. Therefore the measuring procedures considered here are designed to obtain the transport of sediment moving as suspension. No bed load measurements were considered.

To estimate the value at the unmeasured layer (very close to and at the seabed), an extrapolation based on the last three lowest measurements is used [van Rijn, 1993]. It reads as: [van Rijn, 1993]:

$$c_e = e^{az_e+b} \quad (3.14)$$

in which  $c_e$  = estimated concentration in  $\text{kg/m}^3$ ,  $z_e$  = height of the estimated layer above seabed and  $a$  and  $b$  are the regression slope and intercept of the regression line ( $y = ax + b$ ) relating  $y = \ln(c_e)$  and  $x = z$  respectively. The corresponding illustration is shown in Figure 3.12.

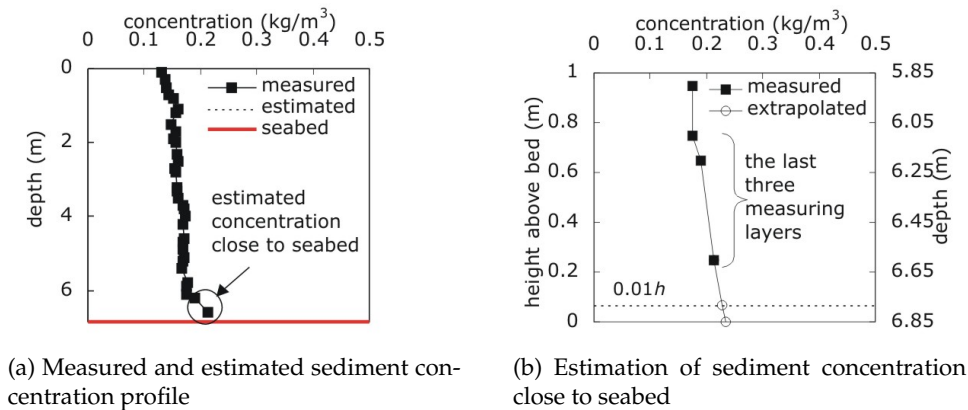


**Figure 3.12: Estimation of current velocity and sediment concentration profiles over an entire water column**

The extrapolation gives a gently sloping concentration profile in the near bed layer towards the seabed resulting in an almost uniform concentration profile over the entire water column. As the sediment particles in the investigation domain have been found to be very fine, most of sediments are expected to be transported in suspension. Therefore the approach for estimating near bed concentration magnitudes used here is assumed to be acceptably representative.

### 3.3.4 Estimation of suspended load transports

For estimating the suspended load transport rates in the measuring stations, Equation 3.15 is used. Since the velocity and concentration measurements are not at the same depth, linear interpolation was carried out to obtain concentration measurement for each measured layer of current velocity. The corresponding process is illustrated in Figure 3.13.

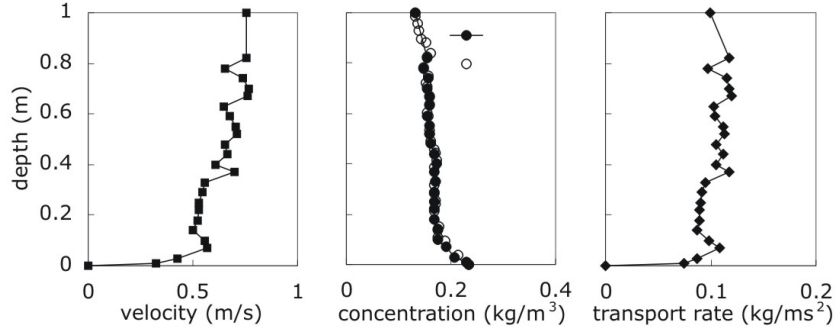


Figure 3.13: Estimation of suspended load transport rate

Having calculated the transport rate as the product of velocity and concentration data in each depth layer, the calculation of depth-integrated suspended load transport ( $\bar{q}_s$ ) has been done by the integration over measured vertical divided by the distance from the reference level to the free surface:

$$\bar{q}_s = \frac{1}{h} \int_a^h u(z)c(z)dz = \frac{1}{h} \int_a^h q_s(z)dz \quad (3.15)$$

in which  $q_s(z)$  = suspended load transport in  $\text{kg}/\text{m}^2\text{s}$  at height  $z$  in m and  $\bar{q}_s$  = depth-integrated suspended load transport in  $\text{kg}/\text{m}^2\text{s}$ .

Suspended load transport per unit width ( $q_s$ ) in  $\text{kg}/\text{ms}$  is obtained by multiplying the depth-integrated suspended load transport with the corresponding water depth:

$$q_s = \bar{q}_s h \quad (3.16)$$

Estimation of suspended load transport in cross section ( $Q_s$ ) in  $\text{kg}/\text{s}$  is done by the integration of suspended load transport over the depth and the measured cross-sectional width:

$$Q_s = \int_0^b q_s(b)db \quad (3.17)$$

in which  $b$  = cross section width in m. The corresponding calculation is illustrated in Figure 3.14.

Accumulated suspended load over an entire tidal phase ( $Q_{s,tot}$ ) in kg is obtained

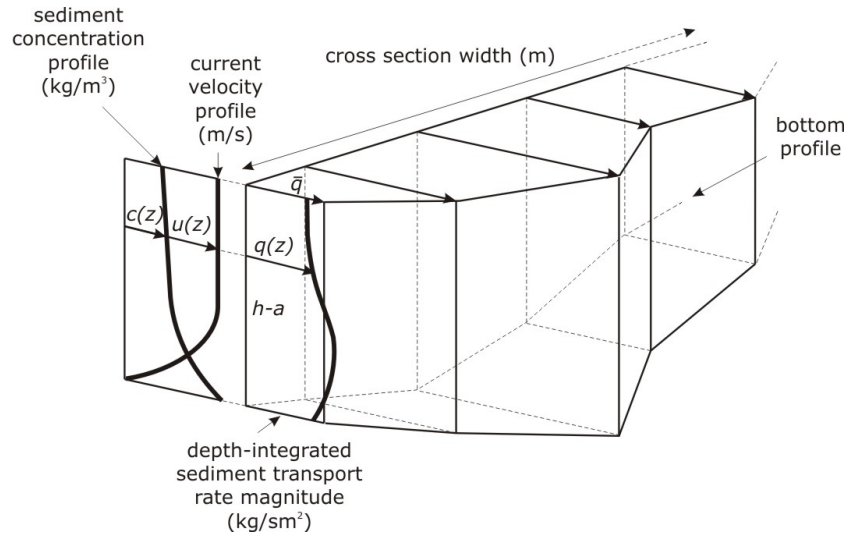


Figure 3.14: Schematisation of calculation of suspended sediment transport load in cross section

by integrating suspended load transport in cross section over a period of a tidal phase:

$$Q_{s,tot} = \int_0^t Q_s(t) dt \quad (3.18)$$

## 3.4 Assessment of measuring uncertainties

### 3.4.1 Accuracy of current measurement

The ADCP device used in the present study is a 1200kHz Direct Reading Broadband type manufactured by RD Instruments and designed with 4 convex transducers at 20° beam angle. By default, it has 1mm/s velocity measurement resolution and can be used to measure up to 5m/s of water current velocity. The maximum measuring range can also be extended up to 20m/s. Based on manufacturer's technical specification, the measuring accuracy is of  $\pm 0.25\%$  of water velocity relative to ADCP or of  $\pm 2.5\text{mm/s}$  at a measured velocity of 1m/s.

Measuring uncertainties may occur in field condition due to inaccuracy of estimated speed of sound (due to errors in temperature and salinity measurements) and vessel movement. Some authors accepted manufacturer designed accuracy of better than 1% or 1cm/s at a measured velocity of 1m/s [Lane et al., 1999; Garabato et al., 2002]. Laboratory and field experiments have been attempted to observe and quantify the accuracy of ADCP measurement. Various deployment methods and analysis approaches were used with no satisfying generic conclusions.

A study for estimating ADCP accuracy was conducted by deploying two ADCPs of similar type (Broadband, 1200kHz) and configuration (0.5m bin size, 12 seconds averaging ensemble) from moving vessels [Jiménez-González et al., 2003]. The corre-

sponding investigation was carried out in the domain of investigation considered in the present study. The analysis considered theoretical logarithmic law velocity profile and re-sampling or Bootstrap method [Efron & Tibshirani, 1993].

The investigation confirmed a standard deviation of 0.14m/s for point measurement up to 1m from bottom and 0.06m/s above 1m from bottom up to the free surface. Furthermore, the calculated depth-integrated velocity value resulted in an estimated accuracy of  $\pm 0.015\text{m/s}$  as 90% confidence level. Comparable result had been reported from an experiment using 1500kHz ADCP with 10seconds averaging ensemble for point measurement. It gives an accuracy of 0.053m/s [van Rijn et al., 2002a]. Recently, several authors also reported the investigation to the deviation obtained from the comparison of different types of acoustical profilers (i.e. ADCP and Argonaut-ADV) of within the range of 0.02 to 0.05m/s [Vermeyen, 2003; Freitag et al., 2003]. Huhta & Ward [2003] reported that the measurement results given by two different acoustical profilers (i.e. ADCP and Argonaut-SW) may deviate of within 6%.

### 3.4.2 Accuracy of sediment concentration measurement

The uncertainties of optical sampling can not be predicted unless a calibration curve giving the predicted value had been previously developed and a reference value considered as a 'true' value is known. In this study, the measuring accuracy of the optical beam transmissometer is estimated by comparing the predicted concentration (Equation 3.13) with those obtained using trap sampler. The concentrations from the trap sampler are considered as the 'true' values.

Standard methods for error analysis are available in the literature. In this study, the uncertainty of optical sampling is represented by the accuracy of the calibration curve in predicting concentration. The accuracy is estimated by the relative error (RE):

$$\text{RE} = \frac{|c_o - c_d|}{c_d} \times 100\% \quad (3.19)$$

in which  $c_o$  = concentration estimated by converting optical transmission to concentration using the calibration curve (Equation 3.13),  $c_d$  = concentration obtained from the trap sampler.

A probability distribution histogram based on a comparison of 479 relative error data is shown in Figure 3.15(a). It can be seen that the relative error distribution shows an asymmetry where most of the data are bunched to the left side of the center (positive skew). Due to the nature of the distribution, the median value is used as the typical or representative value for the data set giving a value of 29.2%. This value will be considered as representative overall accuracy of the optical beam transmissometer used in this study.

Large relative errors occur mainly in lower concentration measurements (see: Figure 3.15(b)). This is also confirmed by the predicted optical attenuation ( $A_t = 100\% - I$ )

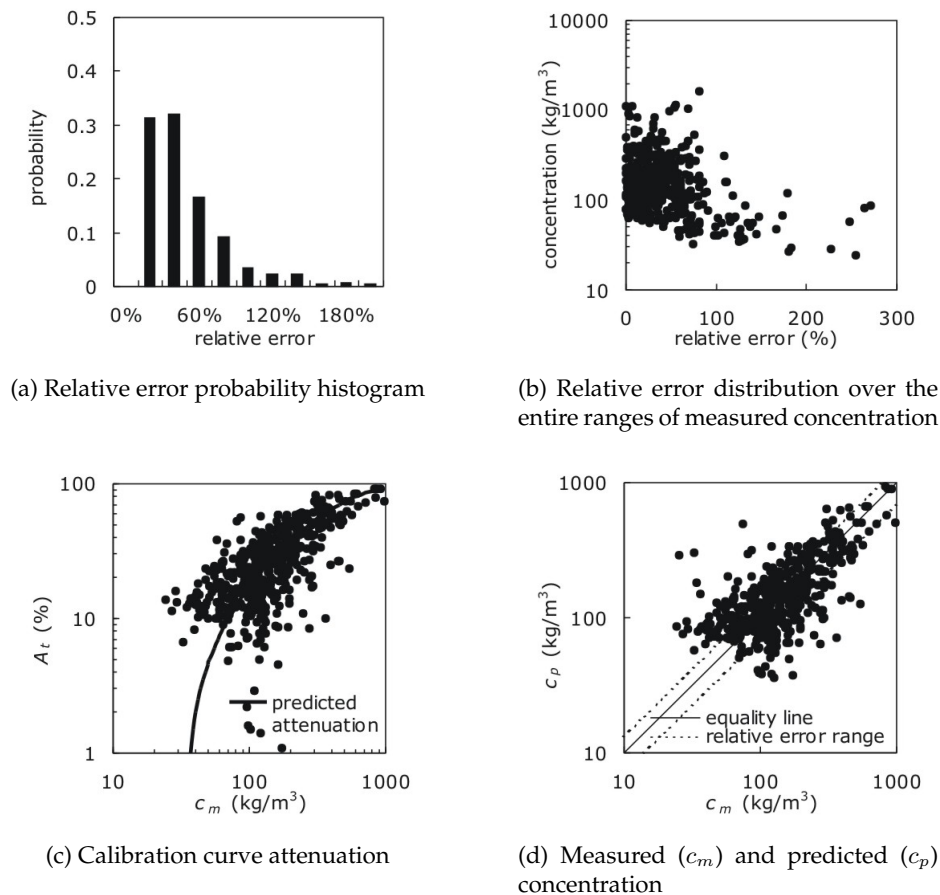


**Figure 3.15: Optical profiling uncertainty assessment**

given by the calibration curve (Figure 3.15(c)). It tends to give asymptotic concentration decreasing in the lower region and limits the measuring ability at concentration of approximately less than  $0.05\text{kg/m}^3$ . Comparison between optically and directly measured suspended sediment concentrations is shown in Figure 3.15(d).

### 3.5 Discussion

How accurate a field measurement of sediment transport can be?

Acoustic Doppler Current Profilers (ADCP) for current velocity measurement and optical beam transmissometer measurement calibrated with filtrated water samples for suspended sediment concentration estimation are used in this study to indirectly estimate the sediment transport rate. For approximating the uncertainty of the resulting sediment transport rate estimation, the accuracy of current velocity and suspended sediment concentration measurements should be taken into account.

Various studies have been made for estimating the accuracy of ADCP for field condition. Most of them have been based on direct comparison to an independent device. The corresponding accuracy is usually given as an absolute value in m/s or in



percentage. According to the study conducted by Jiménez-González et al. [2003] and van Rijn et al. [2002a] the accuracy of ADCP measurement for point measurement in field condition from moving vessel varies from 0.05 to 0.14m/s. Some other authors reported higher accuracy values of between 0.02 and 0.05m/s [Vermeyen, 2003; Freitag et al., 2003]. Huhta & Ward [2003] reported a relative accuracy value being the average deviation of two different acoustical profilers of up to 6% (see: section 3.4.1).

In this study an investigation to the accuracy of suspended sediment concentration measurement has also been carried out (see: section 3.2.2.2). The corresponding accuracy value is estimated using comparison against direct sampling concentration and given as relative error. It is found that the representative relative error of suspended sediment concentration measurement is of 30%.

For determining the accuracy of total load transport measurement, the accumulation of the uncertainties of current and concentration measurements is considered. In addition to that, uncertainty that occurs due to the agreement between the depth measured by CTD and ADCP should also be considered. In the study of the accuracy estimation of acoustical current measurement conducted by Jiménez-González et al. [2003] it was shown that with respect to those calculated for point measurement, the deviation obtained in the depth-integrated measurement is found to decrease. This is due to the compensation effect between discrepancies among point measurements.

Similarly as the total load transport is estimated based on the integration of point measurement of current velocity suspended sediment concentration, its uncertainty should decrease. However, since quantitative investigation is not carried out in this study, the accuracy of total load transport measurement for the condition in question can not be made available.



## Chapter 4

# Sediment Properties and Transport Dynamics

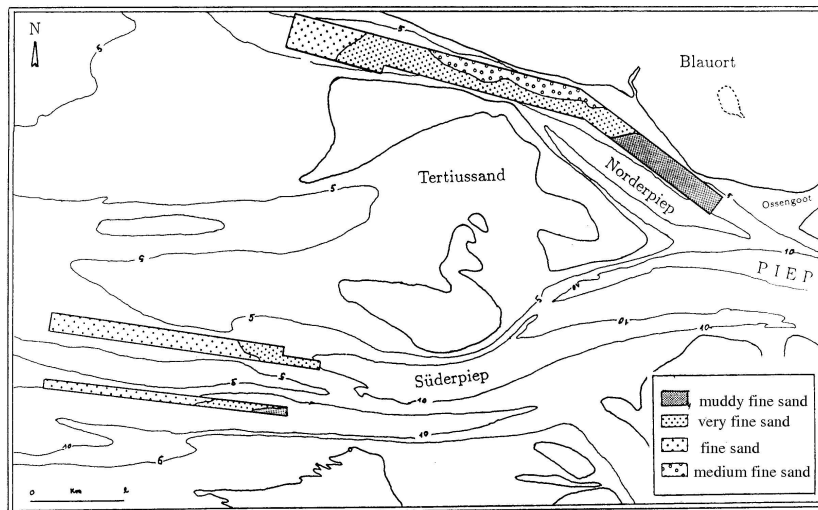
### 4.1 Introduction

In this chapter, an investigation to the properties of sediment (in bed and in suspension) and a comprehensive description of suspended sediment transport dynamics based on the measurement of suspended sediment concentrations and hydrodynamics in the investigation area are discussed. The investigation to bed and suspended sediment properties will be related to the setting and input parameters for the modelling environment in simulating the corresponding behaviour of transport dynamics. An analysis of the transport dynamics is presented to describe generic patterns and characteristics of suspended sediment concentration, current velocity and transport rate dynamics in temporal and spatial series.

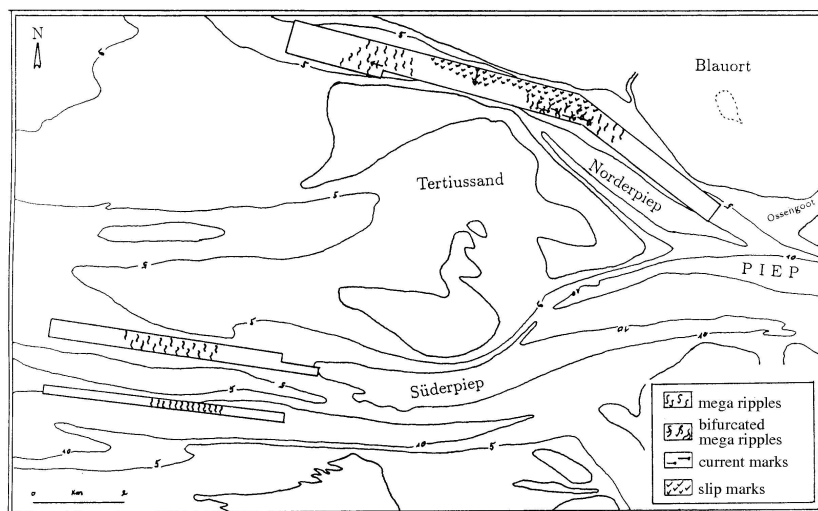
### 4.2 Bed and suspended sediment properties

The range and composition of bed sediment sizes in the tidal channel had previously been described by Kesper [1992] focusing mainly in the Norderpiep and the outer part of Suederpiep. According to his findings, it is concluded that the bed sediments are mainly composed of fine sand (Figure 4.1(a)). Silt and clay fractions dominate the eastern part of the Norderpiep channel mainly at the northern bank. Kesper [1992] also documented a study on bedform measurement along the same area based on Side Scan Sonar surveys (Figure 4.1(b)). It has been found that Norderpiep and the outer part of Suederpiep are dominated with mega ripples. In addition to that, slip and current marks appear to dominate the local bed morphology of the Norderpiep channel.

An investigation on bed sediment properties (size distribution and mud content) had been recently carried out based on grab sampling surveys done in the years 1998 (132 sampling stations) and 2000 (15 sampling stations) mainly along the Piep tidal



(a) Bed sediment composition



(b) Bedform measurement

Figure 4.1: Bed sediment composition and bedform measurement in Norderpiep and Süderpiep channels [Kesper, 1992]

channel and the inner part of the main tidal channel with spatial resolution of about 200 to 400m and, additionally, some sporadic sampling stations along the southern part of Suederpiep channel [Razakafoniaina, 2001; Vela-Diez, 2001]. Figure 4.2 shows the corresponding sampling locations.

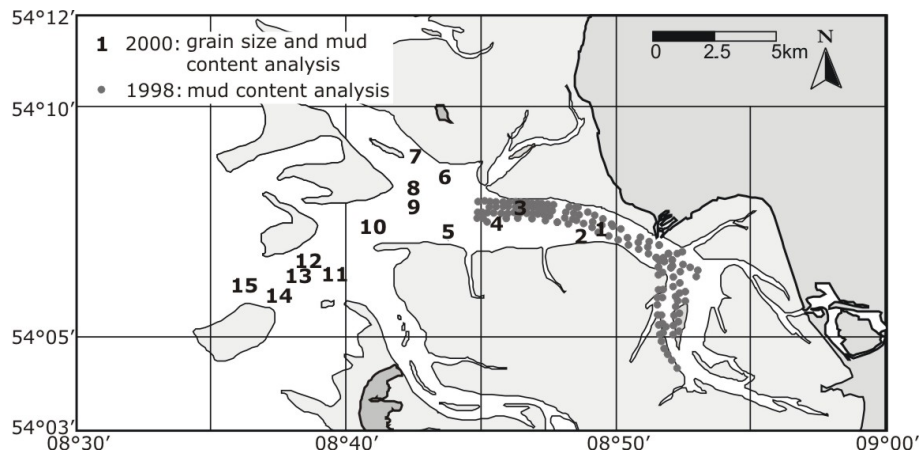


Figure 4.2: Grab sampling locations

Investigation on suspended sediment sizes has also been carried out. The samples were taken from the main channels (cross sections T1, T2 and T3; see: Figure 1.1) at about 1m above seabed during regular measuring campaigns in the years 2000 and 2001 resulting in a total of 233 samples.

Additionally, an investigation on the bottom sediment characteristics and identification of bedform types and dimensions along the main tidal channels (Norderpiep, Suederpiep and Piep channels) based on grab sampling analyses and Side Scan Sonar surveys have also been carried out. The results are summarised in Mayerle et al. [2002]. In this study further efforts have been attempted in the investigation of the sorting parameters of bed sediment and a brief discussion on suspended sediment size measurements. An investigation of the relationship between water depth, silt and clay content and median size of bed sediment samples is also attempted.

#### 4.2.1 Bed sediment sizes distribution

The distribution of bed sediment sizes is obtained based on sieve analysis of 15 bed sediment samples taken in 2000 from the main tidal channels. The results show that the median diameter ( $d_{50}$ ) of 15 bed sediment samples varies from 80 to 230  $\mu\text{m}$ . The sorting parameters of the samples indicate that the sediments are largely (11 out of 15) well sorted with a ratio of  $d_{84}$  to  $d_{16}$  varying from 1 to 2.9 with an average value of 1.9. The geometric standard deviation ( $\sigma_g = (d_{84}/d_{16})^{0.5}$ ) is from 1 to 1.7 with an average value of 1.4. The average ratio of  $d_{90}$  to  $d_{50}$  is 1.4. Most of the samples (10 out of 15) have median sizes equal or less than about 100  $\mu\text{m}$ .

Table 4.1 shows the results of the sorting characteristics of the bed sediment samples. Information of sizes of sediment ( $d_{50}$  and  $d_{90}$ ) presented in Table 4.1 is based on the work carried out by Vela-Diez [2001]. It is shown here that the bed sediment consists mainly of very fine to medium sand with varying percentage of silt and clay fraction, thus, confirming previous studies conducted by Kesper [1992] and Mayerle et al. [2002].

**Table 4.1: Bed sediment samples analysis result**

| Station | Depth<br>(m) | $d_{50}$<br>( $\mu\text{m}$ ) | $d_{90}$<br>( $\mu\text{m}$ ) | $d_{90}/d_{50}$ | $\sigma_g$ | Fine<br>(%) | Sorting      |
|---------|--------------|-------------------------------|-------------------------------|-----------------|------------|-------------|--------------|
| 1       | 10.0         | 103                           | 124                           | 1.2             | 1.3        | 8.1         | Well-sorted  |
| 2       | 6.3          | 104                           | 130                           | 1.3             | 1.0        | 4.7         | Well-sorted  |
| 3       | 14.4         | 137                           | 203                           | 1.5             | 1.5        | 2.7         | Intermediate |
| 4       | 1.0          | 86                            | 115                           | 1.3             | 1.2        | 18.8        | Well-sorted  |
| 5       | 5.0          | 124                           | 189                           | 1.5             | 1.4        | 10.0        | Well-sorted  |
| 6       | 7.0          | 107                           | 222                           | 2.1             | 1.7        | 17.2        | Intermediate |
| 7       | 12.4         | 103                           | 132                           | 1.3             | 1.3        | 12.1        | Well-sorted  |
| 8       | 10.0         | 109                           | 134                           | 1.2             | 1.3        | 23.6        | Well-sorted  |
| 9       | 12.5         | 104                           | 131                           | 1.3             | 1.3        | 21.5        | Well-sorted  |
| 10      | 3.0          | 125                           | 207                           | 1.7             | 1.5        | 3.2         | Intermediate |
| 11      | 7.5          | 230                           | 295                           | 1.3             | 1.6        | 3.8         | Intermediate |
| 12      | 11.0         | 84                            | 117                           | 1.4             | 1.3        | 47.5        | Well-sorted  |
| 13      | 10.5         | 90                            | 136                           | 1.5             | 1.4        | 51.9        | Well-sorted  |
| 14      | 5.0          | 159                           | 210                           | 1.3             | 1.4        | 4.1         | Well-sorted  |
| 15      | 15.4         | 80                            | 123                           | 1.5             | 1.3        | 50.7        | Well-sorted  |
| Minimum | 1            | 80                            | 120                           | 1.2             | 1.0        | 3           |              |
| Maximum | 15           | 230                           | 300                           | 2.1             | 1.7        | 52          |              |

#### 4.2.2 Mud fractions and bed sediment types

Analysis of mud fraction is carried out based on all samples collected in 1998 and 2000. Mud fraction has been found in all bed sediment samples with varying percentage. Measurements indicated that the mud content in the sampling area is in general higher than 5%. Besides, over 50% of the samples (73 out of 132) have mud content exceeding 10%. Additionally, the consolidated fine grained sediments are mostly outcropping in the deeper parts and at the flanks of the channels developing a non-erodible (less mobile) type of bed due to the presence of consolidated mud in bed sediment. Figure 4.3 shows the distribution of consolidated mud in the domain of investigation. Non-cohesive bed sediment zones have been found to be in a good agreement with the development of bedform. Bedforms in the range of 0.2 to 0.4m of heights are generally found where there is no existence of mud. Additionally, time-dependent bedform development was also indicated [Mayerle et al., 2002].

Figure 4.4 shows the relation between mud (silt and clay) fractions in bed sediment samples with water depth and median grain diameter. The tendency of increasing

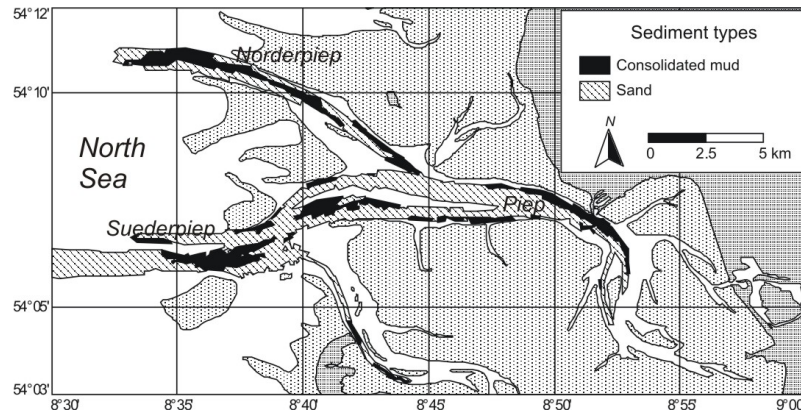
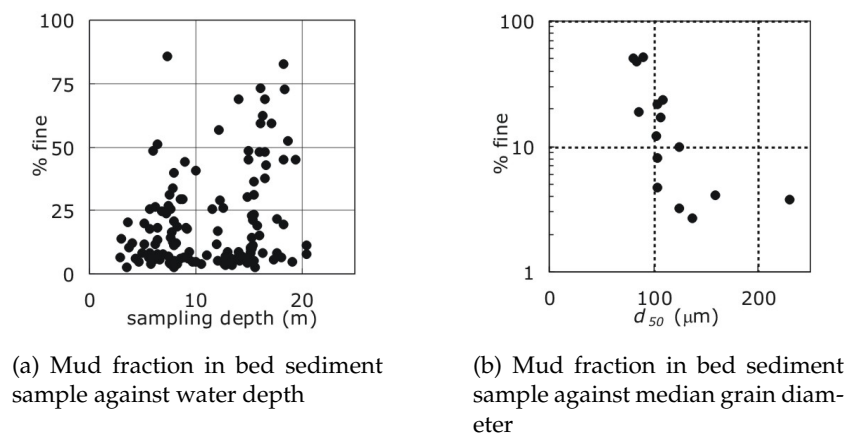


Figure 4.3: Bed sediment types [Mayerle et al., 2002]

mud content with depth in bed sediment samples can be observed. Bed sediment samples with higher silt and clay fractions are usually found in the deeper area of the main channels. Besides, finer sizes ( $d_{50} \approx 100\mu\text{m}$ ) of median values correspond with larger fraction of silt and clay particles in the bed sediment samples ( $\geq 10\%$ ), whereas, higher sand fractions in the bed sediment samples ( $>95\%$ ) were found to correspond with larger median sizes ( $d_{50} > 100\mu\text{m}$ ).



(a) Mud fraction in bed sediment sample against water depth

(b) Mud fraction in bed sediment sample against median grain diameter

Figure 4.4: Relationship of mud fraction in bed sediment sample with water depth and median grain diameter

### 4.2.3 Suspended sediment sizes

The range of median sizes of material moving in suspension in the investigation area has been found to vary from 6 to  $86\mu\text{m}$  [Mayerle et al., 2002] of which about 60% of them have values between 10 to  $25\mu\text{m}$  [Poerbandono et al., 2003]. Figure 4.5 shows the relative frequency of median sizes of material moving in suspension measured using laser granulometer without and with pre-treatment. Discussion of the corresponding analysis follows.

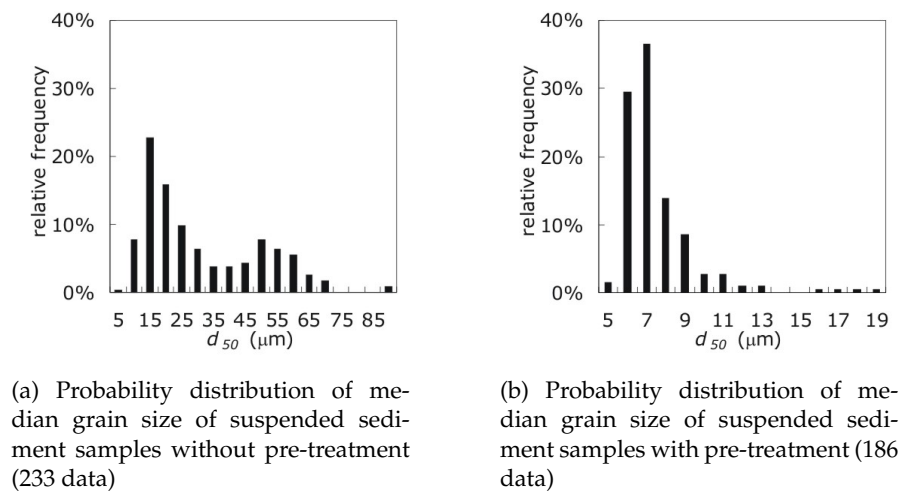


Figure 4.5: Median grain size of suspended sediment samples

#### 4.2.3.1 Ranges of grain sizes

Samples for suspended sediment grain sizes analysis were taken from cross sections T1, T2 and T3 along the three representative main channels at about 1m from seabed during several measuring campaigns covering various magnitudes of tidal ranges (neap and spring) and phases (ebb and flood). The water depths of the sampling locations varies from 5 to 26m, the instantaneous depth-integrated current velocity magnitude varying from effectively zero to 1.6m/s and the sample concentrations were from 0.04 to 1.1kg/m<sup>3</sup>. The amount of the water sample was about 2 litres. About 250ml therefrom was re-sampled for particle size analysis. The grain size analysis has been done using a Galai CIS-1 laser granulometer.

Fine sediment particles in natural coastal environment tend to flocculate developing larger aggregates due to electro-statical forces between particles that exceed gravity forces working on them. The flocculation may also occur during the time between sampling and analysis (resident time). It is suggested that the resident time of water samples should not exceed a few hours [Jantschik et al., 1992]. However, since immediate analysis (on-board) could not be performed, the samples have experienced resident time from 24 hours up to 1 week.

Pre-analysis treatment was done by shooting the water sample with ultrasonic wave in about 10 minutes duration before measurement. It is expected that by such a treatment the aggregates will be separated. It may also happen that the shooting destructs the original particles in the sample and breaks them up. In turn, the particle size analysis may not represent their natural sizes distribution. However, two different sample types (with and without pre-analysis treatment) are considered here.

With respect to those measured without pre-analysis treatment, the pre-analysis treatment gives approximately 36% reduction of the median sizes of the particles in the samples. It is also found that pre-analysis treatment reduces the range of median



grain sizes by a factor of 5. The corresponding comparison is given in Table 4.2.

**Table 4.2: Ranges of median values of suspended sediment samples**

|         | With pre-analysis treatment ( $\mu\text{m}$ ) | Without pre-analysis treatment ( $\mu\text{m}$ ) |
|---------|---|--|
| Minimum | 4   | 6  |
| Maximum | 19  | 86   |
| Range   | 15  | 80   |

#### 4.2.3.2 Materials moving in suspension

A sample has been selected to give a qualitative description of the visual appearance of sediment moving in suspension. Figure 4.6 shows the corresponding photos under microscope with 20 (left) and 40 (right) times exaggeration.

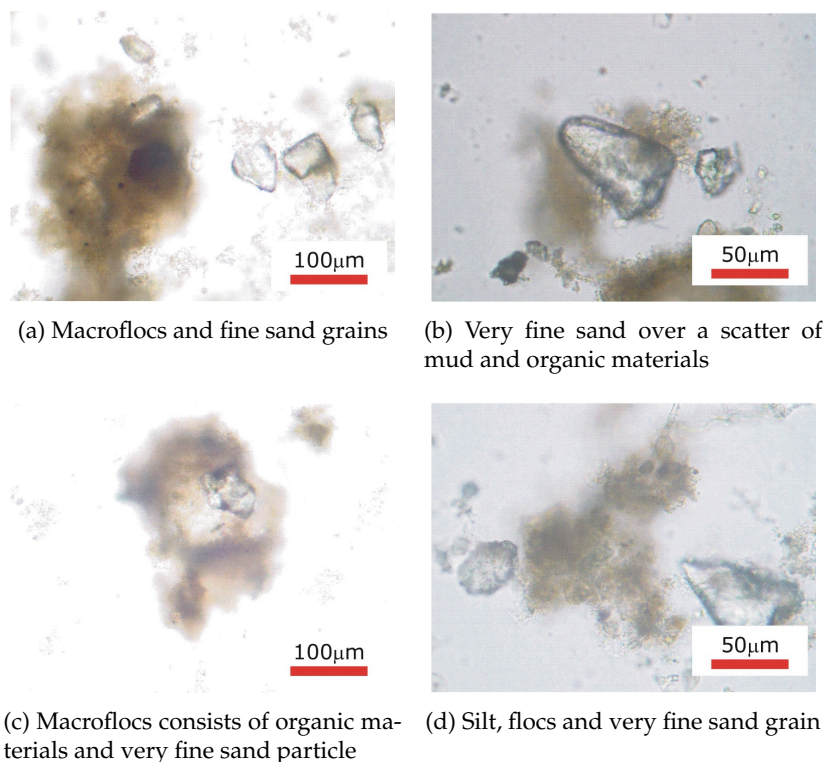


**Figure 4.6: Photos of material moving in suspension without pre-treatment**

This sample was taken from the middle of the Piep channel, on September 11<sup>th</sup>, 2001 during the flood phase. The water depth was 11.8m and the instantaneous depth-integrated velocity was 0.83m/s. The suspended sediment concentration was  $0.12\text{kg}/\text{m}^3$  and the median sediment size of the sample was  $43\mu\text{m}$ . It is shown that it consists of different kinds of materials, mainly very fine sand, mud, organic material and flocs. Some efforts have been attempted to investigate the relationship between

median size of suspended sediment samples with other parameters measured simultaneously in the field during sampling (i.e. current velocity, flow depth, concentration, salinity and temperature). No distinct pattern of particle size distribution over a range of those parameters can be drawn.

### 4.3 Suspended sediment dynamics

The spatial (vertical and within the domain) and temporal (within a tidal cycle and depending on the tidal range) variations of the suspended sediment concentrations and suspended load transports obtained from the measurements were investigated. The results are resumed in Table 4.3.

**Table 4.3: Resume of field measurement data [Poerbandono et al., 2003]**

| Cross section<br>[width]            | Date          | Tidal range<br>(m) | Max. depth-integrated current velocities (m/s) |      | Max. depth-integrated suspended sediment concentration (kg/m <sup>3</sup> ) |      | Tide-integrated suspended load transport ×10 <sup>3</sup> tons |                    |
|-------------------------------------|---------------|--------------------|--|------|---|------|--|--------------------|
|                                     |               |                    | Flood  | Ebb  | Flood   | Ebb  | Flood  | Ebb                |
| T1 [770m]<br>Norderpiep tidal inlet | Mar. 16, 2000 | 3.2                | 1.1  | -1.5 | 0.27  | 0.22 | 18.7   | -18.3              |
|                                     | Mar. 22, 2000 | 4.0                | 1.2  | -1.2 | 0.14  | 0.19 | 18.2   | -17.3              |
|                                     | Jun. 5, 2000  | 3.7                | 1.6  | -1.4 | 0.18  | 0.17 | 18.8 <sup>u</sup>  | -4.7 <sup>u</sup>  |
|                                     | Sep. 5, 2000  | 3.0                | 1.1  | -1.2 | 0.08  | 0.08 | 7.6  | -4.7 <sup>u</sup>  |
|                                     | Sep. 12, 2000 | 3.4                | 1.1  | -1.0 | 0.15  | 0.15 | 10.1   | -8.7               |
|                                     | Dec. 5, 2000  | 2.3                | 0.6  | -0.8 | 0.16  | 0.15 | 1.7 <sup>u</sup>   | -4.6 <sup>u</sup>  |
|                                     | Dec. 12, 2000 | 3.8                | 1.2  | N/A  | 0.21  | N/A  | N/A  | N/A                |
| T2 [2040m]<br>Süderpiep tidal inlet | Mar. 21, 2000 | 4.1                | 1.5  | -1.2 | 0.52  | 0.50 | 86.5   | -79.3              |
|                                     | Jun. 5, 2000  | 3.7                | N/A  | -1.3 | N/A   | 0.25 | N/A  | -41.6              |
|                                     | Sep. 5, 2000  | 3.1                | 1.3  | -1.1 | 0.34  | 0.28 | 34.2   | -27.4              |
|                                     | Sep. 12, 2000 | 3.3                | 1.3  | -1.1 | 0.39  | 0.31 | 50.0   | -40.3              |
|                                     | Dec. 5, 2000  | 2.3                | 0.8  | -0.9 | 0.22  | 0.27 | 29.7   | -30.0              |
| T3 [1200m]<br>Piep tidal channel    | Mar. 14, 2000 | 3.6                | 1.1  | -1.2 | 0.39  | 0.38 | 29.9 <sup>u</sup>  | -14.8 <sup>u</sup> |
|                                     | Mar. 23, 2000 | 4.2                | 1.1  | -1.4 | 0.39  | 0.33 | 30.0   | -29.6              |
|                                     | Jun. 6, 2000  | 3.9                | 1.1  | N/A  | 0.34  | N/A  | 25.2   | N/A                |
|                                     | Jun. 14, 2000 | 3.6                | 1.1  | -1.2 | 0.27  | 0.29 | 18.8   | -22.9              |
|                                     | Sep. 6, 2000  | 2.9                | 0.9  | -0.9 | 0.24  | 0.28 | 15.5 <sup>u</sup>  | -17.7              |
|                                     | Sep. 13, 2000 | 3.5                | 1.3  | N/A  | 0.28  | N/A  | 17.7   | N/A                |
|                                     | Dec. 6, 2000  | 2.5                | 0.8  | -0.9 | 0.19  | 0.18 | 13.9   | -15.0              |
|                                     | Jun. 22, 2001 | 3.9                | 1.2  | N/A  | 0.23  | N/A  | 23.7   | N/A                |
|                                     | Jun. 28, 2001 | 3.6                | 1.1  | -1.1 | 0.21  | 0.26 | 16.7   | -13.1              |
| Sep. 11, 2001                       | 3.1           | 1.0                | -1.1   | 0.25 | 0.27  | 21.2 | -20.8  |                    |

Notes:

u = underestimated value due to incomplete coverage of tidal phase

N/A = measurements not available

The investigation considers only the measurement results from the main channels (Norderpiep, Süderpiep and Piep). Typical examples presented here are based on

a data set obtained during spring tide on 21, 22 and 23 March 2000. The measured tidal ranges at the Buesum port was approximately 4m. Most of the part of this section is based on the work carried out by Poerbandono et al. [2003]. Based upon the investigation to the measurement results, the significant features of the dynamics of suspended sediment concentration and transport are described. The spatial variability is represented by the variation of concentration and transport in the main channels. The temporal variability of the dynamics includes the variation of concentration and transport dynamics during different tidal period (spring and neap tides) and phases (low water, flood phase, high water and ebb phase).

### 4.3.1 Suspended sediment concentrations

The maximum depth-integrated suspended sediment concentrations along cross sections T1 (Norderpiep), T2 (Suederpiep) and T3 (Piep) resulted  $0.27\text{kg}/\text{m}^3$ ,  $0.52\text{kg}/\text{m}^3$  and  $0.39\text{kg}/\text{m}^3$  respectively. Higher values were found at the main tidal inlet (cross section T2). The smallest ranges of concentration is observed in cross section T1. A dependency of the maximum suspended sediment concentrations and suspended load transports due to the tidal range was identified quite clearly in cross sections T2 and T3 and to a certain extent in cross section T1 (Figure 4.7).

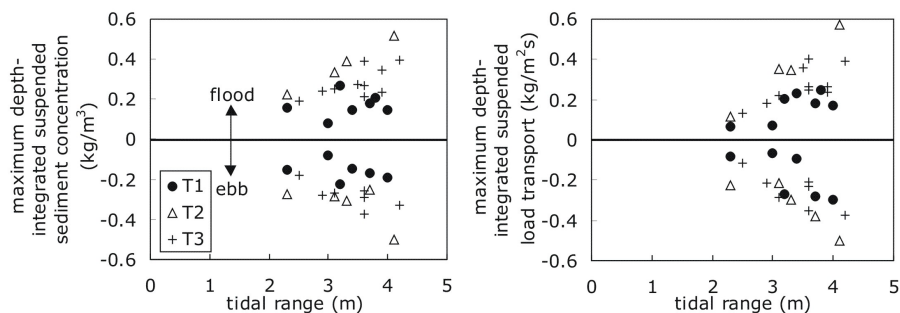


**Figure 4.7: Variation of maximum depth-integrated suspended sediment concentration and suspended load transport with tidal range**

The results indicate that the suspended sediment concentrations and transports become increasingly important with increasing strength of the tide. Much higher values are transported during spring tides. Besides, with a few exceptions there is fairly a good balance between the maximum suspended sediment concentrations observed during ebb and flood phases.

The minimum depth-integrated suspended sediment concentration values along cross sections T1, T2 and T3 varied from 0.04 to 0.12, 0.05 to 0.16 and 0.06 to 0.17 $\text{kg}/\text{m}^3$  respectively. Minimum values were measured during slack water at high and low water levels. During the measurements the slack water lasted over a period of 60 to 90 minutes. No distinct pattern of the magnitude of the minimum concentration values with respect to moon or tidal phases, high or low water could be identified.

Due to the small sizes of the sediment grains moving as suspension, in general fairly uniform vertical distributions of suspended sediment concentration were found. In Figure 4.8, the vertical distribution of velocity, concentration and suspended load transport during slack water (high and low water) and at maximum velocity (ebb and flood) are shown.

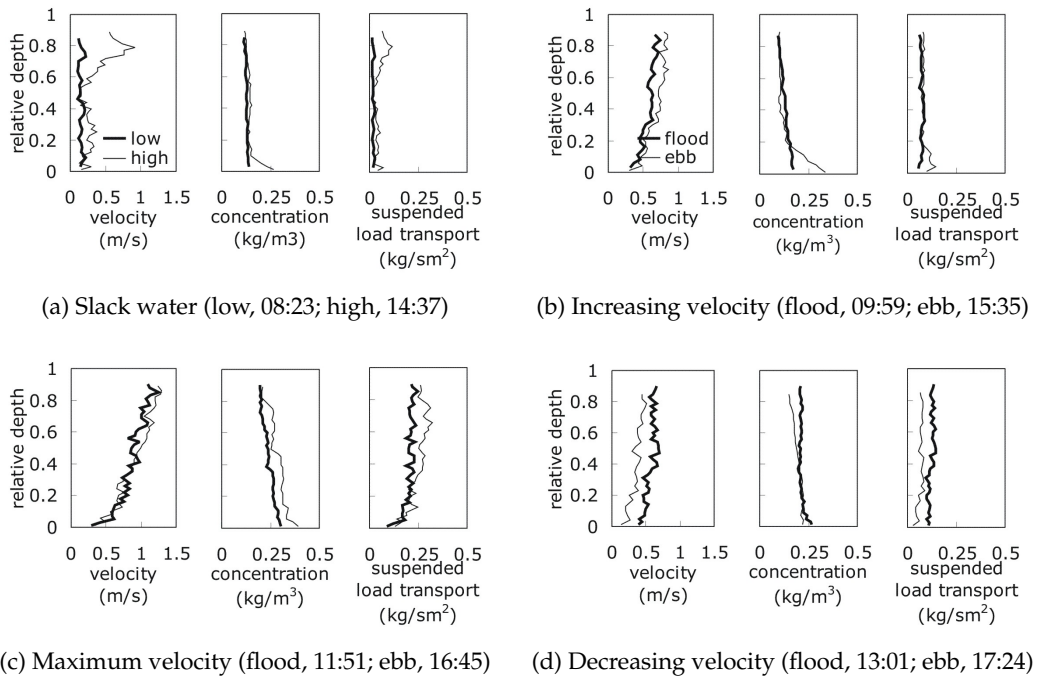


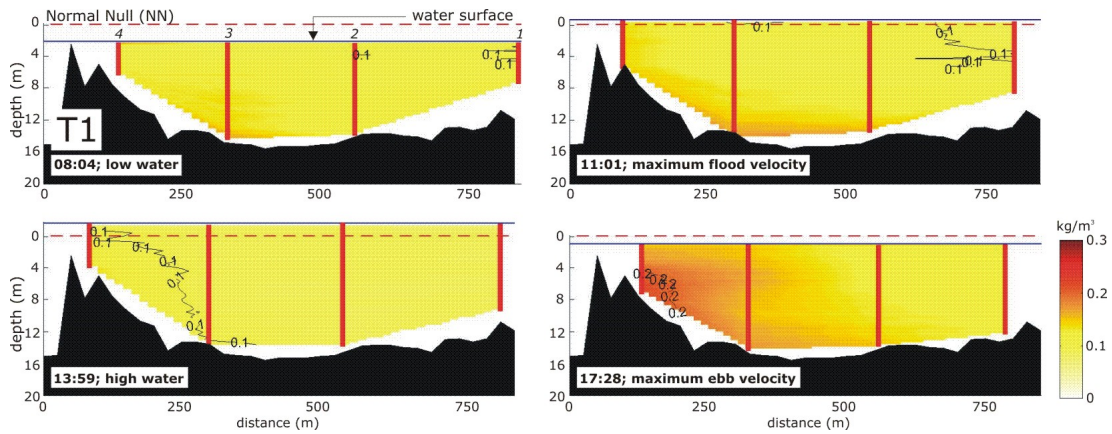
**Figure 4.8: Vertical distributions of velocity, suspended sediment concentration and suspended load transport at station 4 of cross-section T3 on March 23, 2000**

The corresponding typical examples are resulted from an investigation of the measurements on March 23, 2000 at station 4 of cross section T3. The suspension number  $Z$  (defined as  $w_s/\kappa u_*$ ) for the vertical suspended sediment concentration distributions estimated from the measurements in question ranged from  $1/6$  to  $1/36$  assuming parabolic eddy diffusivity and reference level at 1% of water depth [Rouse, 1937]. It is interesting to notice also the increase in the suspended sediment concentration near the bottom during the accelerating phase (Figure 4.8(b)).

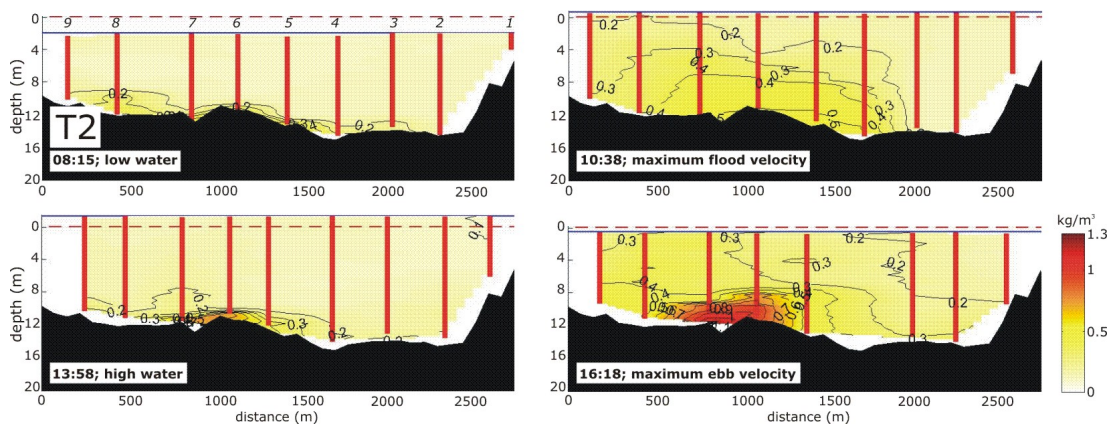
Figure 4.9 shows the cross-sectional variation of the suspended sediment concentrations for the measurements carried out at cross-sections T1, T2 and T3 on March 21 to 23, 2000. The values interpolated from the measured verticals are indicated on the same figure. Only the results obtained during slack water at high and low water levels and at maximum ebb and flood currents are shown. The variations of suspended sediment concentration over the width of the cross-sections show fairly uniform distributions during slack water. At maximum flood and ebb currents higher suspended sediment concentration values resulted.

Figures 4.10 to 4.12 show the variations of depth-integrated current velocities, sus-

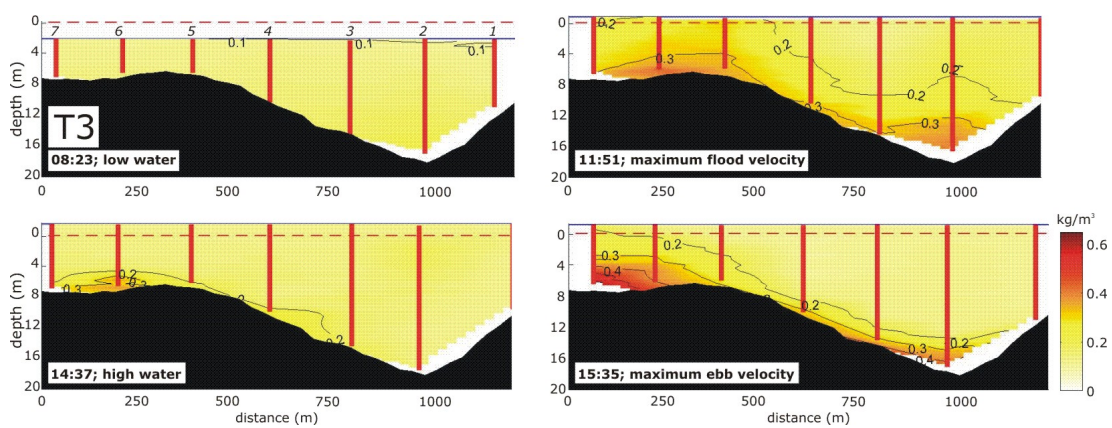




(a) Cross-sectional distribution of suspended sediment concentration at cross sections T1 on March 22, 2000 during low water, maximum flood velocity, high water and maximum ebb velocity



(b) Cross-sectional distribution of suspended sediment concentration at cross sections T2 on March 21, 2000 during low water, maximum flood velocity, high water and maximum ebb velocity



(c) Cross-sectional distribution of suspended sediment concentration at cross sections T3 on March 23, 2000 during low water, maximum flood velocity, high water and maximum ebb velocity

**Figure 4.9: Cross-sectional distribution of suspended sediment concentration**

pendent sediment concentrations and suspended load transports over a tidal cycle. The cross-sections considered are T1, T2 and T3 for the measurements carried out on March 21 to 23, 2000.

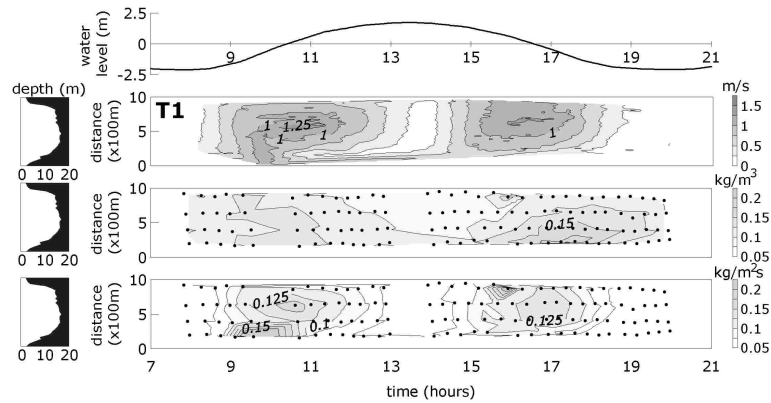


Figure 4.10: Depth-integrated velocity, suspended sediment concentration and suspended load transport variation over tidal cycle in Norderpiep

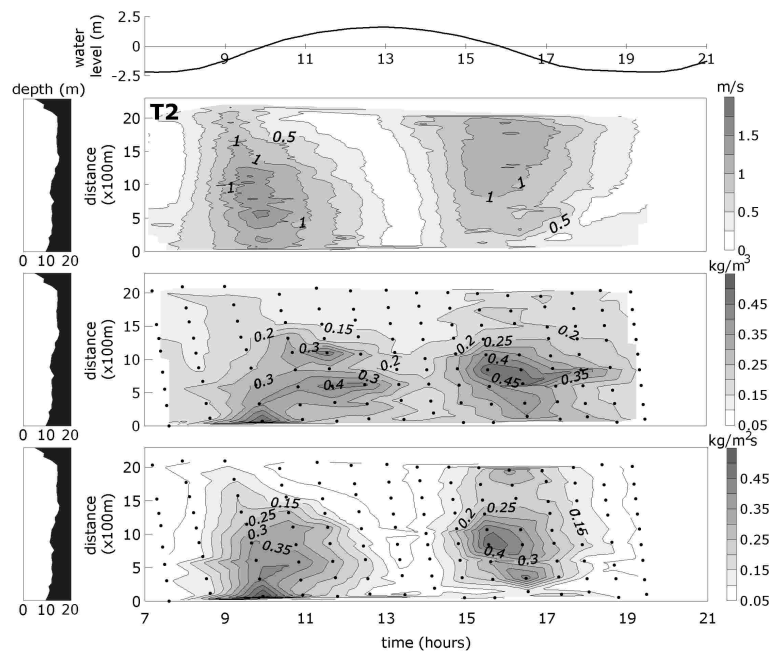


Figure 4.11: Depth-integrated velocity, suspended sediment concentration and suspended load transport variation over tidal cycle in Suederpiep

The values shown in Figures 4.10 to 4.12 were integrated from the measured verticals and from cross-sectional measurements at different times. The results show that during a tidal cycle the suspended sediment concentrations and suspended load transports increase from a minimum value during slack water (high and low water level) to maximum values which usually occur just after the maximum flood and ebb current velocity. During slack water minimum current velocities, suspended sediment con-

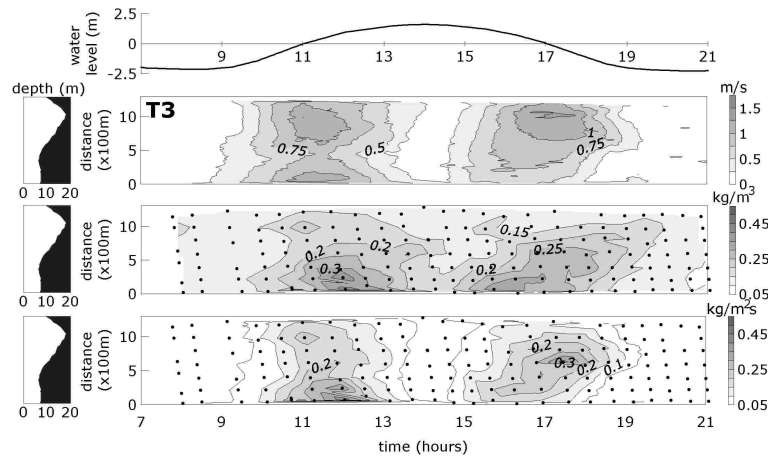


Figure 4.12: Depth-integrated velocity, suspended sediment concentration and suspended load transport variation over tidal cycle in Piep

centrations and suspended load transports values with fairly uniform variations over the width resulted. During maximum flood and ebb currents non-uniform variations of these quantities over the width can be seen.

### 4.3.2 Suspended load transports

The variations in suspended sediment load transport in cross-section as well as the tide-integrated suspended load transport during the ebb and flood phases were estimated. A dependency of the maximum suspended load transport in cross section and tide-integrated suspended load transport on the tidal range was identified (Figure 4.13).

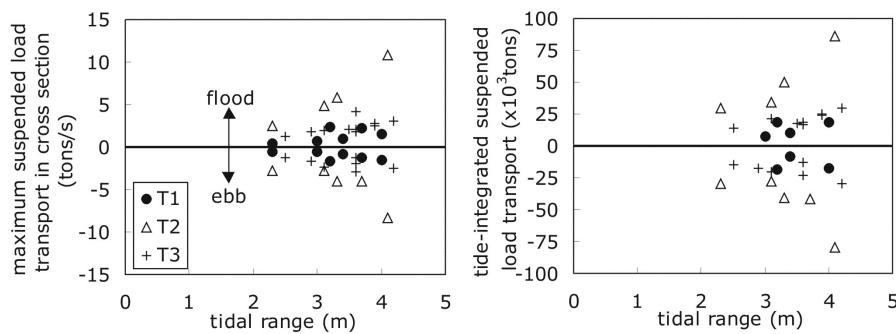
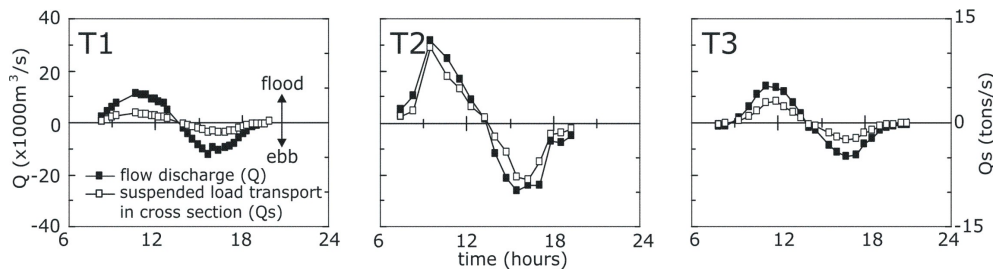


Figure 4.13: Variation of the maximum suspended load transport in cross section (left) and tide-integrated suspended load transport (right) with tidal range

Bearing in mind the accuracy in the measurements and the involved interpolations in space and time fairly similar values resulted for the ebb and flood phases. From the amount of tide-integrated suspended load transport entering and leaving the system through the two inlets (cross sections T1 and T2) it was found that approximately

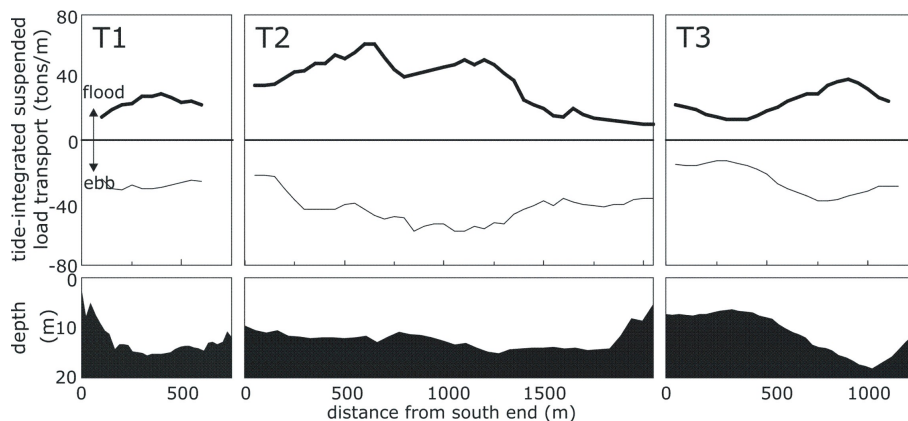
80% is conveyed through the cross-section T2. There is an increase in the amount of suspended sediment transported with the strength of the tide. The tendency of increasing amount of suspended sediment transported with the strength of the tide was found mainly in cross section T2 and to some extent in cross section T3. The ranges of approximate ebb to flood ratios of tide-integrated suspended load transport at cross sections T1, T2 and T3 resulted 0.86 to 0.98, 0.8 to 1.01 and 0.79 to 1.22 respectively.

Figure 4.14 shows the variations of the flow discharge and suspended load transport in cross section along T1, T2 and T3 (March 21 to 23, 2000) with time. It can be seen that the maximum discharges and suspended load transport in cross section along T2 resulted much higher than along the other two cross-sections (T1 and T3). Compared to the values found in cross section T1, the maximum sediment suspended load transport in cross section at T3 and T2 can be up to a factor 2 and 6 respectively.



**Figure 4.14: Variation of flow discharges and suspended load transport in cross section along T1, T2 and T3 on March 21 to 23, 2000**

Figure 4.15 displays the variation of the estimated distributions of tide-integrated suspended load transport (flood and ebb phases) over the width. There is a balance between the amount of tide-integrated suspended load transport during the ebb and flood phases.



**Figure 4.15: Variation of the tide-integrated suspended load transport along cross sections T1, T2 and T3 on March 21 to 23, 2000**



## 4.4 Discussion

What are the main characters of sediment transport dynamics in the study area?

It is found that the composition of the sediments is mainly very fine to fine sands with varying fractions of silt and clay and in some cases tend to be cohesive. In the location where the mud content in the bed sediment is predominant, the cohesive properties of sediment increase its resistance to be eroded. Bed sediment with larger mud content is found mainly in the deeper part of the main channels. In those particular location the consolidated mud layer is outcropped and resulting in a less mobile bed sediment.

The typical median value of the bed sediment grain ( $d_{50}$ ) is of about  $100\mu\text{m}$  and the  $d_{90}$  is approximately 1.2 to 2 times the  $d_{50}$ . The sizes of the particles in suspension were found to be much smaller than the ones taken from the bed samples having a range of 6 to  $86\mu\text{m}$ . The corresponding ranges of the settling velocities are approximately between 0.02 to  $6\text{mm/s}$ .

Due to the small sizes of the particles transported in suspension and high turbulence levels a background concentration level is always present with a value of about  $0.1\text{kg/m}^3$ . The magnitude of the background concentrations observed in cross sections T1, T2 and T3 are independent to the tidal conditions and locations. The vertical distribution of the suspended sediment concentrations and suspended load transport is fairly uniform. As a result most of the sediment is transported in suspension.

With respect to the amount of suspended sediment concentration and suspended load transport, a clear dependency on the tidal range was identified. Higher suspended sediment concentrations and suspended load transport pertain to higher tidal range. This pattern is also observed regarding the maximum suspended load transport in cross section and tide-integrated suspended load transport. It was found that Suederpiep channel is responsible for most of the suspended sediment entering and leaving the area. In the Norderpiep channel, less sediment materials are transported.

Within the limits of accuracy of measurements in calm weather conditions no clear pattern in terms of ebb and flood domination of the channels could be identified. However, the amount of sediment balance can be estimated. In this case, a careful attention should be paid due to the uncertainty in the data acquisition and estimation procedures.



## Chapter 5

# Prediction of Sediment Transport Dynamics

### 5.1 Introduction

In this chapter the prediction of sediment transport dynamics is carried out using empirical sand transport formulae proposed by Bijker [1971] and van Rijn [1984a,b]. The concept, derivation and condition at which these formulae were developed have been previously discussed in section 2.3.1. The transported sediment is assumed to be the total transport as an algebraic summation of bed and suspended load transports (see: Equation 2.25). In the prediction of the rate of sediment transport for the condition in question, two different approaches are applied:

1. Based on the measured velocity: the bed shear stress is estimated using logarithmic current velocity distribution theory based on the instantaneously measured local velocity.
2. Based on the model simulation: the bed shear stress is predicted based on the numerical simulation of two-dimensional velocity field.

In the first approach, empirical equations for sand transport prediction are used. The depth-integrated sediment concentration ( $\bar{c}$ ) is calculated based on the predicted total load transports ( $q_{tot}$ ) and the locally measured depth-integrated velocity magnitude ( $\bar{u}$ ) (see: Equation 2.26). In the latter one, equilibrium sand transport and advection-diffusion equations are used. In case of using equilibrium sand transport equations, Equation 2.26 is also used to calculate the depth-integrated sediment concentration from the predicted total load transport. In case of using advection-diffusion equation, the depth-integrated concentration is available and provided by the modelling tools.

### Performance evaluation

For evaluating the prediction performance, comparisons between predicted and measured concentrations as well as sediment transports are analysed. To qualify the performance of the prediction, the agreement between computed and measured values is quantified using RMAE and scores of discrepancy factor (see: section 2.3.3).

Additionally, the absolute and relative discrepancies (errors) of the predicted values with respect to those measured in the field is also calculated to dimensionalise the agreement. The time averaged absolute discrepancy given in the unit of the parameter being evaluated is quantified using:

$$\Delta_x = \frac{1}{t_1 - t_0} \int_{t_0}^{t_1} \sqrt{[x(t) - x'(t)]^2} dt \quad (5.1)$$

in which  $\Delta_x$  = absolute discrepancy of a calculated value  $x$  with respect to the measured value  $x'$  and  $t$  = time. The relative discrepancy given in % is calculated using Equation 3.19 for determining the relative error (RE) and rewritten to give the time averaged value as:

$$\overline{\text{RE}} = \frac{1}{t_1 - t_0} \int_{t_0}^{t_1} \frac{\Delta_x(t)}{x'(t)} dt \quad (5.2)$$

For the use of RMAE method, the concentration measurement is assumed to have an accuracy of 30% (see: section 3.4.2). Since no precise information of the accuracy estimation of sediment transport measurement was found for the conditions in question, the evaluation of sediment transport prediction is done using absolute and relative error analysis as well as the score of discrepancy factor.

The agreement between the calculated and measured values over temporal and spatial series is discussed. The temporal agreement is represented by the discrepancy variations over the measured period (a tidal cycle) focusing on the conditions during slack water and peak velocity periods. The spatial agreement is represented by the discrepancy variations over all measuring stations and along the three different cross sections (T1, T2 and T3).

### Data sets

Field measurement data obtained from the year 2000 are used here and classified into 5 sets. Each data set represents conditions with a particular tidal range. Data sets 1 is used for testing the sensitivity of the formulae due to several input parameters. The best input parameter setting that fit the measurements will be determined based on fitting the calculated values to the measured ones employing data set 1, 4 and 5 representing condition with maximum, mean and minimum tidal ranges. The validation is done using data sets 2 and 3. Further details about the data considered in this study are given in Table 5.1.

Table 5.1: Measurement data sets

| Data set | Measuring campaign | Date | Tidal range (m) | Cross section | Measuring stations | Duration (hours) | Remarks                              |
|----------|--------------------|------|-----------------|---------------|--------------------|------------------|--------------------------------------|
| 1        | March, 2000        | 22   | 4.0             | T1            | 4                  | 12:00            | Sensitivity analysis and calibration |
|          |                    | 21   | 4.1             | T2            | 9                  | 11:55            |                                      |
|          |                    | 23   | 4.2             | T3            | 7                  | 13:04            |                                      |
| 2        | June, 2000         | 5    | 3.7             | T1            | 4                  | 06:36            | Calibration                          |
|          |                    | 5    | 3.7             | T2            | 12                 | 08:26            |                                      |
|          |                    | 6    | 3.9             | T3            | 7                  | 08:12            |                                      |
| 3        | September, 2000    | 5    | 3.1             | T1            | 4                  | 10:28            | Validation                           |
|          |                    | 5    | 3.1             | T2            | 12                 | 09:54            |                                      |
|          |                    | 6    | 2.9             | T3            | 7                  | 10:47            |                                      |
| 4        | September, 2000    | 12   | 3.3             | T1            | 4                  | 11:38            | Validation                           |
|          |                    | 12   | 3.3             | T2            | 10                 | 10:59            |                                      |
|          |                    | 13   | 3.5             | T3            | 7                  | 04:34            |                                      |
| 5        | December, 2000     | 5    | 2.3             | T1            | 4                  | 05:33            | Sensitivity analysis and calibration |
|          |                    | 5    | 2.3             | T2            | 10                 | 10:50            |                                      |
|          |                    | 6    | 2.5             | T3            | 6                  | 12:06            |                                      |

A data set contains time-series measured parameters (i.e. current velocities and sediment concentrations) that are obtained from cross sectional measurements along T1, T2 and T3. A cross sectional measurement may content 4 to 12 measuring stations (profiles). At least 20 observation points were obtained within each measuring campaign. In each measuring station, measurement of current velocity and suspended sediment concentration profiles over an entire tidal cycle at about 20 to 40 minutes intervals was carried out from a moving vessels. For the data sets in question, over 1400 time-series field measurement data have been made available.

### Sediment grain size and settling velocity

The discussion of the sizes of bed sediment in the main channel has been presented in section 4.2.1. It has been found that most of bed sediment samples have median diameters of ranging between 80 and 230 $\mu\text{m}$  (see: Table 4.1). As most of them are very close to 100 $\mu\text{m}$ , for the modelling purpose the representative size of bed sediment is therefore assumed to be uniform having  $d_{50}$  of 100 $\mu\text{m}$ . Figure 5.1(a) shows a plot of chosen representative bed sediments ( $d_{50}$  and  $d_{90}$ ) in a range of 15 actual distribution curves of bed sediment samples .

The sediment settling velocity is assumed to be a function of the size of sediment moving in suspension and calculated using Stoke's formulae (Equation 2.1). The discussion of the sizes of sediment moving as suspension has been presented in section 4.2.3. It has been found that the sizes of sediment moving as suspension are varying from 6 to 86 $\mu\text{m}$ . Using Stoke's formulae, the corresponding approximate settling velocities range between 0.02 and 6mm/s. In the calculation, the water and sediment densities are assumed respectively equal to 1020kg/m<sup>3</sup> and 2650kg/m<sup>3</sup>, giving an ap-

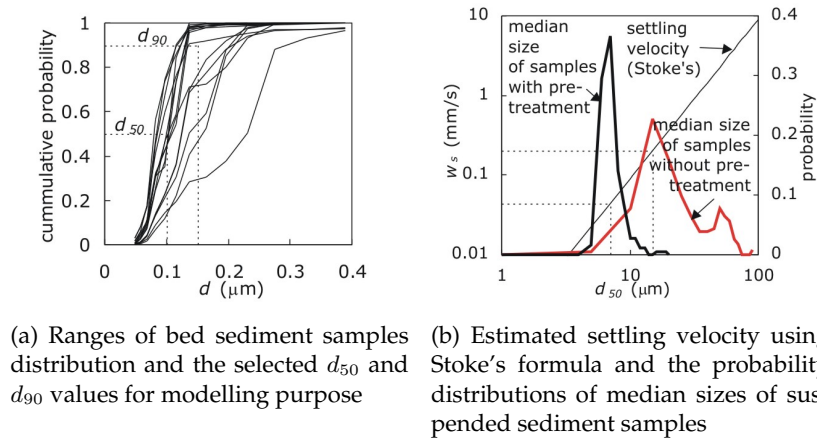


**Figure 5.1: Validity of the selected representative bed sediment sizes ( $d_{50}$  and  $d_{90}$ ) and settling velocity ( $w_s$ ) of sediment moving in suspension**

proximate relative density ( $s$ ) of 2.6. The kinematic viscosity ( $\nu$ ) and acceleration due to gravity ( $g$ ) are assumed respectively to be  $1.3 \times 10^{-6} \text{m}^2/\text{s}$  and  $9.81 \text{m}/\text{s}^2$ .

Figure 5.1(b) shows the probability distribution of the median size of suspended sediment samples and the estimated settling velocity based on the calculation using Stoke's formulae. In Figure 5.1(b) the measured median particle diameters of 233 suspended sediment samples are considered. As two kind of treatments in suspended sediment sample analysis were carried out (see: section 4.2.3), two outcomes are conceived: for sample with and without pre-treatment. The maximum probability of the median size of suspended sediment sample without pre-treatment has been found to be of approximately  $15 \mu\text{m}$  whereas for the samples with pre-treatment of approximately  $7 \mu\text{m}$ . It corresponds with an approximate settling velocity of roughly close to  $0.1 \text{mm}/\text{s}$  which is used as an initial guess for the modelling purpose.

## 5.2 Prediction based on the measured velocity

In this section, the prediction of sediment transport and concentration dynamics based on the measured velocity is discussed. The current velocity profiles measured from the field are used for estimating the bed shear stress. Based on this estimation, the sediment transports are calculated using the empirical equations proposed by Bijker [1971] and van Rijn [1984a,b].

### 5.2.1 Estimation of bed shear stress

For empirically calculating sediment transport an estimate magnitude of bed shear velocity ( $u_*$ ) and, hence, bed shear stress ( $\tau_b$ ) is required. The estimation of bed shear velocity magnitude is carried out by fitting the instantaneously measured current velocity profiles from ADCP with the theoretical logarithmic current velocity distribution (Equation 2.5) assuming the bed to be fully rough. The bed shear stress is then

calculated using Equation 2.3. Since no available measurement data of wave orbital velocities can be provided the bed shear stress is assumed to be due to the current only.

Recently, Cheng et al. [1999] applied such an approach in a coastal area with bidirectional flow (tidal current) for predicting roughness length ( $z_0$ ) and bed shear velocity ( $u_*$ ). In the corresponding work, current velocity profile measurement using an ADCP was carried out in a fix position over long period (45 days) with relatively short recording interval (every 2 minutes) and high vertical resolution (5cm). Independent measurement for verifying the measured current profile was available. A tight data selection was applied. In the selection, bad measurements and fittings (between measured and theoretical current velocity profile;  $r^2 < 0.8$ ) are rejected resulting in 33 to 100 good profiles (out of about 144) daily. Accuracy assessment of the  $z_0$  and  $u_*$  predictions are calculated using a statistical technique following Gross & Nowell [1983]. In the application of such a technique sufficient number of data is required in order to reduce error.

Quantitative assessment of the uncertainty of the application of such an approach is not available in this study. This is due to the data acquisition method employed during field measurement. Instantaneous measurement with relatively large time interval from a moving vessel does not allow the application of statistical technique for estimating the uncertainty of the application of the theoretical logarithmic current velocity distribution. All measured current velocity profiles are used to estimate the bed shear velocity and, hence, bed shear stress. An example taken from cross sectional measurement in cross section T3 (Piep channel) on March 23, 2000 shows that only 27% of data have  $r^2 \geq 0.8$  (Figure 5.2(a)). However, a tendency of increasing estimated bed shear velocity due to the increasing depth-integrated velocity magnitude as also demonstrated in the work carried out by Cheng et al. [1999] is observed (Figure 5.2(b)).

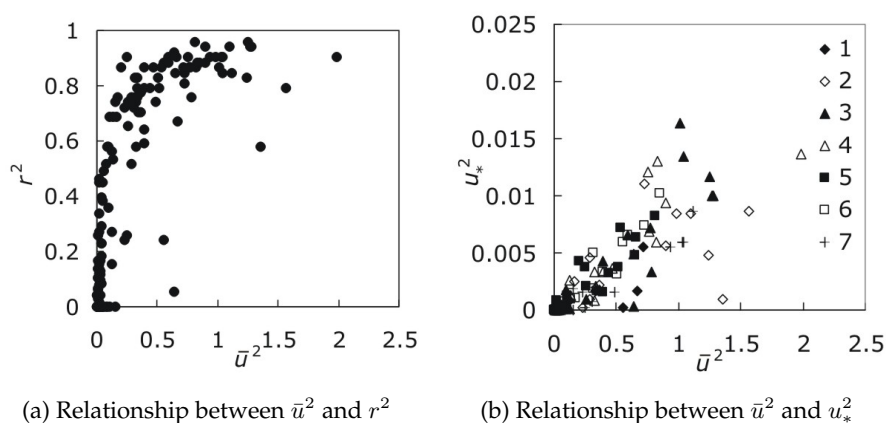


**Figure 5.2: Typical example of bed shear velocity estimation taken from measurement in cross section T3 (Piep channel) on March 23, 2000**

Figure 5.2 confirms that although the data acquisition procedure and the estimation approach is relatively less precise but the resulting bed shear velocity magnitude

does follow the cyclic pattern of current dynamic in a tidal flow environment. For a given depth-integrated velocity magnitude ( $\bar{u}$ ) the estimated bed shear velocity ( $u_*$ ) is within one order of magnitude.

The transport stage parameter ( $T$ ) to be used in van Rijn formulae is calculated using Equation 2.21. The grain-related bed shear stress ( $\tau'_b$ ) is calculated using Equation 2.22. The grain-related Chézy coefficient ( $C'$ ) is calculated using Equation 2.23. The critical bed shear stress ( $\tau_{b,cr}$ ) is calculated using Shields parameter (Equation 2.9) considering dimensionless particle diameter ( $D_*$ ) calculated using Equation 2.2 and converted to critical Shields parameter ( $\theta_{cr}$ ) using Equation 2.10. The calculation gives an approximate critical bed shear stress of  $0.18\text{N/m}^2$  for the considered  $d_{50}$  of  $100\mu\text{m}$ .

The effective bed roughness height ( $k_s$ ) is proposed by Bijker [1971] and van Rijn [1984b] to delineate the edge between bed and suspended load layer. In Bijker formulae,  $k_s$  value is required, for example, to calculate the ripple factor ( $\mu$ ) using Equation 2.28. Accordingly, the Chézy coefficient may be calculated using Equation 2.8 and the Chézy coefficient related to  $d_{90}$  can be calculated using Equation 2.29. In van Rijn formulae,  $k_s$  is required for calculating the reference concentration ( $c_a$ ) using Equation 2.54.

The  $k_s$  values can be empirically estimated, for example, based on the predicted roughness length ( $z_0$ ) from the application of logarithmic current velocity distribution theory or based on the predicted (or measured) bedform dimensions (height and length). Since no reliable prediction and independent measurements (for validating the prediction) of the corresponding magnitudes are available, such parameters are *a-priori* determined and will be used as a calibration parameter.

## 5.2.2 Sediment transport prediction

The prediction of sediment transport using empirical sand transport formulae is relatively simple and straight forward. The calculation procedures for bed load and suspended load transports using Bijker's and van Rijn's equations have been discussed in section 2.3.1. Several physical parameters should be firstly determined and given to the equations. The corresponding discussion follows.

### Sensitivity analysis

The effect of calibration factor ( $b$ ) used in Bijker formulae is investigated. The investigation is carried out to evaluate the most proper  $b$  value that gives the best agreement between measured and computed values. The result is evaluated using Relative Mean Average Error (RMAE) method and the score of discrepancy factor (percentage of data within a factor of 2). Data sets 1 and 5 representing respectively maximum and minimum tidal ranges are employed. The evaluation confirmed that the use of  $b$  value of 2 gives minimum RMAE and at the same time most of data within a factor of 2. Therefore, the  $b$  value of 2 is chosen and used for the rest of the calculation of sediment



transport and concentration based on the measured velocity.

Originally, van Rijn formulae do not have any calibration factor ( $b$ ). However, if a calibration factor is incorporated in the equation for predicting the total load transport, the corresponding agreement has been found to be improved. The use of  $b$  value of 2 is found to give the most optimum agreement between the calculated and the measured values and for the prediction purpose will be used to do the rest of the calculation of sediment transport and concentration based on the measured velocity. In the corresponding calculation, data sets 1 and 5 representing respectively maximum and minimum tidal ranges are employed. The agreement is evaluated using Relative Mean Average Error (RMAE) method and the score of discrepancy factor (percentage of data within a factor of 2).

Sensitivity tests of transport calculation due to bed sediment size ( $d_{50}$ ), suspended sediment settling velocity ( $w_s$ ) and equivalent bed roughness height ( $k_s$ ) using Bijker and van Rijn formulae are carried out. The results are shown in Figures 5.3 and 5.4.

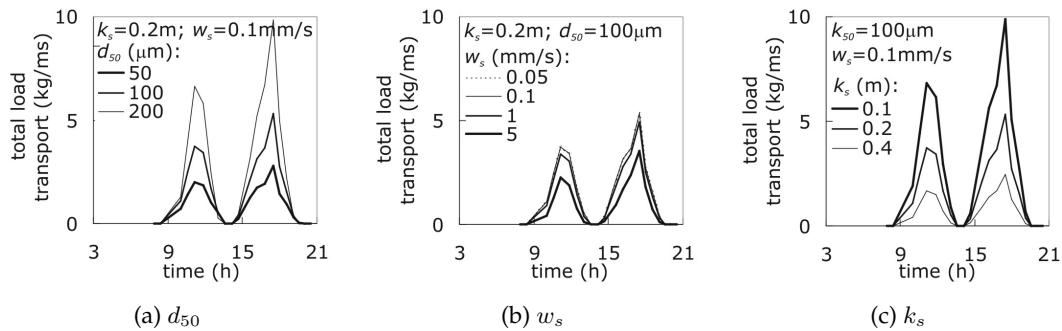


Figure 5.3: Sensitivity of total load transport prediction using Bijker's empirical formulae

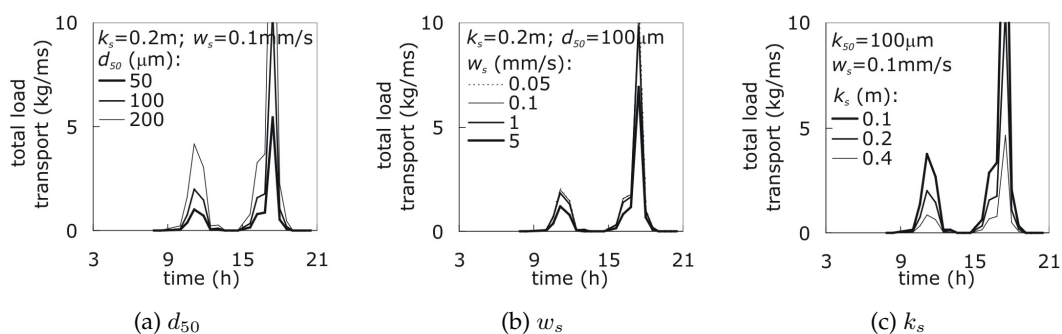


Figure 5.4: Sensitivity of total load transport prediction using van Rijn's empirical formulae

From Figures 5.3(a) and 5.4(a), it can be seen that the use of different values of median size of bed sediment ( $d_{50}$ ) gives a significant effect to the computed transport. Using Bijker formulae, increasing  $d_{50}$  within a factor of 2 (from 100 to 200  $\mu\text{m}$ ) gives an increase in the calculated transport up to a factor of 1.8. The effect of increasing  $d_{50}$  is more pronounced in the calculated transport using van Rijn formulae. Increasing  $d_{50}$

within a factor of 2 gives an increase of calculated transport up to a factor of 2.

From Figures 5.3(b) and 5.4(b), it can be seen that the sediment settling velocity ( $w_s$ ) is found to play an important role for a value of 1mm/s or higher. Using Bijker formulae, an increasing  $w_s$  value within a factor of 5 (from 1 to 5mm/s) gives a reduction in the predicted total load transport up to about 1kg/ms. Similar tendency with less reduction is also observed in the calculation of transport using van Rijn formulae. The effect of  $w_s$  value to the calculated transport is also more pronounced within  $w_s$  value of approximately higher than 1mm/s. Less significant effect can be found on the use of  $w_s$  value of equal or less than approximately 0.1mm/s.

From Figures 5.3(c) and 5.4(c), it can be seen that the effective bed roughness height ( $k_s$ ) is found to play an important role in the computed transport. Using Bijker formulae, an increasing  $k_s$  value within a factor of 4 (from 0.1 to 0.4m) gives a reduction in the calculated total load transport up to a factor of 4. Bijker formulae are found to be more sensitive to the changes of  $k_s$  value. Similar tendency with less reduction is also observed in the calculation of total load transport using van Rijn formulae.

### Calibration

To determine the best setting for appropriately predicting the total load transport, several tests were carried out to adjust the input parameters that gives the best agreement between measured and computed values. The bed sediment sizes is initially assumed to be uniform having  $d_{50}$  of 100 $\mu\text{m}$  and  $d_{90}$  of 150 $\mu\text{m}$ . In the tests, data sets 1, 4 and 5 were employed. To verify the validity of the chosen grain size, various  $d_{50}$  values (of 80, 100, 120, 160 and 200 $\mu\text{m}$ ) are tested and the results confirm that the use of  $d_{50}$  value of 100 $\mu\text{m}$  gives the best agreement with the measurement either for Bijker or van Rijn formulae.

In the next step, calibration due to  $k_s$  value is carried out. In the test,  $k_s$  values ranging from 0.2 to 0.45m with 0.05m increment are used. The results suggest the use of  $k_s$  values of 0.4 and 0.35m respectively for Bijker or van Rijn formulae in order to obtain the best agreement with the measurement. In the final step the use of  $w_s$  values of 0.02, 0.1, 0.4, 1 and 5mm/s are tested. The results recommend the use of  $w_s$  value of 0.1mm/s or smaller for obtaining the best agreement using either Bijker or van Rijn formulae. The optimum settings for the empirical total load transport calculation based on data sets 1, 4 and 5 are summarised in Table 5.2.

**Table 5.2: Input parameter settings for total load transport prediction using empirical formulae**

|          | $b$ | $d_{50}$<br>( $\mu\text{m}$ ) | $d_{90}$<br>( $\mu\text{m}$ ) | $k_s$<br>(m) | $w_s$<br>(mm/s) |
|----------|-----|-------------------------------|-------------------------------|--------------|-----------------|
| Bijker   | 2   | 100                           | 150                           | 0.40         | 0.1             |
| van Rijn | 2   | 100                           | 150                           | 0.35         | 0.1             |

### Validation

In the sensitivity tests and calibration, the empirical formulae were found to be able to give prediction results within the order of measured values. To verify the findings, the settings obtained in the previous section (see: Table 5.2) are used here to calculate the total load transport. The results are validated against data sets 2 and 3. Typical examples of the comparison between measured and calculated total load transports are shown in Figure 5.5. An observation point in each cross section is chosen to illustrate measured and predicted total load transport using Bijker and van Rijn formulae. Table 5.3 summarises the corresponding performance.

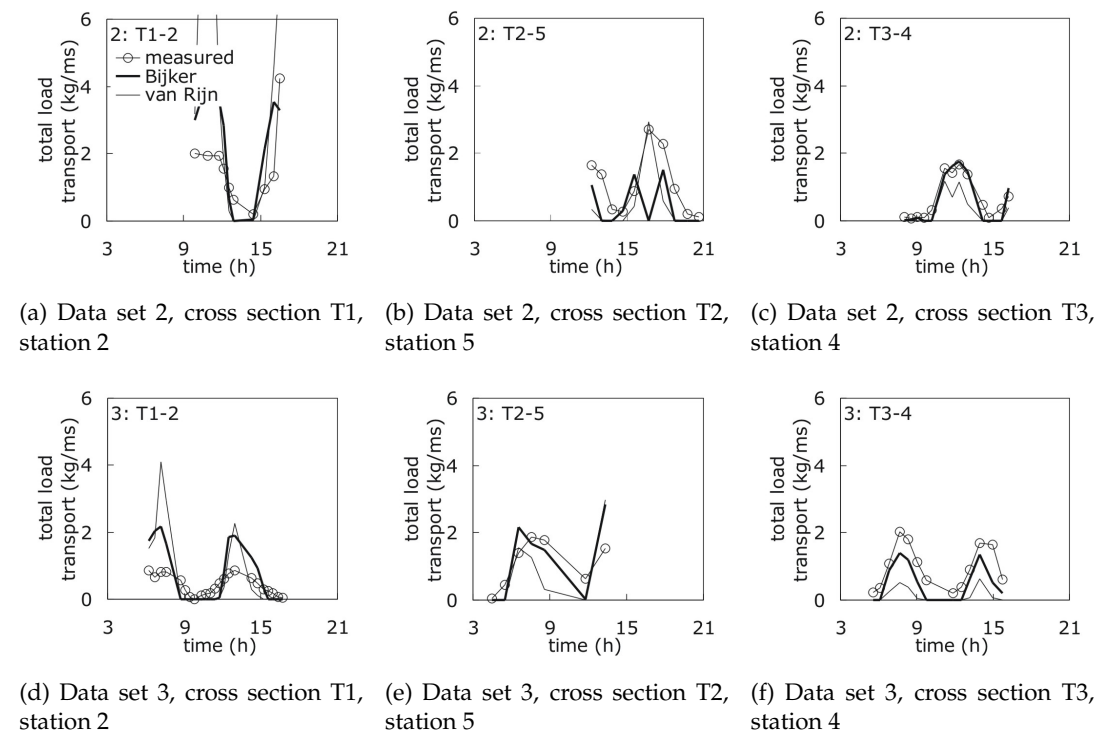


**Figure 5.5: Comparison between measured and predicted total load transport using empirical formulae**

**Table 5.3: Performance of total load transport prediction using empirical formulae**

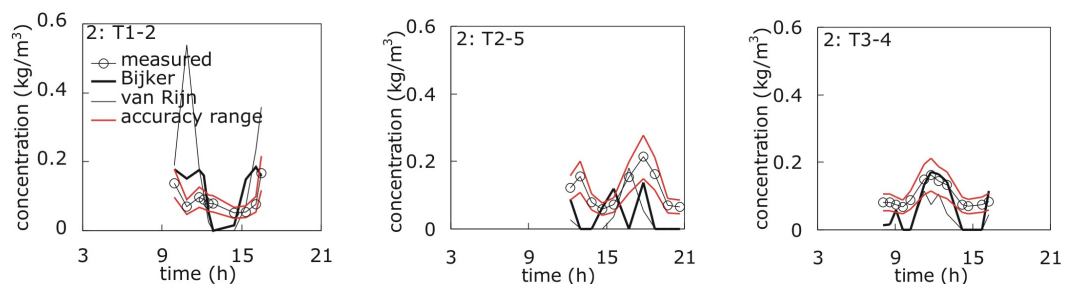
|          | Absolute error | Relative error | Data within a factor of 2 |
|----------|----------------|----------------|---------------------------|
| Bijker   | 0.44kg/ms      | 59%            | 38%                       |
| van Rijn | 0.59kg/ms      | 75%            | 18%                       |

The validation confirms a comparable performance of the prediction of total load transport using Bijker and van Rijn formulae. However, a slightly better prediction is achieved by the calculation using Bijker formulae. In this case, Bijker formulae give 38% of data within a factor of 2, whereas van Rijn formulae only 18%. The absolute

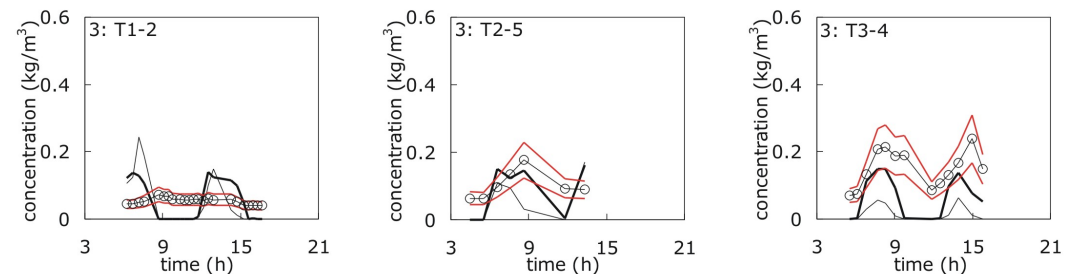
error is within 0.5kg/ms. The overall accuracy is within a relative error value of 60 to 75%. In case of using Bijker formulae, the predicted total load transports in cross section T1, may deviate up to a factor of 3. Better prediction results are observed in cross section T2. However, a deviation of up to a factor of 2 can still be observed. In cross section T3, the predicted transports agree quite well with the measurement with a deviation of less than a factor of 2. Using van Rijn formulae, major disagreements can be observed in cross section T1, the southern part of cross section T2. The corresponding deviation can be up to a factor 3. In cross section T3 the predicted total load transports are generally underestimated.

### Prediction of depth-integrated concentration

The depth-integrated concentration is calculated based on the predicted total load transport, the depth-integrated velocity magnitude from locally measured current velocity profiles and the measured local water depth. The performance of the calculation is verified against data sets 2 and 3. Typical examples of the comparison between measured and calculated depth-integrated concentrations are shown in Figure 5.6. An observation point in each cross section is chosen to illustrate measured and predicted values using Bijker and van Rijn formulae. Performance evaluation of depth-integrated concentration prediction is given in Table 5.4.



(a) Data set 2, cross section T1, station 2      (b) Data set 2, cross section T2, station 5      (c) Data set 2, cross section T3, station 4



(d) Data set 3, cross section T1, station 2      (e) Data set 3, cross section T2, station 5      (f) Data set 3, cross section T3, station 4

**Figure 5.6: Comparison between measured and predicted depth-integrated concentration using empirical formulae**

In Figure 5.6 it can be seen that both formulae are able to give prediction of depth-

**Table 5.4: Performance of depth-integrated concentration prediction using empirical formulae**

|          | RMAE | Absolute error        | Relative error | Data within a factor of 2 |
|----------|------|-----------------------|----------------|---------------------------|
| Bijker   | 0.42 | 0.08kg/m <sup>3</sup> | 68%            | 38%                       |
| van Rijn | 0.55 | 0.09kg/m <sup>3</sup> | 82%            | 17%                       |

integrated concentrations within the order of magnitudes of those measured from the field. However, the results tend to be most of the time underestimated. Proper prediction results during slack water conditions can not be well performed. Around slack water the estimated bed shear stress is lower than the critical value resulting in zero concentration prediction. In reality, during slack water the turning of velocity direction produces residual currents that keeps the fine sediment particles to remain in suspension. Using Bijker formulae, the predicted concentrations in cross section T1 tend to be overestimated mainly during peak velocity. In cross sections T2 and T3 better agreement can only be observed during peak velocity. No distinct pattern of either underestimation or overestimation of predicted concentration with respect to the measuring station can be drawn. Similar tendency as has been observed in the application of Bijker formulae is also observed in the use of van Rijn formulae. In cross section T1 the predicted concentration tends to be overestimated mainly during peak velocity. In cross sections T2 and T3 the results are generally underestimated.

### 5.3 Prediction based on model simulations

In this section, the prediction of sediment transport and concentration dynamics based on the simulated velocity is discussed. The numerical simulation of flow field is carried out using a two-dimensional horizontal area (2DH) type model. The modelling environment used is DELFT3D-MOR. The descriptions of the DELFT3D-MOR model can be found in Roelvink & van Banning [1994].

#### Modelling environment

The DELFT3D-MOR is designated to simulate the integration of the effects of waves, currents and sediment transports on morphological development in rivers, estuaries and coasts on time scale of days to years [Roelvink & van Banning, 1994]. In the modelling system each of these process is separated into individual component or module being WAVES, FLOW, TRANSPORT and BOTTOM. For modelling the complete process of morphological development the MAIN module controls the coupling process between modules. A single module can also be operated individually. The simulation of physical processes is done on a finite-difference curvilinear grid.

### Meldorf Bight Model

A computational grid covering the Meldorf Bight comprising about 36,000 elements with grid spacing ranging from 80 to 250m was made available for this study [Palacio et al., 2001; Mayerle & Palacio, 2002]. Bathymetric data from recent echo soundings was interpolated on the grid using linear triangulation [Winter & Mayerle, 2003]. Boundary conditions being time-series water levels were derived from larger model domain covering the German Bight and continental shelf area (North Sea) using nesting procedures [Zielke et al., 2000]. In the larger domains, astronomical tidal constituents and meteorological influence are used to produce the water level at the boundary of smaller model domains. Figure 5.7 illustrates the nesting procedures.

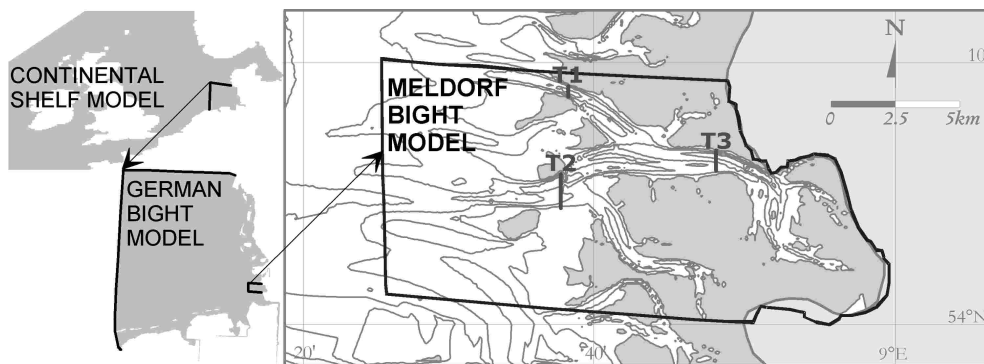
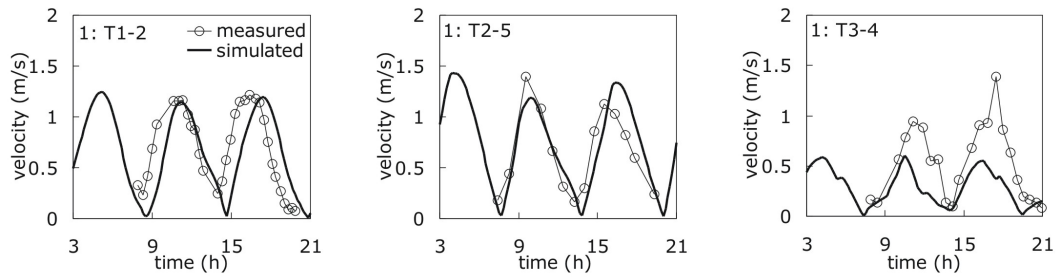


Figure 5.7: Nesting scheme of the Meldorf Bight Model

#### 5.3.1 Flow simulation

The initial set-up, calibration and validation of the flow model used in this study are fully discussed in Palacio [2001], Palacio et al. [2001] and Mayerle & Palacio [2002]. In the corresponding studies, evaluation of hydrodynamic model performance considered in this study is discussed. It was found that with respect to those measured from the field the model gives water level discrepancy of less than 6% for water level, about 2% for tidal range and about 3% for tidal period. The velocity discrepancy was found to be about 0.2m/s. It was also found that the influence of wave field modelling at the open sea boundary in the tidal channel is negligible.

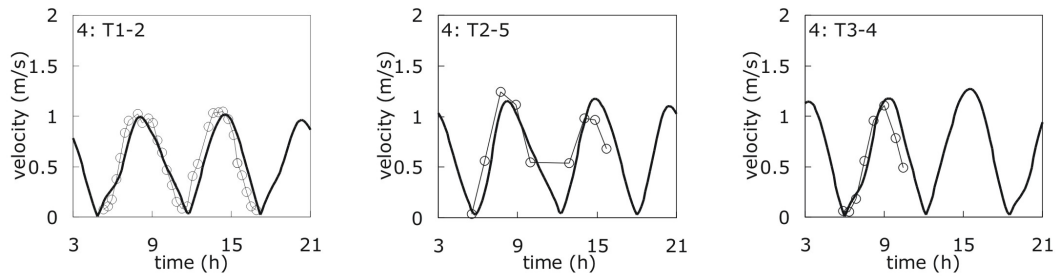
For all of the measuring period carried out in the year 2000, flow simulations have been made available. Good agreement between measured and simulated velocity have been found in most of all observation points. Better agreement resulted at cross sections T2 and T3. Larger disagreement in cross section T1 is caused by the underestimation in the northern bank and overestimation in the southern bank. Examples of the comparison between measured and simulated depth-integrated velocity magnitudes taken from data sets 1, 4 and 5 representing typical tidal ranges (maximum, average and minimum) are given in Figure 5.8.



(a) Data set 1, cross section T1, station 2, tidal range 4m

(b) Data set 1, cross section T2, station 5, tidal range 4.1m

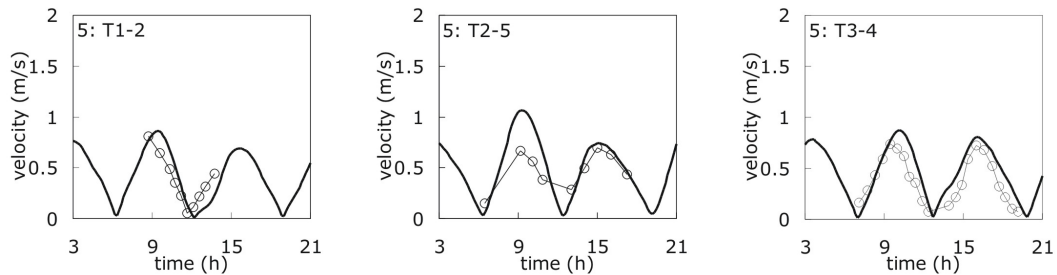
(c) Data set 1, cross section T3, station 4, tidal range 4.2m



(d) Data set 4, cross section T1, station 2, tidal range 3.3m

(e) Data set 4, cross section T2, station 5, tidal range 3.3m

(f) Data set 4, cross section T3, station 4, tidal range 3.5m



(g) Data set 5, cross section T1, station 2, tidal range 2.3m

(h) Data set 5, cross section T2, station 5, tidal range 2.3m

(i) Data set 5, cross section T3, station 4, tidal range 2.5m

**Figure 5.8: Comparison between measured and simulated depth-integrated velocity magnitudes**

Detailed evaluation results of the flow simulation is summarised in Table 5.5. In terms of depth-integrated velocity magnitudes, it gives an absolute discrepancy of slightly less than 0.2m/s and thus confirmed the previous evaluation in the initial set-up, calibration and validation of the flow model carried out by Palacio [2001], Palacio et al. [2001] and Mayerle & Palacio [2002]. The absolute discrepancy of the simulated unit discharge is of 3.1m<sup>2</sup>/s.

Larger disagreements occur mainly in the simulation results for data sets 1. It correlates with the extreme (the highest) tidal ranges. For the highest tidal range, the simulated flow tends to be underestimated mainly during the flood phase and overestimated during the ebb phases. The overestimation is more pronounced during the ebb phase. Some underestimation can also be observed mainly in cross section T3.

**Table 5.5: Absolute error of flow simulation and the corresponding unit discharge**

| Data set | Flow (m/s) | Unit discharge (m <sup>2</sup> /s) |
|----------|------------|------------------------------------|
| 1        | 0.23       | 4.1                                |
| 2        | 0.21       | 3.0                                |
| 3        | 0.18       | 2.6                                |
| 4        | 0.16       | 2.4                                |
| 5        | 0.18       | 3.2                                |
| Mean     | 0.19       | 3.1                                |

On the other hand, overestimated flow simulations to the seaward direction can be observed as shown by the simulated results for cross section T2.

### 5.3.2 Sediment transport simulation

In the modelling environment, several modes for sediment transport simulation are provided. It includes simulation (1) using equilibrium sand transport equations (mode 1), (2) using cohesive sediment transport equations (mode 2) and (3) using solution of advection-diffusion equation (mode 3). Modes 1 and 3 are applied in this study.

To predict time-series sediment transport for several given periods and observation points, the TRANSPORT module receiving flow field simulation stored in a communication file from the FLOW module is considered. The communication file also stores many other information (e.g. modelling time frame and increment, physical parameters used and computational grid system) and is used to communicate with the TRANSPORT module being the input data for sediment transport simulation.

In the modelling system the TRANSPORT module computes bed and suspended load transports. The bed load transport is determined based on an empirical formula. For computing the suspended load transport, two different options are available and provided by the model:

- using an empirical equation for directly calculating the total (bed and suspended) load transport.
- using an advection-diffusion equation for determining the actual concentration ( $c_s$ ); an equilibrium concentration ( $c_{se}$ ) is calculated using an empirical formula and the difference ( $c_{se} - c_s$ ) is considered as sink or source term.

In case of using empirical formulae (mode 1), the equilibrium total load transports are directly calculated based on the simulated flow. In case of using the advection-diffusion equations (mode 3), the actual concentration computed by the module is the depth-integrated concentration ( $c_s$ ) and is defined by:

$$c_s = \frac{1}{\zeta + z_b} \int_{-z_b}^{\zeta} c(z) dz \quad (5.3)$$



in which  $c_s$  = computed actual depth-integrated concentration,  $\zeta$  = water level,  $-z_b$  = bed level and  $z$  = vertical coordinate. The actual depth-integrated concentration ( $c_s$ ) is computed from the advection-diffusion equation (see: 2.62).

For the modelling purposes a calibration coefficient termed as  $\alpha$ -factor (previously termed as  $b$ ; see: section 5.2.2) is included in both formulae and should be properly specified. Additionally, another parameter for transport relations should also be specified. This employed sediment grain size parameters ( $d_{50}$  and  $d_{90}$ ), effective bed roughness height ( $k_s$ ) and settling velocity ( $w_s$ ). Sensitivity analysis due to those aforementioned parameters is carried out.

### 5.3.2.1 Equilibrium transport formulae

The option provided by the DELFT3D-MOR model for predicting the total load transport and depth-integrated concentration using equilibrium sediment transport formulae is investigated here. The model gives only the total load transport values based on the simulated flow. No concentration prediction result is provided. Therefore, depth-integrated concentrations are obtained from the predicted total load transports.

#### Sensitivity analysis and calibration

Sensitivity tests with respect to the several parameters are made. It includes the sediment grain ( $d_{50}$ ), effective bed roughness height ( $k_s$ ) and sediment settling velocity ( $w_s$ ). Optimum setting that gives the best fit with the measurement will be determined based on a calibration using data sets 1, 4 and 5. The validation will be made employing data sets 2 and 3. Figures 5.9 and 5.10 show the sensitivity of total load transport prediction results due to the changes in  $w_s$ ,  $k_s$  and  $d_{50}$  values using respectively Bijker and van Rijn formulae.

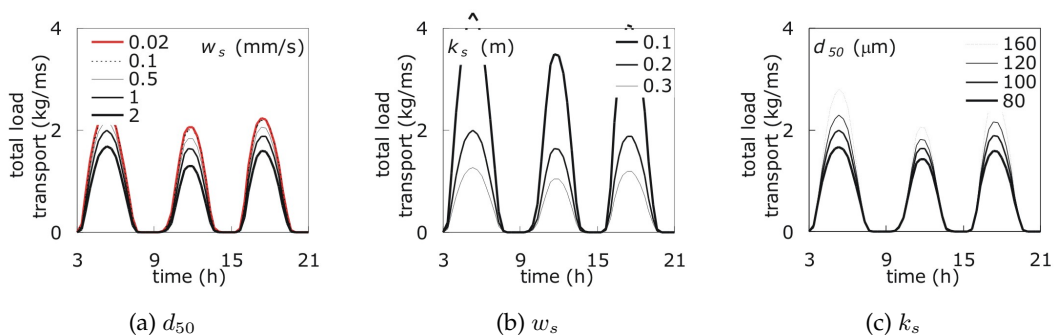


**Figure 5.9: Sensitivity of total load transport prediction using Bijker's equilibrium formulae**

Bijker formulae are found to be less sensitive to the changes of particle size. The use of  $d_{50}$  values of 80, 120 and 160  $\mu\text{m}$  gives a reduction in the simulated total load transport of 25 and 12%, whereas for van Rijn formulae it gives a reduction of 40 and 30%. In terms of  $d_{50}$  value, van Rijn formulae tend to give higher prediction results.

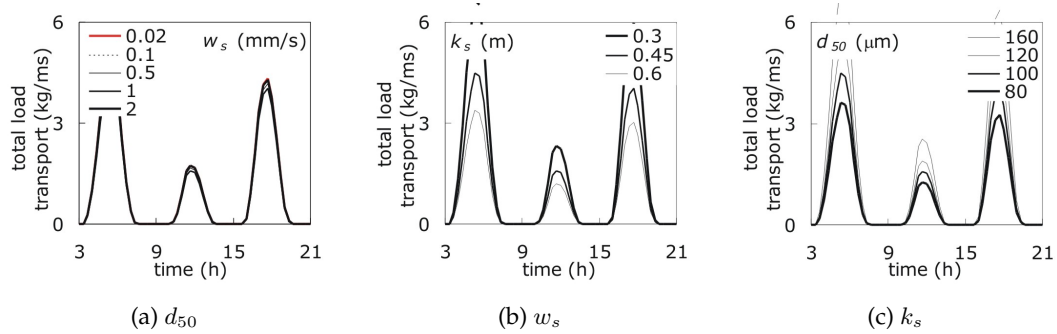


**Figure 5.10: Sensitivity of total load transport prediction using van Rijn's equilibrium formulae**

The changes in sediment settling velocity ( $w_s$ ) gives a minor influence in the simulated total load transport. However, the effect of the use of  $w_s$  value of higher than 1mm/s is quite important especially in the calculation using Bijker formulae. In this case, a reduction on the simulated total load transport of up to about 35% is resulted for the changes in  $w_s$  value from 2 to 4mm/s. For van Rijn formulae, the reduction is less distinct. It only gives a reduction of about 16%.

The equivalent bed roughness height is found to play an important role in governing the magnitude of the predicted total load transport. For Bijker formulae, increasing  $k_s$  value within a factor of 3 (from 0.1 to 0.3m) resulted in a proportional reduction within the same factor. Similar response is also shown by van Rijn formulae.

The sensitivity tests suggest that with respect to those given by Bijker formulae, van Rijn formulae tend to give higher results. Therefore, in the calibration, the higher ranges of input parameters are designated to van Rijn formulae. Calibration is made based on the use of  $k_s$  values ranging from 0.1 to 0.3m for Bijker formulae and from 0.3 to 0.6m for van Rijn formulae. The  $w_s$  values used in the calibration are from 0.02 to 4mm/s with an increment of a factor of 2. The  $d_{50}$  is assumed to be uniform and the  $d_{90}$  is assumed to be 1.5 times the  $d_{50}$ . In the calibration, the use of  $d_{50}$  ranging from 80 to 160 $\mu\text{m}$  is considered. The results are evaluated based on data sets 1, 4 and 5.

It is confirmed that simulated results within the order of measured values are given by the  $d_{50}$  value of 80 and 100 $\mu\text{m}$ ,  $w_s$  value of 0.1 or 1mm/s and  $k_s$  value of about 0.3 and 0.6m respectively for Bijker and van Rijn formulae. Finer calibration is made considering the aforementioned ranges of input parameters and the resulting best settings are given in Table 5.6.

**Table 5.6: Input parameter settings for total load transport prediction using equilibrium formulae**

|          | $\alpha$ -factor | $d_{50}$<br>( $\mu\text{m}$ ) | $d_{90}$<br>( $\mu\text{m}$ ) | $w_s$<br>(mm/s) | $k_s$<br>(m) |
|----------|------------------|-------------------------------|-------------------------------|-----------------|--------------|
| Bijker   | 3                | 100                           | 150                           | 0.1             | 0.3          |
| van Rijn | 3                | 80                            | 120                           | 0.1             | 0.6          |

### Validation

The input parameter setting obtained in the previous section (see: Table 5.6) is validated here against data sets 2 and 3. The result is shown in Table 5.7. Typical examples of the comparison between measured and simulated total load transports are given in Figure 5.11.

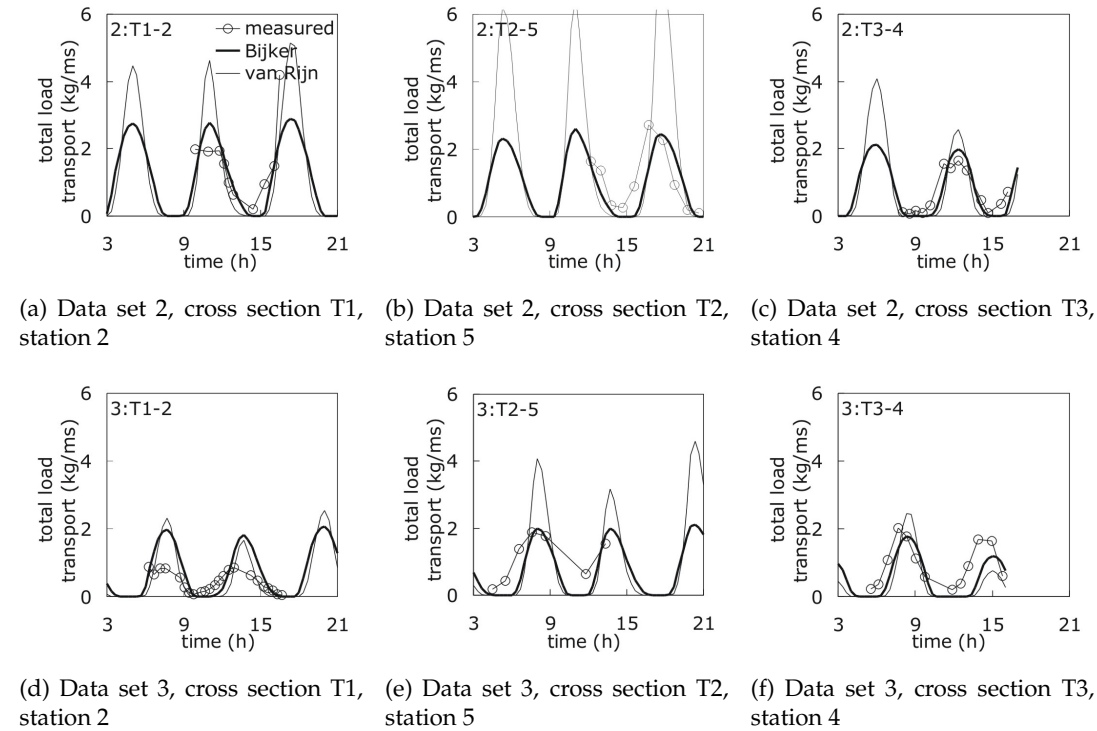


**Figure 5.11: Comparison between measured and predicted total load transport using equilibrium formulae**

**Table 5.7: Performance of total load transport prediction using equilibrium formulae**

|          | Absolute error | Relative error | Data within a factor of 2 |
|----------|----------------|----------------|---------------------------|
| Bijker   | 0.46kg/ms      | 65%            | 35%                       |
| van Rijn | 0.62kg/ms      | 80%            | 26%                       |

It is found that a slightly better agreement between predicted and measured total load transport is given by Bijker formulae. This is observed in most of the measuring stations (observation points). However major discrepancies can still be found mainly in the southern part of cross sections T2 and T3. In those locations the predicted values tend to be underestimated. The corresponding deviation can be up to a factor of 2.

The predicted total load transport using van Rijn formulae tend to be overestimated. This can be observed mainly in cross section T1 and in the northern part of cross section T2. In most cases the predicted total load transport during the accelerat-

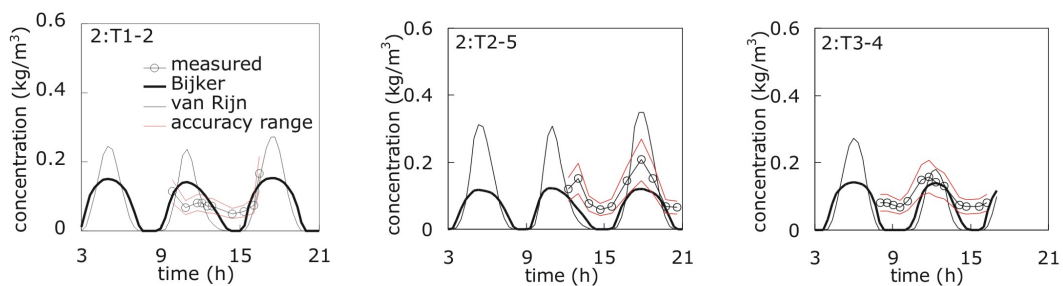
ing and decelerating velocities tend to be underestimated. Although such a tendency is also shown by the prediction results using Bijker formula, the is more pronounced in the prediction results using van Rijn formulae.

### Calculation of depth-integrated concentration

Depth-integrated concentration is calculated based on the predicted total load transports, flow simulations and water depths from model bathymetry. The results are compared with the measured values. Data sets 2 and 3 are used to verify the performance. Detailed evaluation of the corresponding verification performance is given in Table 5.8. Typical examples of the comparison between measured and predicted depth-integrated concentrations are given in Figure 5.12.

**Table 5.8: Performance of depth-integrated concentration prediction using equilibrium formulae**

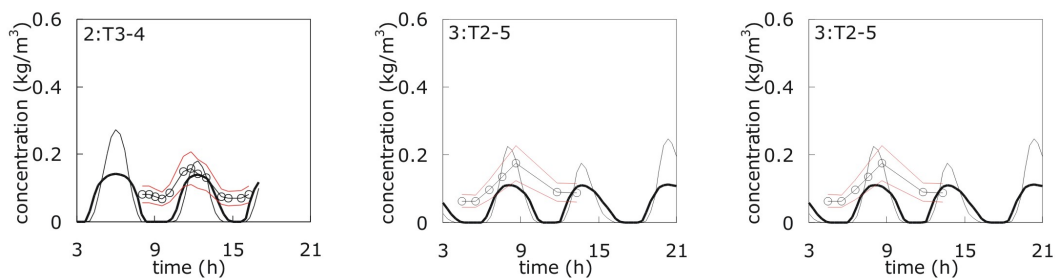
|          | RMAE | Absolute error        | Relative error | Data within a factor of 2 |
|----------|------|-----------------------|----------------|---------------------------|
| Bijker   | 0.32 | 0.06kg/m <sup>3</sup> | 58%            | 38%                       |
| van Rijn | 0.46 | 0.08kg/m <sup>3</sup> | 73%            | 23%                       |



(a) Data set 2, cross section T1, station 2

(b) Data set 2, cross section T2, station 5

(c) Data set 2, cross section T3, station 4



(d) Data set 3, cross section T1, station 2

(e) Data set 3, cross section T2, station 5

(f) Data set 3, cross section T3, station 4

**Figure 5.12: Comparison between measured and predicted depth-integrated concentration using equilibrium formulae**

From Figure 5.12 it can be observed that the calculated concentrations from the

predicted flows and total load transports are within the order of magnitude of those measured from the field. The background concentrations during slack waters can not be properly reproduced. The calculation gives zero concentration values during slack waters. Such a tendency is shown by both formulae. According to the RMAE criteria, the predicted concentration based on the simulated velocity performs a slightly better agreement with respect to those measured from the field.

Compared to those given by van Rijn formulae, Bijker formulae generally perform a better prediction results. This is due to the response to the increasing and decreasing velocities. The prediction of depth-integrated concentration using Bijker formulae shows a gentle development of increasing and decreasing values during deposition and resuspension, whereas van Rijn formulae tend to give a sudden increase and decrease of concentration dynamics.

The spatial variability of concentration dynamics has been found to be similar to those observed in the prediction of depth-integrated concentration based on the locally measured velocity. The predicted depth-integrated concentration in cross section T1 is generally overestimated. Slight overestimation is also observed occasionally in the northern part of cross sections T2. Better agreement can be observed in the prediction results for cross sections T2 and T3. However this only occurs during peak velocities. For a condition with the lowest tidal range the predicted concentrations are most of the time underestimated.

### 5.3.2.2 Advection-diffusion equation

Preliminary works on the use of the solution of advection-diffusion equation for depth-integrated concentration and sediment transport predictions in the domain in question have been initiated by Winter & Mayerle [2003]. In the works, analysis of model sensitivity and calibration were carried out using data set 1 representing condition with the highest tidal range ( $\geq 4\text{m}$ ). The sediment grain is assumed to be uniform with  $d_{50}$  of  $100\mu\text{m}$  and  $d_{90}$  of  $150\mu\text{m}$ . The effect of locally generated wave with wave height of  $0.3\text{m}$  to the simulated concentration had been found to be negligible. It gave predicted concentration simulated with and without waves of less than  $0.01\text{kg}/\text{m}^3$ .

Model sensitivity for depth-integrated concentration and sediment transport predictions focusing on data set 1 had also been previously carried out and summarised in Winter & Mayerle [2003]. The  $\alpha$ -factor gives linear effects to the result and the use of  $\alpha$ -factor of 1 to 5 gives results in the order of measured concentration. The use of  $d_{50}$  of 40 to  $160\mu\text{m}$  gives concentration differences of within a factor of 2. The effect of  $w_s$  considering values of 0.1 to  $4\text{mm}/\text{s}$  was found to have minor effect. However, it becomes more important during slack water. The use of varying  $k_s$  from 1mm to 0.5m gives concentration differences of within three order of magnitude [Winter & Mayerle, 2003].

The best input parameter settings evaluated using RMAE considering equivalent

bed roughness size ( $k_s$ ) and coefficients in the empirical formulae ( $\alpha$ -factor and  $w_s$ ) were determined. The corresponding findings are summarised in Table 5.9. It gives average RMAE over all observation points of 0.17 and 0.28 considering respectively for Bijker and van Rijn formulae.

**Table 5.9: Input parameter settings based on data set 1 [Winter & Mayerle, 2003]**

|          | $\alpha$ -factor | $d_{50}$<br>( $\mu\text{m}$ ) | $d_{90}$<br>( $\mu\text{m}$ ) | $w_{ss}$<br>(mm/s) | $w_{sb}$<br>(mm/s) | $k_s$<br>(m) | RMAE |
|----------|------------------|-------------------------------|-------------------------------|--------------------|--------------------|--------------|------|
| Bijker   | 3                | 100                           | 150                           | 0.1                | 1                  | 0.1          | 0.17 |
| van Rijn | 3                | 100                           | 150                           | 0.1                | 0.1                | 0.3          | 0.28 |

### Prediction of depth-integrated concentration

In this study, further work is attempted to investigate the application of the numerical model for all data sets representing conditions with various tidal ranges.

#### Sensitivity analysis

Additional analysis for evaluating model sensitivity employing data set 5 representing condition with the minimum tidal range is carried out here. Various setting parameters are considered. It includes the  $\alpha$ -factor,  $d_{50}$ ,  $w_s$  and  $k_s$  values. Figures 5.13 and 5.14 show the corresponding results.

The use of  $\alpha$ -factor ranging from 1 to 5 gives linear increases to the results for Bijker and van Rijn formulae. The use of  $d_{50}$  values of 50, 100 and 200 $\mu\text{m}$  and  $d_{90}$  of 1.5 times  $d_{50}$  was found to be significant for Bijker formulae in controlling the range of simulated concentration. Larger  $d_{50}$  leads to larger range (differences between minimum and maximum) of simulated concentration. For van Rijn formula, the use of those three different  $d_{50}$  leads to a discrepancy of simulated concentration up to a factor of 2.

Sensitivity tests confirmed that the use of larger settling velocity decreases the simulated concentration. Such an effect is more pronounced particularly for the value of above 1mm/s. To obtain simulated concentration within the order of measured values, settling velocity of about 0.1mm/s should be used.

The changes of  $k_s$  values in the resulting simulated concentration in van Rijn formulae is less pronounced. Bijker formulae are more sensitive to the changes of  $k_s$ . For Bijker formula, the use of increasing  $k_s$  values within a factor of 2, 4, 8 and 16 ranging from 0.05 to 0.8m lead to a decrease in simulated concentration within a factor of 2, 5, 11 and 25. Similar trend was also found in van Rijn formulae. The use of increasing  $k_s$  values within a factor of 2, 4, 8 and 16 ranging from 0.1 to 1.6m lead to a decrease in simulated concentration within a factor of 2, 4, 8 and 18.

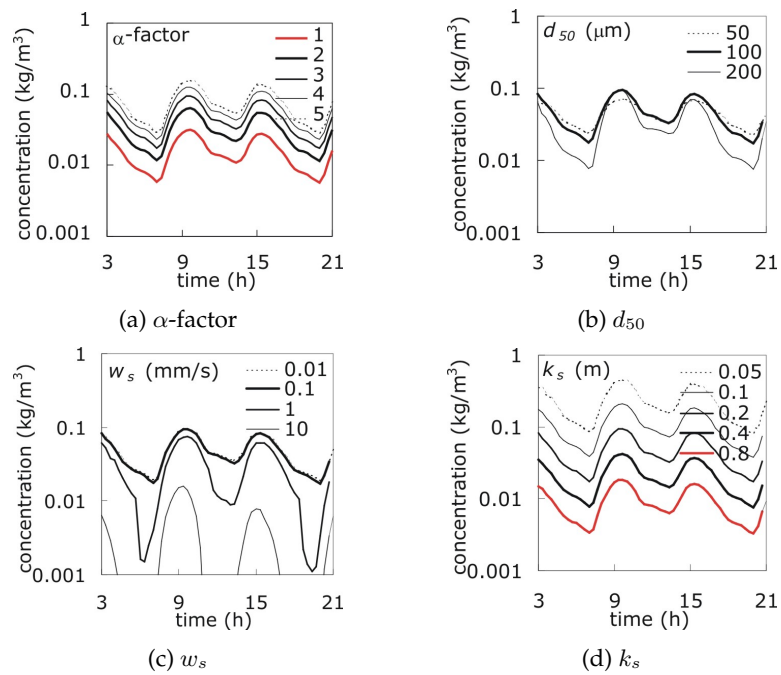


Figure 5.13: Sensitivity of depth-integrated concentration prediction using Bijker's advection-diffusion equation

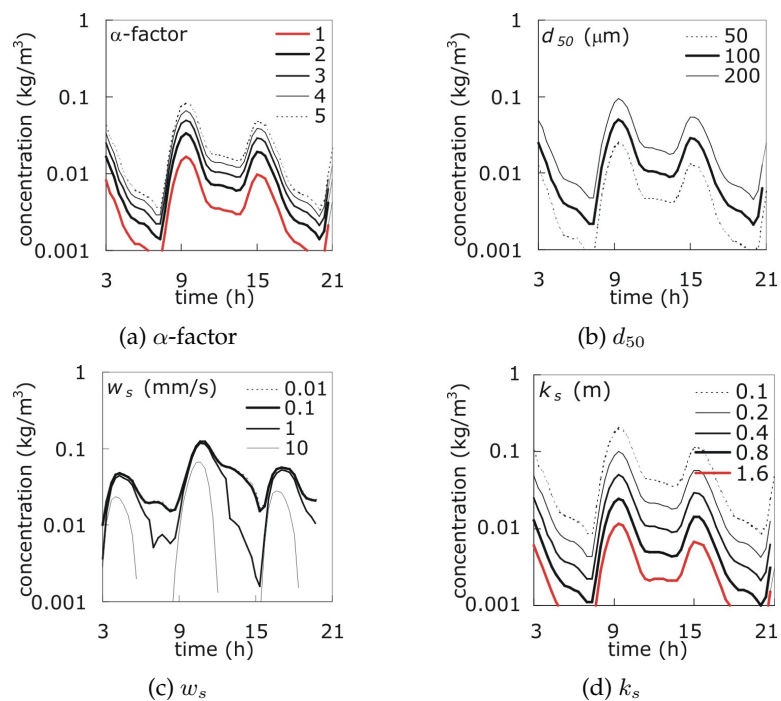


Figure 5.14: Sensitivity of depth-integrated concentration prediction using van Rijn's advection-diffusion equation

### Calibration

Model calibration is carried out here considering field measurement classified in data sets 1, 3 and 4. To avoid exhausting efforts by running all possible combinations of input parameter settings, the  $\alpha$ -factor is fixed at a value of 3, the settling velocity of sediment in suspension ( $w_{ss}$ ) and for the transport relation ( $w_{sb}$ ) is set to 0.1mm/s. The sediment grain sizes are for the time being assumed to uniform over all measuring cross sections with  $d_{50}$  and  $d_{90}$  of respectively 100 and 150  $\mu\text{m}$ . The remaining calibration parameter would only be the equivalent bed roughness height ( $k_s$ ). In the calibration,  $k_s$  values used for Bijker formulae are from 0.05 to 0.25m, whereas, for van Rijn formulae are from 0.05 to 0.55m. Using the aforementioned ranges of  $k_s$  values, both formulae have been found to be able to reproduce time-series depth-integrated concentration within the order of measured values. The best  $k_s$  value fitting data sets 1, 4 and 5 for Bijker formulae should be of 0.2m, whereas for van Rijn formulae of 0.3m. To fit the measurement, higher equivalent bed roughness values is usually required by van Rijn formula. Resuming the calibration results, the best input parameter settings based on average RMAE of all observation points are summarised in Table 5.10.

**Table 5.10: Input parameter settings for depth-integrated concentration prediction using advection-diffusion equation**

|          | $\alpha$ -factor | $d_{50}$<br>( $\mu\text{m}$ ) | $d_{90}$<br>( $\mu\text{m}$ ) | $w_s$<br>(mm/s) | $k_s$<br>(m) |
|----------|------------------|-------------------------------|-------------------------------|-----------------|--------------|
| Bijker   | 3                | 100                           | 150                           | 0.1             | 0.2          |
| van Rijn | 3                | 100                           | 150                           | 0.1             | 0.3          |

### Validation

The input parameter setting obtained in the previous section is validated here against data sets 2 and 3. Typical examples of the comparison between measured and predicted depth-integrated concentrations are shown in Figure 5.15. Only prediction and measurement results from stations 2, 5 and 4 from respectively cross sections T1, T2 and T3 are shown here to illustrate the agreement. The corresponding performance is summarised in Table 5.11.

**Table 5.11: Performance of depth-integrated concentration prediction using advection-diffusion equation**

|          | RMAE | Absolute<br>error     | Relative<br>error | Data within<br>a factor of 2 |
|----------|------|-----------------------|-------------------|------------------------------|
| Bijker   | 0.12 | 0.05kg/m <sup>3</sup> | 41%               | 75%                          |
| van Rijn | 0.40 | 0.08kg/m <sup>3</sup> | 73%               | 52%                          |



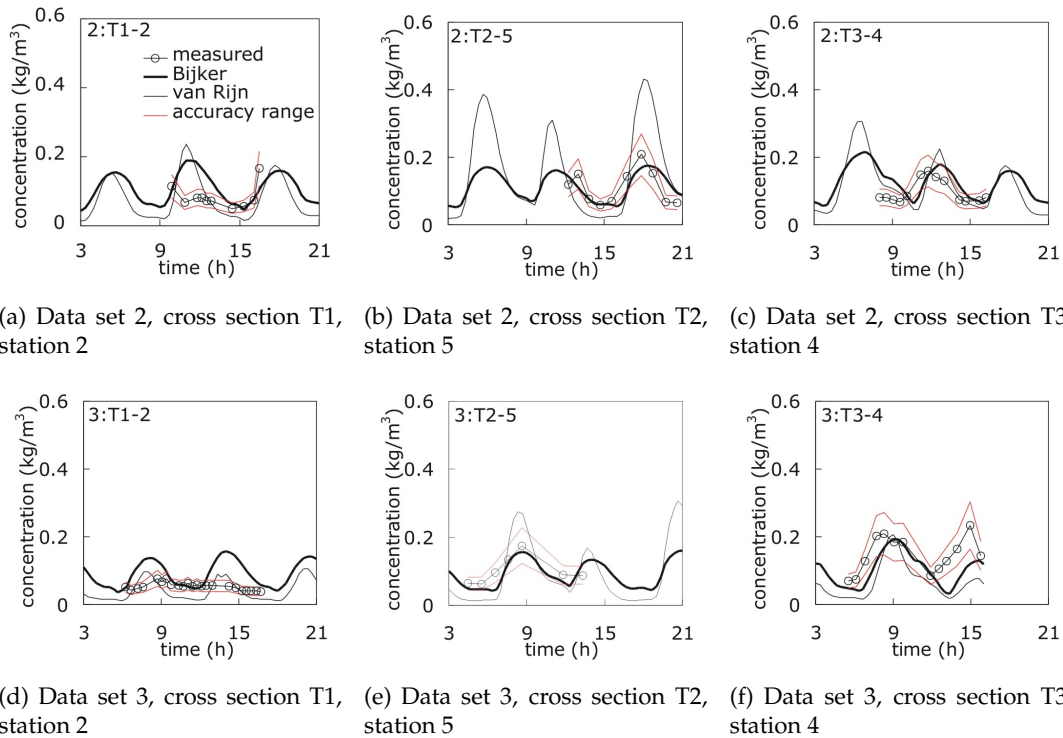


**Figure 5.15: Comparison between measured and predicted depth-integrated concentration using advection-diffusion equation**

In terms of RMAE and relative error, Bijker formulae gives better performance with respect to those given by van Rijn formulae. Considering the absolute error, both formulae give a comparable results. The average absolute errors ranges between 0.05 to 0.08kg/m<sup>3</sup>. An increasing performance qualification with respect to those predicted using the equilibrium transport formulae can be observed.

Good agreement between measured and simulated values is performed by the model in almost all of the observation points. The disagreement is resulted from major discrepancies in the southern part of cross sections T2 and T3. This occupies about 40% of observation points. In those observation points, the simulated concentration tend to be underestimated. Such tendencies are shown by both formulae. For van Rijn formulae, the underestimation is even more pronounced during slack waters. In addition to that, a tendency of larger disagreement during extreme tidal ranges (highest and lowest) can be observed. This can be seen in data sets 1 and 5. During those periods, the simulated value tend to be underestimated. This is shown by the prediction results using both formulae.

### Transport prediction

Investigation to the simulation of total load transport is presented here. In the simulation, the optimum input parameter settings obtained in the previous section (see: Table 5.10) are applied. Data sets 2 to 3 are used to verify the simulation performance.

It is found that comparable performance of simulated total load transports using Bijker and van Rijn formulae are resulted. Detailed evaluation of the performance of the optimum parameter setting for total load transport simulation using advection-diffusion equation is given in Table 5.12. Typical examples of the comparison between the measured and simulated total load transports are presented in Figure 5.16.

**Table 5.12: Performance of total load transport prediction using advection-diffusion equation**

|          | Absolute error | Relative error | Data within a factor of 2 |
|----------|----------------|----------------|---------------------------|
| Bijker   | 0.56kg/ms      | 70%            | 42%                       |
| van Rijn | 0.68kg/ms      | 78%            | 31%                       |

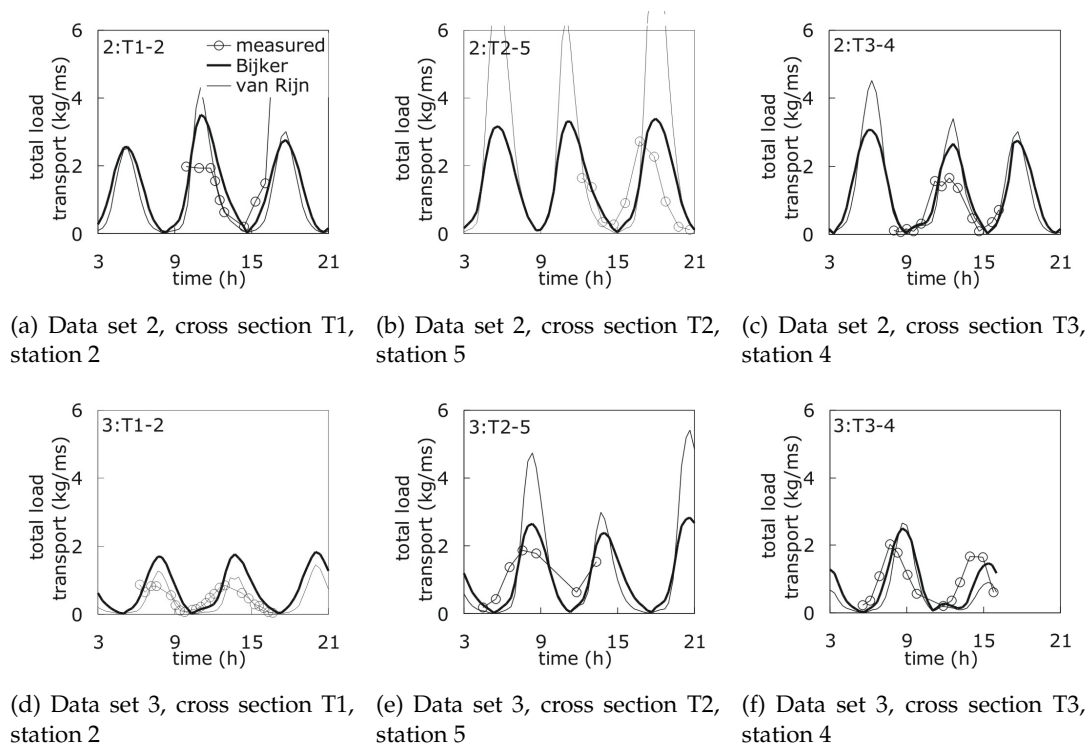


**Figure 5.16: Comparison between measured and predicted total load transport using advection-diffusion equation**

Major disagreement is found mainly in the southern part of cross section T2. Here, the simulated total load transports tend to be underestimated. The underestimation is up to a factor of 2 for particularly data set 1 (highest tidal range). In cross section T1 and in the northern part of cross sections T2 and T3, the simulated total load transports tend to be slightly overestimated. Good agreement is achieved mainly in the southern part of cross section T2. The average RMAE values over all observation points are of about 0.4 and the average absolute errors are of about 0.6kg/ms.

## 5.4 Discussion

Could concentration and sediment transport dynamics be properly predicted?

The calibration and validation of depth-integrated concentration and sediment (total load) transport predictions have been presented. In the prediction, two different approaches were used: (1) based on the locally measured current velocity for estimating the bed shear stress and (2) the bed shear stress is estimated based on the numerical simulation of two-dimensional velocity field. In the first case, empirical sand transport formulae are used. In the latter case, equilibrium sand transport and advection-diffusion equations are used.

The best input parameter settings based on representative (maximum, mean and minimum) tidal ranges have been determined. The corresponding parameters are the sediment grain ( $d_{50}$  and  $d_{90}$ ), sediment settling velocity ( $w_s$ ) and equivalent bed roughness height ( $k_s$ ). The validation of the prediction has been carried out. In the validation, the prediction performance is quantified. Investigation to the agreement between measured and predicted values has also been done. It considers the variability of the agreement over a tidal cycle and along the three different cross sections. Based on the present analysis, the following findings can be drawn:

- The predicted depth-integrated concentration and total load transport have been found to be within the magnitudes of those measured from the field. This is shown by the prediction based on the locally measured as well as based on the numerically simulated velocities. The accuracy of the depth-integrated concentration predictions are approximately between a factor of 1.4 to 1.8, whereas for the total load transport predictions of 1.7 to 2. In general, the predicted values performed by Bijker formulae fit better with the measured ones than those given by van Rijn formulae.
- Single setting parameter (uniform bed sediment grain sizes ( $d_{50}$  and  $d_{90}$ ), settling velocity ( $w_s$ ) and effective bed roughness height ( $k_s$ )) is found to be able to be used for reproducing the dynamics of sediment concentration and total load transport. However, major disagreements in several particular observation points are found. For some particular locations, adjustment of the setting parameter to give a better fit may be required. As the  $w_s$  value is found to give minor influence to the results, additional calibration effort to achieve a better fit should consider the use of a combination of different  $d_{50}$  and  $k_s$  values.
- Increasing performance is observed by the prediction results using the solution of advection-diffusion equations with respect to those given by the equilibrium or empirical sand transport formulae. On the other hand the use of advection-diffusion equations unfortunately require higher computational effort. In case of using equilibrium or empirical sand transport equations based respectively on

the locally measured and numerically simulated velocity, none of both empirical formulae (i.e. Bijker and van Rijn formulae) are able to properly predict the background concentration during the slack water. It leads to an underestimation of the predicted total load transports during resuspension and deposition.

- In case of the prediction based on the locally measured velocity no distinct pattern of spatial agreement can be observed. The deviation of the predicted values tends to be randomly distributed over all observation points. In case of the prediction based on the simulated velocity, a tendency of consistent deviation for some particular locations in the cross sections can be observed. In cross section T1 (Norderpiep channel), the predicted depth-integrated concentrations and total load transports tend to be overestimated and are leading to larger disagreement. Such an overestimation is more pronounced in the middle of the channel. Better agreement is achieved in cross sections T2 and T3 (Suederpiep and Piep channels). However, larger deviation can still be found mainly in the northern part of Suederpiep and Piep channels. The total load transports agree quite well in the middle part of Suederpiep channel and in the southern part of Piep channels.

Could the performance of the prediction results be (significantly) improved?

The performance of the prediction results has been obtained by averaging the agreement between measured and predicted values over all measuring stations. The RMAE, absolute error, relative error and percentage of data within a factor of 2 presented in this chapter are therefore an average value over all observation points. Consequently, the temporal and local variations of the agreement respectively for a particular measuring period or cross section can not be clearly identified.

Further investigation is hence attempted here to evaluate the depth-integrated concentration and total load transport prediction considering variability over a temporal series (measuring periods) and spatial series (cross sections). In the investigation, additional sensitivity tests and calibrations due to the effect of changing mainly the  $d_{50}$  and  $k_s$  values are done and addressed to determine an optimum input parameter setting that might give the best fits with the measurement for a particular cross section or measuring period.

It should be noted that as no distinct pattern of the distribution of the agreement over spatial series in the use of locally measured velocity for predicting bed shear stress can be clearly identified, this adjustment might only be applicable for the use of the prediction based on the simulated velocity. Based on the present analysis, the following findings are drawn:

- As major overestimation is commonly found mainly in cross section T1 (Norderpiep) and in the northern part of cross section T3 (Piep), the use of relatively

higher  $k_s$  value (than those given to the rest of the measuring locations) may improve the agreement. The relative ratio of  $k_s$  value for Norderpiep and the northern part of Piep channels with respect to the rest of the measuring stations may be up to a factor of 2.

- Alternatively, for reducing overestimation in cross section T1 (Norderpiep) and in the northern part of cross section T3 (Piep) the use of relatively smaller  $d_{50}$  value may also improve the agreement. It gives a reduction in the predicted ranges of depth-integrated concentration and total load transport. Such an adjustment is however valid only for Bijker formulae.
- As major underestimation is commonly found mainly in cross section T2 (Suederpiep), the use of relatively smaller  $k_s$  value (than those given to the rest of the measuring locations) may improve the agreement. The relative ratio of  $k_s$  value for Suederpiep channel with respect to the rest of the measuring stations may up to a factor of 2.
- Occasionally, in addition to the  $k_s$  adjustment, the use of relatively higher  $d_{50}$  value may also improve the agreement mainly in the southern part of Suederpiep channel as it gives a higher ranges of concentration dynamics. The recommended  $d_{50}$  value is of  $200\mu\text{m}$ . Field data support this adjustment as larger bed sediment grain sizes are found along the southern part of Suederpiep channel and along the southern part of its elongation up to the intersection with the Norderpiep channel.
- The  $k_s$  value has been determined based on the optimum fit for all representative (maximum, minimum and average) tidal ranges. It is found that the best  $k_s$  value that fits each data set varies from period to period. It suggest a relationship between an optimum  $k_s$  value with the tidal range.

Related to the latest aforementioned item, investigation of the role of  $k_s$  in sand transport equations in controlling the predicted concentration and sediment transport is carried out. In this study,  $k_s$  has been used as a calibration parameter. A uniform  $k_s$  over the entire location and period was assumed. It was found that the use of varying  $k_s$  can improve the agreement in several particular locations (observation points). This encourages that the  $k_s$  for sediment transport simulation should vary within spatial series. Such an evidence is suggested by the relationship between the nature of local bed morphology and higher  $k_s$  to give a better fit with the measurement. For example, the mega ripples as well as the slip and current marks in the Norderpiep channel is found to correlate with the requirement of a relatively higher  $k_s$ .

In the flow model simulation spatially distributed  $k_s$  over the entire domain was made available. The corresponding discussion is given in Palacio [2001]. The use of spatially varying  $k_s$  was found to give a good agreement between the measured

and simulated velocities. Suggestion of the use of higher relatively  $k_s$  values in the sediment transport model simulation for the Norderpiep channel and the northern part of Piep channel is found to have a good correlation with the spatial  $k_s$  distribution in the flow model simulation. Figure 5.17 shows the spatial  $k_s$  distribution in the flow model domain. In the corresponding figure the sea bottom profiles from the model bathymetry and the  $k_s$  value relative to the seabed are also shown.

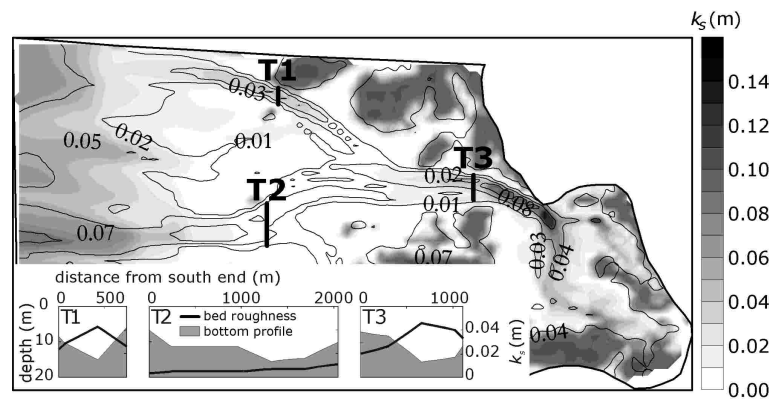
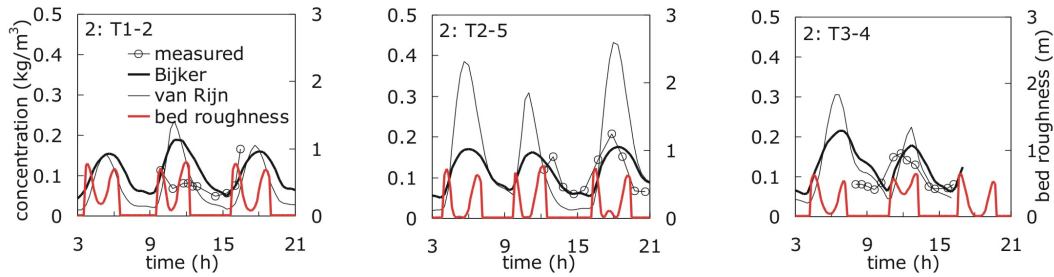


Figure 5.17: Spatial  $k_s$  distribution in the flow model simulation

A time dependent development of effective bed roughness heights in the investigation area has been observed and documented in Razakafoniaina [2001] and Mayerle et al. [2002]. The works were based on field measurement and numerical model simulations. In the study, empirical formulae for predicting bedform dimensions (height and length) and effective bed roughness heights based on the predicted bedform dimensions proposed by van Rijn [1984c] and Yalin [1985] were applied. It was found that  $k_s$  values vary during a tidal cycle. Besides, different values are found during the neap and spring tides. Within a tidal cycle, the predicted effective bed roughness heights is developed during peak velocity and disappeared during slack water. During the neap tide (tidal range 2.4m), the bed roughness is rarely developed, whereas during the spring tide (tidal range 3.5m), bedforms were developed at all monitoring points. In a period with storm surge (water level rise of 4m), no bedforms are developed except during the water level rise [Mayerle et al., 2002].

An evidence of time dependent effective bed roughness height development over a tidal cycle is also found in this study. Such a tendency is observed in all of data sets and in most of all observation points. The corresponding typical examples are shown in Figure 5.18. The effective bed roughness height is developed during the peak concentration and disappeared during slack water. Having observed the tendency of underestimation and overestimation of the simulated concentration using the solution of advection-diffusion equation, incorporation of time dependent  $k_s$  development in the sediment transport simulation might reduce the overestimation during peak velocity and the underestimation during slack water. It should be noted that the  $k_s$  value is

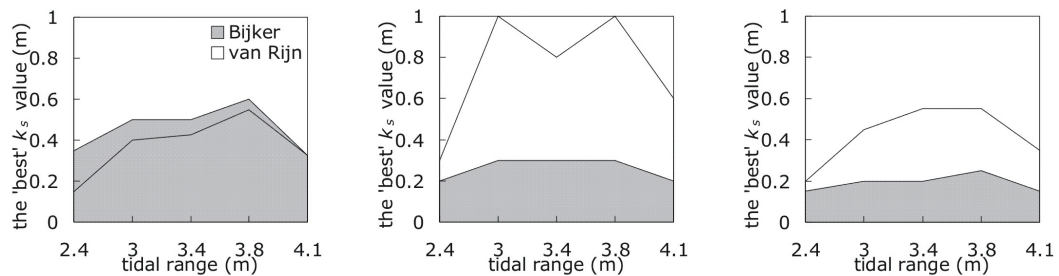
an equivalent effect of the nature of bed morphology that influences the current structure and hence bed shear stress. Therefore, this should be validated with the field evidence in order to verify if such a phenomena does occur physically in the nature, although in the field, temporal bedform development is very hard to be precisely observed. However, if such a trend can be included in the sediment transport simulation the agreement can be significantly improved.



(a) Data set 2, cross section T1, station 2 (b) Data set 2, cross section T2, station 5 (c) Data set 2, cross section T3, station 4

**Figure 5.18: Time-dependent effective bed roughness height ( $k_s$ ) development in conjunction with simulated and measured time series concentration**

In this study, the relation between the best  $k_s$  value that fit a data set against tidal range is investigated. From the investigation it is found that there is a distinct pattern of the required  $k_s$  value for a certain tidal range. Figure 5.19 shows the relationship between 'best'  $k_s$  value that gives the best fit with field measurement data of each data set.



(a) Using empirical equation and based on locally measured current velocity (b) Using equilibrium sand transport formulae and based on numerical flow field simulation results (c) Using solution of advection-diffusion equations and based on numerical flow field simulation results

**Figure 5.19: Relationship between  $k_s$  value and tidal range**

It can be seen that at the extreme tidal ranges, the use of smaller  $k_s$  value is required. This is confirmed by an indication of an underestimated prediction during those extreme periods (data sets 1 and 5). The use of smaller  $k_s$  value can overcome the underestimation in the simulated concentrations and total load transports. This could represent the physical processes occurred in the nature, in which there is an optimum tidal range for bedforms to disappear, develop or be washed away. Such an evidence

is also shown by [Mayerle et al., 2002] from the numerical simulation during neap, spring and storm conditions. Further investigation to evaluate the flow modelling as well as field observation for observing the bedform development in conjunction with the tidal range is needed to confirm this finding.



## Chapter 6

# Evaluation of Prediction Results

### 6.1 Introduction

In this chapter further discussion of the results of depth-integrated concentration and sediment transport dynamics prediction is presented. Three different prediction approaches used in this study can be distinguished as:

- Prediction 1: based on measured velocity and using empirical sediment transport equations;
- Prediction 2: based on simulated velocity and using equilibrium sand transport formulae; and
- Prediction 3: based on simulated velocity and using solution of advection-diffusion equation.

Comparisons of the prediction performances based on those three different approaches are given. Application of the modelling results for extreme tidal conditions (neap and spring tides) using the best prediction approach is shown. The importance of suspended load as the primary mode of transport in the investigation area is also described.

### 6.2 Concentration and transport dynamics

The validation performance of the prediction results for the depth-integrated concentration dynamics based on the investigation carried out in the previous chapter is summarised in Table 6.1. An increasing performance based upon three different prediction approaches can be observed. Prediction results based on the numerically simulated velocity are relatively better than those given based on the locally measured velocity. With respect to those given by equilibrium transport formulae, the solution of advection-diffusion equation gives better prediction quality. Compared to those given by van Rijn formulae, Bijker formulae perform better prediction results.

**Table 6.1: Performance comparison of depth-integrated concentration prediction**

|                                     | Measured velocity  |          | Model simulation     |          |                      |          |
|-------------------------------------|--------------------|----------|----------------------|----------|----------------------|----------|
|                                     | Empirical formulae |          | Equilibrium formulae |          | Adv.-diff. equations |          |
|                                     | Bijker             | van Rijn | Bijker               | van Rijn | Bijker               | van Rijn |
| RMAE                                | 0.42               | 0.55     | 0.32                 | 0.46     | 0.12                 | 0.40     |
| Absolute error (kg/m <sup>3</sup> ) | 0.08               | 0.09     | 0.06                 | 0.08     | 0.05                 | 0.08     |
| Relative error (%)                  | 68                 | 82       | 58                   | 73       | 41                   | 73       |
| Factor of 2 (%)                     | 38                 | 17       | 38                   | 23       | 75                   | 52       |

It is confirmed that the best depth-integrated concentration prediction can be performed based on the numerical velocity simulation combining with the application of Bijker formulae and using the solution of advection-diffusion equations. The prediction quality is found to be better than the present status of concentration prediction accuracy in which most of data (in this case 75%) are within a factor of 2 (see: section 2.3.3).

Table 6.2 summarises the validation performance of the prediction results for the total load transport dynamics based on the investigation carried out in the previous chapter. It can also be seen here that according to the score of discrepancy factor and using Bijker formulae a comparable performance based upon three different prediction approaches can be generally observed. Prediction results based on the use of advection-diffusion equations are however slightly better than those given based on the other two approaches. In case of using van Rijn formulae an increasing performance between the prediction based on the locally measured and numerically simulated velocity can be observed. Compared to those given by van Rijn formulae, in general Bijker formulae perform better prediction results.

**Table 6.2: Performance comparison of total load transport prediction**

|                        | Measured velocity  |          | Model simulation     |          |                      |          |
|------------------------|--------------------|----------|----------------------|----------|----------------------|----------|
|                        | Empirical formulae |          | Equilibrium formulae |          | Adv.-diff. equations |          |
|                        | Bijker             | van Rijn | Bijker               | van Rijn | Bijker               | van Rijn |
| Absolute error (kg/ms) | 0.44               | 0.59     | 0.46                 | 0.62     | 0.56                 | 0.68     |
| Relative error (%)     | 59                 | 75       | 65                   | 80       | 70                   | 78       |
| Factor of 2 (%)        | 38                 | 18       | 35                   | 26       | 42                   | 31       |

This investigation confirms that the best total load transport prediction can still be achieved based on the numerical velocity simulation combined with the application of Bijker formulae and using the solution of advection-diffusion equations. The prediction quality is found to be below the present status of sediment transport prediction

accuracy. In this case only about 40% of data are within a factor of 2.

### 6.2.1 Comparison of concentration predictions

Further investigation is attempted here to describe the concentration dynamics based on the three different prediction approaches and separately using Bijker and van Rijn formulae. Comparisons between the prediction results based on the three different approaches with respect to those measured from the field are also described. Typical prediction examples from cross sections T1, T2 and T3 representing Norderpiep, Suederpiep and Piep channels are given.

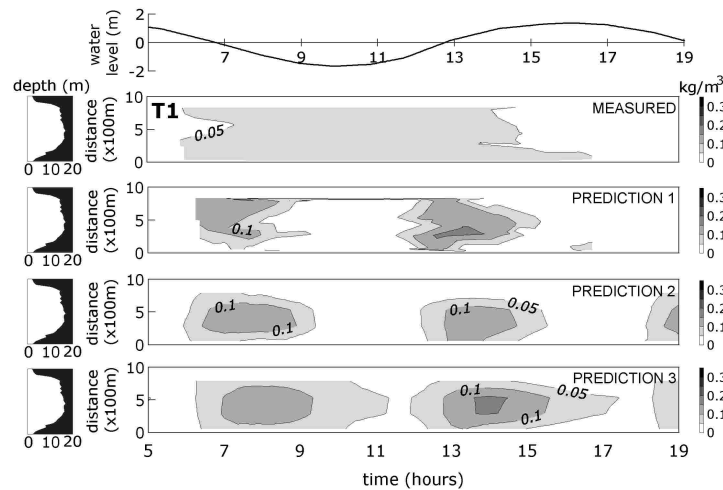
#### 6.2.1.1 Norderpiep channel

The concentration dynamics in the Norderpiep has been found to vary within a very low range of approximately  $0.05$  to  $0.1\text{kg/m}^3$ . For decreasing tidal range, even less variation in concentration can be observed. Typical comparisons of two-dimensional concentration dynamics in cross section T1 (Norderpiep) predicted using Bijker and van Rijn formulae based on the three different prediction approaches are given in Figure 6.1. Data set 3 measured on September 5, 2000 representing the average tidal range (3.1m) is chosen to depict the corresponding dynamics. In the example given in Figure 6.1 the variation of measured depth-integrated concentration in the Norderpiep varied only between  $0.04$  to  $0.08\text{kg/m}^3$ .

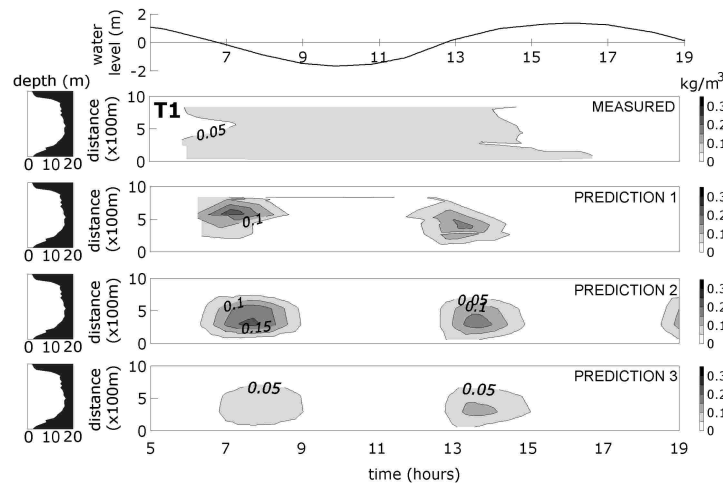
In the Norderpiep the predicted depth-integrated concentrations tend to be overestimated. It is shown by Bijker and van Rijn formulae with a deviation of up to a factor of 3 mainly during the peak velocity of the flood phase. Exceptionally, the overestimation tends to occur in the use of van Rijn formulae based on the predictions 1 and 2 during the flood phase. The predicted background concentration performed by Bijker formulae based on the prediction 3 is found to be closer to the measured values. However an overestimation of up to a factor of 2 and 3 respectively during the ebb and flood phases can still be observed.

Such an overestimation is due to the use of uniform setting parameters for the whole domain. It has been investigated that, in fact, local variability of concentration dynamics should be reproduced using various combination of  $k_s$  and occasionally  $d_{50}$  values. In case of Norderpiep channel, the use of higher  $k_s$  value is recommended to give the reduction effect to the concentration range. In case of using Bijker formulae, the use of smaller  $d_{50}$  can occasionally be considered.

It can also be observed here that the predicted maximum depth-integrated concentration using the solution of advection-diffusion equation based on the simulated velocity (Prediction 3) shows an occurrence of time lag. With respect to those predicted based on the locally measured velocity (Prediction 1), the prediction of peak concentration based on the simulated velocity tend to be lagged of approximately up to 1 hour.



(a) Bijker

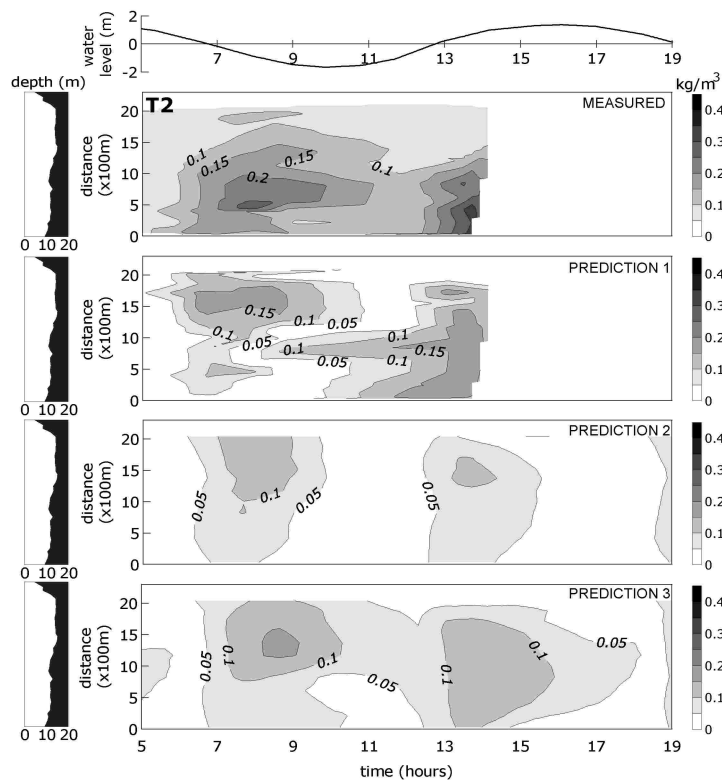


(b) van Rijn

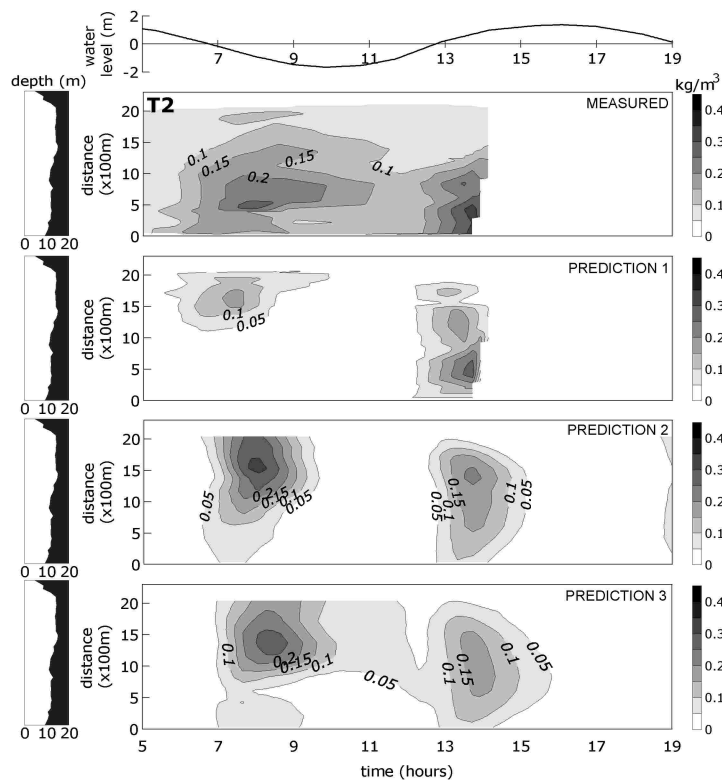
Figure 6.1: Comparison between measured and predicted depth-integrated concentration in cross section T1

### 6.2.1.2 Suederpiep channel

The Suederpiep channel has been found to have the largest depth-integrated concentration variation. In this cross section, a clear response to the increasing tidal range has also been observed. Typical comparisons of two-dimensional concentration dynamics in cross section T2 (Suederpiep) predicted using Bijker and van Rijn formulae based on the three different prediction approaches are given in Figure 6.2. Data set 3 measured on September 5, 2000 representing the average tidal range (3.1m) is chosen to depict the example. During this day the depth-integrated concentration varied between 0.06 to 0.33kg/m<sup>3</sup>. From the measurement, it can be observed that higher concentration range occur mainly in the southern part of the channel. Additionally, increasing maximum concentration can also be observed during the flood phase towards the southern bank of the channel. Background concentration tends to occur a while after the low water and remain up to short before increasing velocity.



(a) Bijker



(b) van Rijn

Figure 6.2: Comparison between measured and predicted depth-integrated concentration in cross section T2

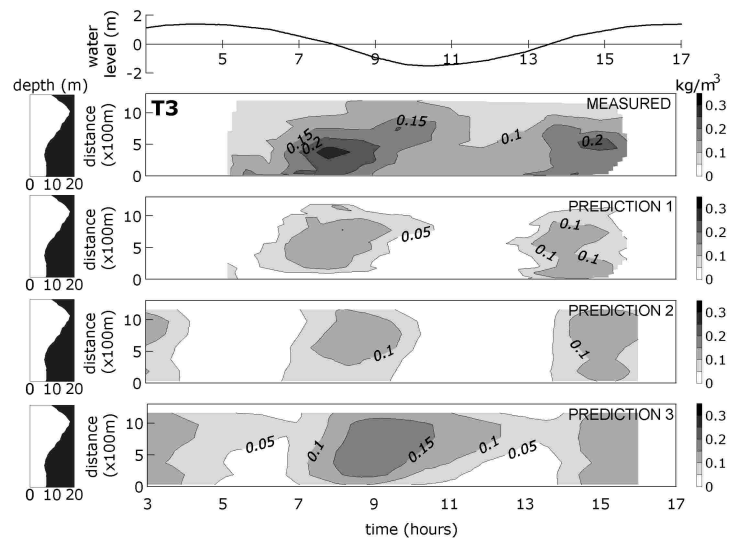
The prediction results generally follow the dynamic pattern of the depth-integrated concentration magnitudes. However, tendency of higher concentration during the flood phase can not be followed. The increasing range of depth-integrated concentration towards the southern part of the channel can be reasonably reproduced. The predicted depth-integrated concentration based on the simulated velocity using Bijker formulae tend to be underestimated. The corresponding deviation can be up to a factor of 2. However, the tendency of increasing depth-integrated concentration magnitudes towards the southern part of the channel can still be observed. Using van Rijn formulae the predicted maximum depth-integrated concentrations have been found to be closer to those measured from the field. However, major disagreement can be observed mainly during the slack water and occasionally during the decreasing and increasing velocity. In the prediction results, the tendency of increasing depth-integrated concentration magnitudes towards the southern part of the channel based on mainly the locally measured velocity can still be observed.

From the measurement it can be observed that the background concentration of up to approximately  $0.1\text{kg/m}^3$  has been found to occupy the entire cross section and over an entire tidal cycle. The predicted background concentrations based on the simulated velocity and using the solution of advection-diffusion equation tend to be underestimated and occupy only the middle part of the channel. The corresponding deviation is up to a factor of 2. This is shown generally either by Bijker as well as van Rijn formulae. However the remaining background concentration towards the southern part of the channel can still be observed.

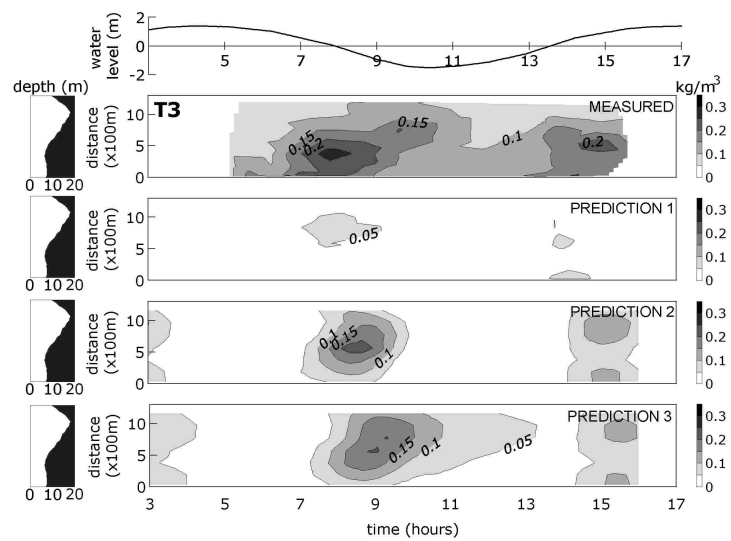
### 6.2.1.3 Piep channel

Similar investigation is carried out for the prediction results in cross section T3 (Piep). The Piep channel has been found to have a unique local bed morphology and sediment characteristics. In the northern part of the channel the bed sediment is mainly consists of consolidated mud and bedforms rarely exist. In the southern part of the channel the bed sediment consists of mainly fine sand with mud content of less than approximately 5%. Such a phenomena influences the transport behaviour. With respect to those observed in the northern part of the channel, in the southern part of the channel higher ranges of concentration dynamics have been clearly observed.

Typical comparisons of two-dimensional concentration dynamics in cross section T3 (Piep) predicted using Bijker and van Rijn formulae based on the three different prediction approaches are given in Figure 6.3. Data set 3 measured on September 6, 2000 representing the average tidal range (2.9m) is chosen to depict the comparison. During this day the depth-integrated concentration varied between  $0.07$  to  $0.3\text{kg/m}^3$ . From the measurement, it can be observed that higher concentration range occur mainly closer to the southern part of the channel. Additionally, higher maximum concentration can be observed during the ebb phase.



(a) Bijker



(b) van Rijn

Figure 6.3: Comparison between measured and predicted depth-integrated concentration in cross section T3

Up to some extents the prediction results are able to reproduce the significant features of depth-integrated concentration dynamics in this cross section. The tendency of decreasing magnitude of maximum depth-integrated concentration during the flood phase can be followed. Higher background concentration towards the northern part of the channel during the ebb phase and closer to the low water can also be followed. However, the prediction of depth-integrated concentration magnitudes generally tend to be underestimated. Extreme example is shown by the prediction using van Rijn formulae based on the locally measured velocity.

The best prediction results are given by the use of the solution of advection-diffusion equation and based on the simulated velocity. In this case, Bijker formulae is able to reproduce the dynamic of concentration during peak velocity and slack water. However an underestimation of maximum concentration can still be observed. Using van Rijn formulae, the predicted maximum concentration agree better with the measurement but the predicted background concentrations tend to be underestimated.

It can also be observed here that the predicted maximum depth-integrated concentration using the solution of advection-diffusion equation based on the simulated velocity demonstrates an occurrence of time lag. With respect to those measured from the field, the prediction of peak concentration based on the simulated velocity tend to be lagged of approximately up to 1 hour. This is shown by the use of Bijker and van Rijn formulae.

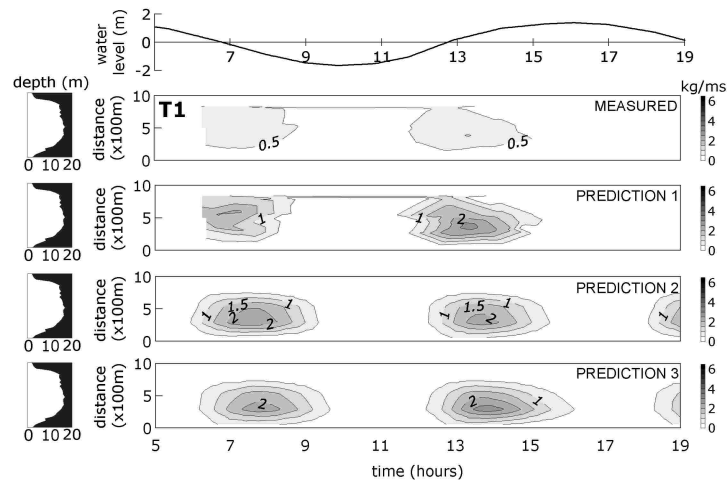
## 6.2.2 Comparison of total load transport predictions

Similar investigation as those performed for the depth-integrated concentration prediction is presented here to describe the dynamics of total load transports based on the three different prediction approaches and separately using Bijker and van Rijn formulae. Comparisons between the prediction results based on the three different approaches with respect to those measured from the field are also described. Typical prediction examples from cross sections T1, T2 and T3 representing Norderpiep, Suederpiep and Piep channels are given.

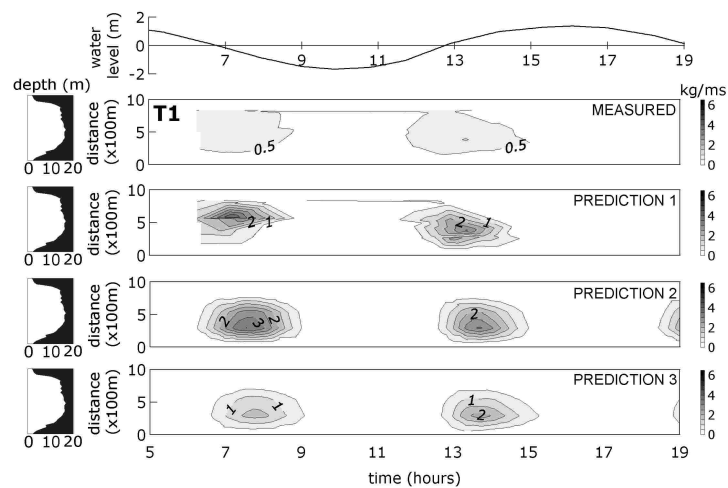
### 6.2.2.1 Norderpiep channel

Typical comparisons of total load transport dynamics in cross section T1 (Norderpiep) predicted using Bijker and van Rijn formulae based on the three different prediction approaches are given in Figure 6.4. Data set 3 measured on September 5, 2000 representing the average tidal range (3.1m) is chosen to depict the example. In this example the variation of measured total load in the Norderpiep varies between 0 to 1kg/ms. Sediments are transported only around maximum ebb or flood velocities. Although the background concentrations do exist but since the current velocity is effectively zero, during the slack water no sediment is transported.





(a) Bijker



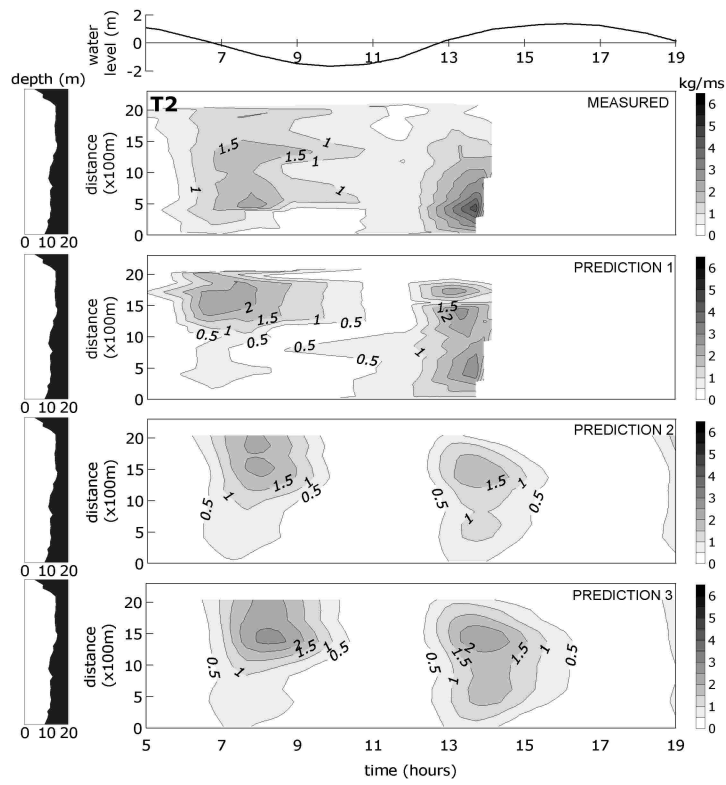
(b) van Rijn

**Figure 6.4: Comparison between measured and predicted total load transport in cross section T1**

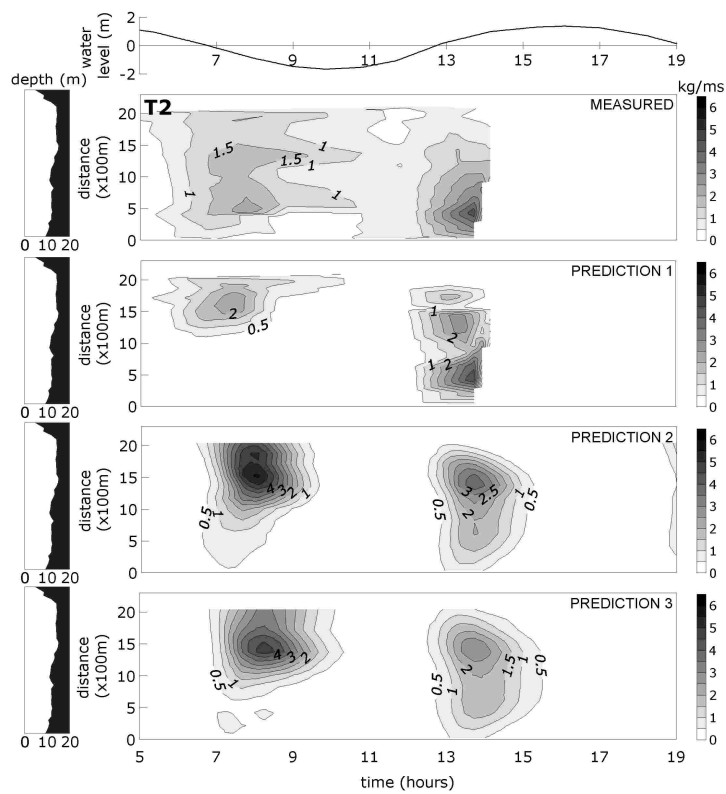
All prediction approaches generally perform a comparable agreement. Although in all cases the corresponding predicted magnitudes tend to be overestimated, the tendency of sediment transportation around maximum velocities can still be observed. The corresponding overestimation can deviate up to a factor of 6. This is mainly due to the overestimated depth-integrated concentration prediction. The prediction results also demonstrate that around slack water no sediment is transported.

### 6.2.2.2 Suederpiep channel

Typical comparisons of total load transport dynamics in cross section T2 (Suederpiep) predicted using Bijker and van Rijn formulae based on the three different prediction approaches is given in Figure 6.5. Data set 3 measured on September 5, 2000 representing the average tidal range (3.1m) is chosen to depict the example. During this day the total load transport in this cross section varied between 0.5 up to 4.3kg/ms.



(a) Bijker



(b) van Rijn

Figure 6.5: Comparison between measured and predicted total load transport in cross section T2

From the measurement, it can be observed that during the ebb phase the maximum total load transport in Suederpiep channel is almost equally distributed along the southern and northern parts of the channel. Higher maximum total load transport is observed during the flood phase and concentrated in the southern bank of the channel. It is expected that during the slack water no sediment material is transported. Unfortunately, the measurement does not show a clear distinction between the conditions during the slack water and flood or ebb phase. Total load transport of about 0.5 to 1kg/ms can still be observed in the entire cross section around slack water and remains until short before increasing velocity.

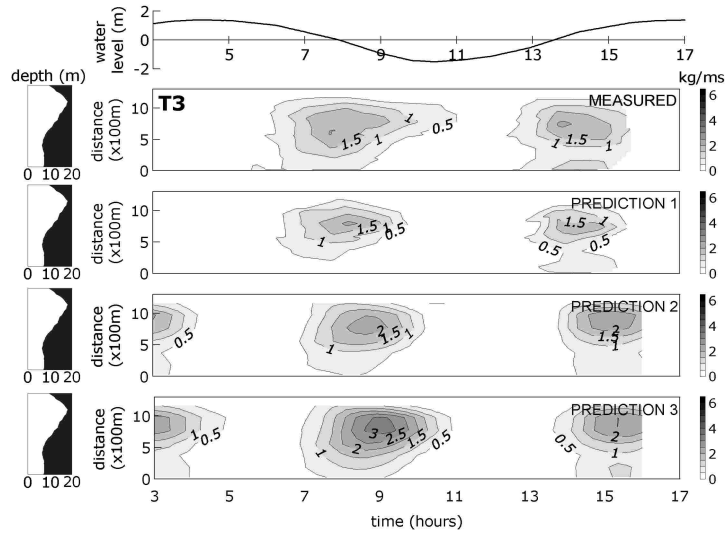
Neglecting the condition during the slack water, the predicted total load transports using the three different approaches perform a comparable agreement especially during maximum velocity in the ebb and flood phases. However, an overestimation in the predicted total load transport during the ebb phase of up to a factor of 3 can be observed especially in the use of van Rijn formulae based on the simulated velocity. The tendency of increasing total load transports during the flood phase is not shown by the prediction results based on the numerically simulated velocity. Although such a tendency is shown by the prediction based on the locally measured velocity, the concentrated total load transport towards the southern bank of the channel can not be reproduced.

### 6.2.2.3 Piep channel

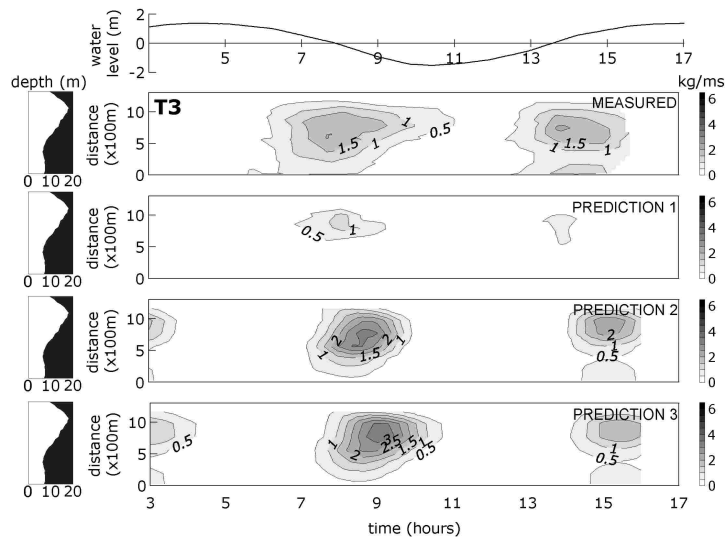
Figure 6.6 shows typical comparisons of total load transport dynamics in cross section T3 (Piep) predicted using Bijker and van Rijn formulae based on the three different prediction approaches. Data set 3 measured on September 6, 2000 representing the average tidal range (3.1m) is chosen to depict the example. During this day the total load transports varied between 0 to 2.1kg/ms.

From the measurement, it can be observed that higher total load transports are concentrated mainly in the middle part of the channel. The maximum total load transports during ebb and flood phases are approximately equal. During the ebb phase the decreasing total load transports are sustained longer towards the slack water. This can be seen closer to the northern part of the cross section. During the flood phase the maximum total load transports are somehow split into two parts: in the northern and southern part of the channel.

The tendency of zero total load transports during the slack water and maximum total load transports during ebb or flood phases can be properly predicted. A time lag of about 1 hour is shown by the prediction based on the simulated velocity. In some cases the predicted maximum total load transports tend to be slightly overestimated with a deviation of up to a factor of 1.5. The trend of sustaining total load transport during the ebb phase towards the slack water can be reproduced using the advection-diffusion equation and based on the simulated velocity.



(a) Bijker



(b) van Rijn

Figure 6.6: Comparison between measured and predicted total load transport in cross section T3

## 6.3 Cross sectional and tide-integrated transports

The prediction of total load transport in cross section (cross sectional integrated transport) is investigated here. The total load transport in cross section is an integration of total load transport (per unit width) in all measuring stations of a transect. This represents the total transported sediment over the entire cross section. The result is visualised as a time series plot. In the plot, the measured and predicted values are shown and evaluated. In case of using the prediction approach based on the locally measured velocity, the continuously measured current velocity profiles along the transect are used to estimate the bed shear stresses and hence the total load transports. In case of using the prediction approach based on the numerical flow simulation, the cross sectional integrated total load transport predictions are provided by the model.

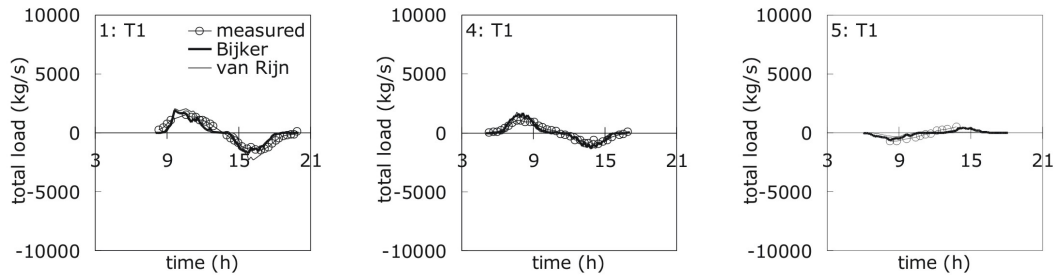
In the investigation, the tendency of the predicted values to be within the order of magnitude of the measured ones is analysed and quantified in terms of absolute and relative error as well as percentage of data within a factor of 2. The relationship between the predicted magnitudes and the tidal ranges is explored. Additionally, the tendency of the predicted values to show flood or ebb domination is discussed. For this particular case, the tide-integrated transport is calculated by integrating all total load transport in cross section over a tidal phase. Representative examples of this investigation are given. Data sets 1, 4 and 5 are chosen to represent the three different tidal conditions (i.e. maximum, average and minimum tidal ranges).

### 6.3.1 Cross sectional integrated transport

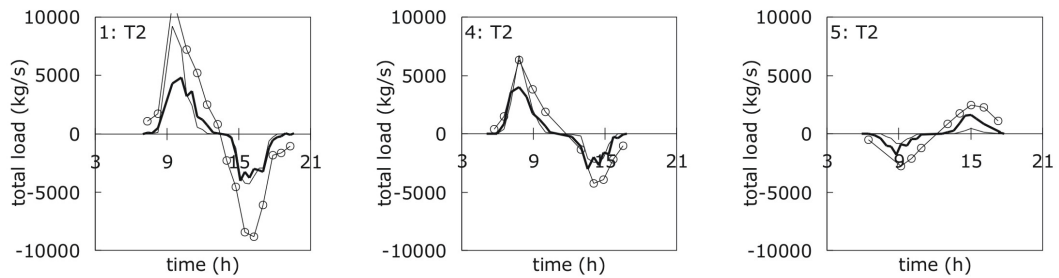
Figures 6.7, 6.8 and 6.9 show consecutively the comparisons between the predicted and measured total load transport in the cross section based on the three different prediction approaches: prediction based on the locally measured velocity and using empirical sand transport formulae (Prediction 1), prediction based on the numerical velocity simulation and using empirical sand transport formulae (Prediction 2) and prediction based on the numerical velocity simulation and using the solution of advection-diffusion equation (Prediction 3).

The predicted total load transports in cross sections are generally within the order of magnitude of the measured ones. The cyclic pattern of total load transport dynamics in cross section over a tidal cycle can be followed. The tendency of the decreasing magnitude of predicted total load transports in cross sections with decreasing tidal range can be observed. Bearing in mind the accuracy of the field estimation, the overall accuracy of the predicted values is of approximately 1ton/s. In terms of relative error the overall accuracy of the predicted values is of about 50%. For the prediction approach based on the numerically simulated velocity a time lag of the maximum magnitude of load transports in cross sections can be seen.

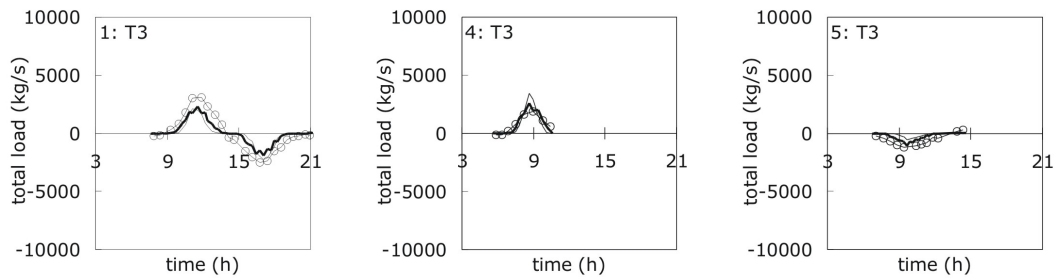
Good agreement is generally achieved by all prediction approaches in cross section T1 (Norderpiep). In this channel, the decreasing magnitudes of total load transports



(a) Cross section T1, data set 1, 22 March 2000, tidal range 4m (b) Cross section T1, data set 4, 12 Sep. 2000, tidal range 3.3m (c) Cross section T1, data set 5, 5 Dec. 2000, tidal range 2.3m



(d) Cross section T2, data set 1, 21 March 2000, tidal range 4.1m (e) Cross section T2, data set 4, 12 Sep. 2000, tidal range 3.3m (f) Cross section T2, data set 5, 5 Dec. 2000, tidal range 2.3m



(g) Cross section T3, data set 1, 23 March 2000, tidal range 4.2m (h) Cross section T3, data set 4, 13 Sep. 2000, tidal range 3.5m (i) Cross section T3, data set 5, 6 Dec. 2000, tidal range 2.5m

**Figure 6.7: Comparison of measured and predicted total load transport in cross sections T1, T2 and T3 using empirical formulae**

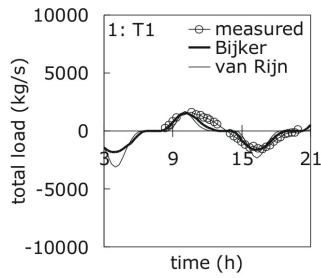
in cross sections with decreasing tidal range can be clearly observed. The average deviation of the predicted values with respect to those measured from the field is of about 0.3ton/s. The average percentage of data within a factor of 2 is of about 50%. Bijker formulae generally perform better agreement with the measurement. The best prediction is achieved by the use of advection-diffusion equation. In this channel the predicted maximum magnitude of total load transport in cross section does not show a significant time lag.

In cross section T2 (Suederpiep) all prediction approaches tend to give an underestimated results. Major disagreement occur in the prediction results at maximum tidal range. The corresponding deviation can be up to a factor of 4. However, the decreasing magnitudes of total load transports in cross sections with decreasing tidal range can still be observed. The average deviation of the predicted values with respect to those measured from the field is of about 1.5ton/s. The average percentage of data within a factor of 2 is of about 30%. The best prediction is achieved by the use of advection-diffusion equation. Bijker and van Rijn formulae tend to perform a comparable agreement.

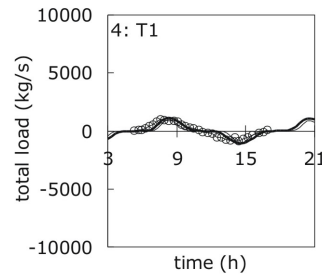
All approaches perform similar tendency of the predicted values in cross section T3 (Piep). Underestimated results can generally be observed for the extreme (maximum and minimum) tidal ranges. Larger disagreement occurs in the prediction results at maximum tidal range. The decreasing magnitudes of total load transports in cross sections with decreasing tidal range can not be straightly observed. However, significant reduction of the magnitude during the minimum tidal range can be seen. The average deviation of the predicted values is less than 1ton/s. The average percentage of data within a factor of 2 is of about 35%. Better prediction is performed by the use of numerically simulated velocity. Bijker formulae generally perform better agreement with the measurement.

Having investigated all prediction approaches in each cross section, it can be concluded that comparable performance quality is achieved by the prediction approach based on the locally measured and numerically simulated velocity. In the first case, the predicted value tend to show a good agreement of the peak transport and in the latter case a time lag of the peak transport occur in some cross sections (T2 and T3) and almost in all measuring periods. However, the prediction approach based on the numerically simulated velocity perform better agreement in terms of the average magnitude of the predicted values.

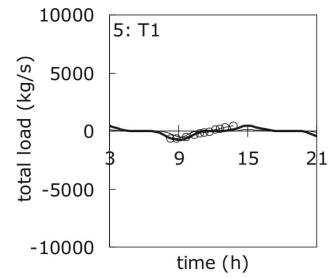
In order to reproduce the main features of sediment transport dynamics in the investigation area, this investigation also confirms the appropriateness of using Bijker formulae based on the numerically simulated velocity and the solution of advection-diffusion equations. Careful attention should be paid to the lag of the predicted total load transport in cross section T2 (Suederpiep) and T3 (Piep), as well as the underestimation of the predicted values in cross section T2 (Suederpiep). This limits the quality of the prediction.



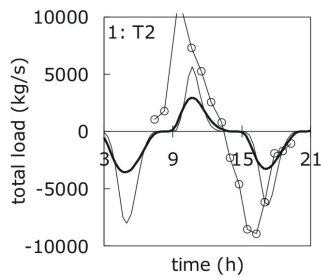
(a) Cross section T1, data set 1, 22 March 2000, tidal range 4m



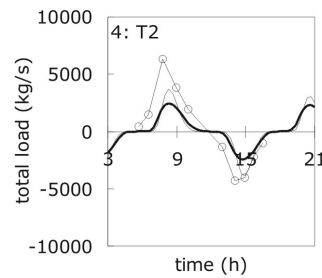
(b) Cross section T1, data set 4, 12 Sep. 2000, tidal range 3.3m



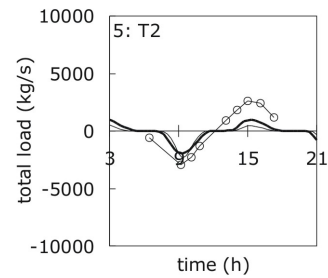
(c) Cross section T1, data set 5, 5 Dec. 2000, tidal range 2.3m



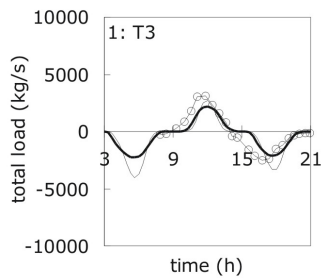
(d) Cross section T2, data set 1, 21 March 2000, tidal range 4.1m



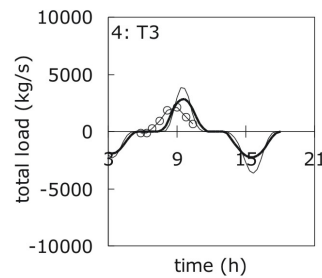
(e) Cross section T2, data set 4, 12 Sep. 2000, tidal range 3.3m



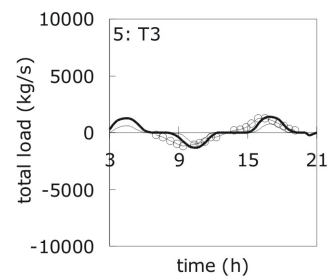
(f) Cross section T2, data set 5, 5 Dec. 2000, tidal range 2.3m



(g) Cross section T3, data set 1, 23 March 2000, tidal range 4.2m



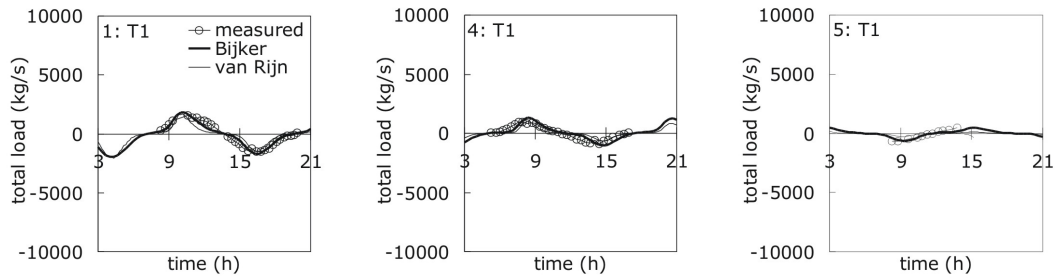
(h) Cross section T3, data set 4, 13 Sep. 2000, tidal range 3.5m



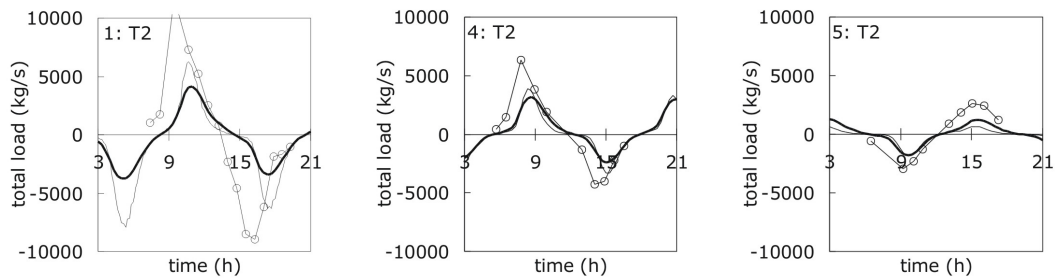
(i) Cross section T3, data set 5, 6 Dec. 2000, tidal range 2.5m

**Figure 6.8: Comparison of measured and predicted total load transport in cross sections T1, T2 and T3 using equilibrium formulae**

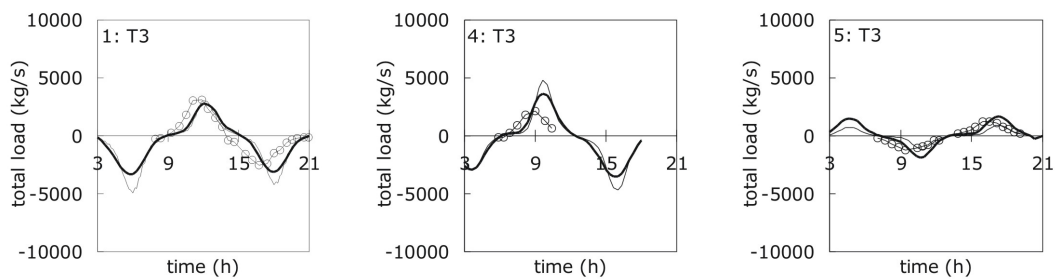




(a) Cross section T1, data set 1, 22 March 2000, tidal range 4m (b) Cross section T1, data set 4, 12 Sep. 2000, tidal range 3.3m (c) Cross section T1, data set 5, 5 Dec. 2000, tidal range 2.3m



(d) Cross section T2, data set 1, 21 March 2000, tidal range 4.1m (e) Cross section T2, data set 4, 12 Sep. 2000, tidal range 3.3m (f) Cross section T2, data set 5, 5 Dec. 2000, tidal range 2.3m



(g) Cross section T3, data set 1, 23 March 2000, tidal range 4.2m (h) Cross section T3, data set 4, 13 Sep. 2000, tidal range 3.5m (i) Cross section T3, data set 5, 6 Dec. 2000, tidal range 2.5m

**Figure 6.9: Comparison of measured and predicted total load transport in cross sections T1, T2 and T3 using advection-diffusion equation**

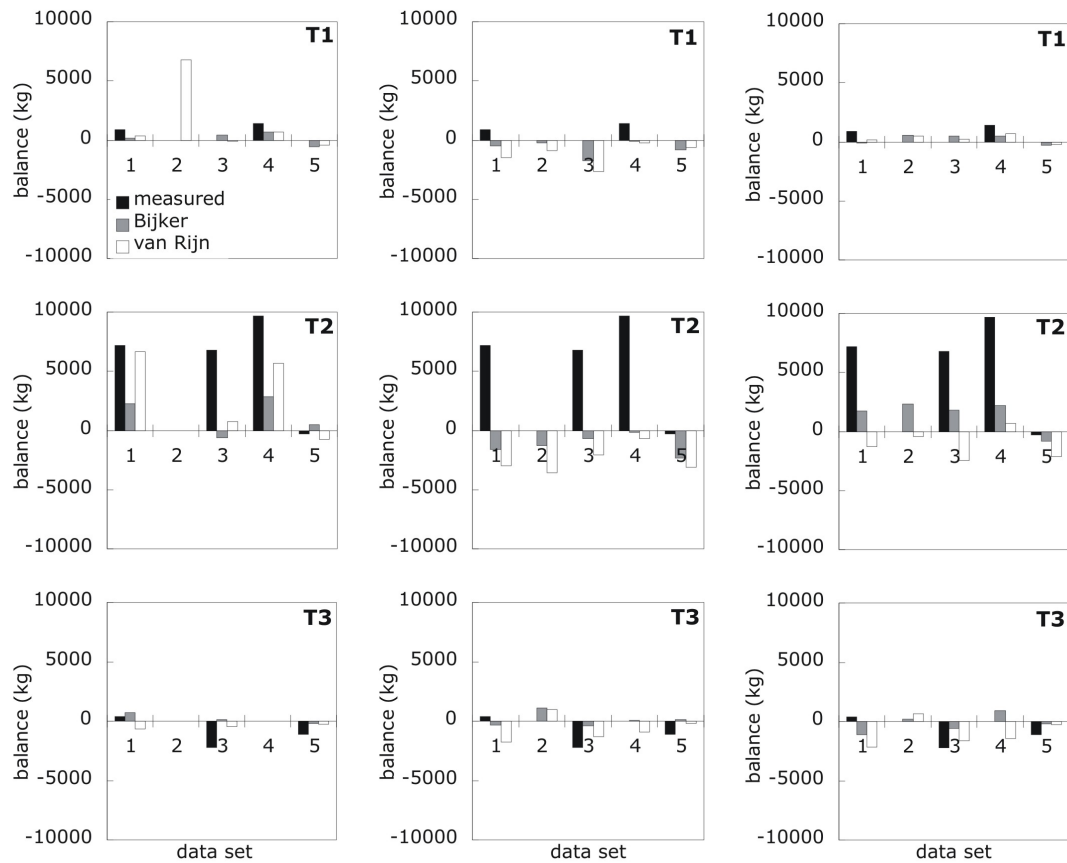
### 6.3.2 Tide-integrated transport

It is in fact very difficult to evaluate if the prediction results can also show the trend of ebb or flood domination (negative or positive balance) of the transported sediment material in a cross section. This is due to the uncertainty of the corresponding estimated values from the field. The uncertainty is resulted from the inaccuracy and the accumulated uncertainties of the measurement and estimation techniques of the total load transport in a measuring cross section. However, the negative or positive balance of the transported sediment material in a cross section can still be calculated. Based on this calculation, a comparison of measured and predicted balance values is carried out. In the comparison, the tendency of ebb or flood domination is evaluated.

In Figure 6.10 comparisons between measured and predicted sediment balances in cross sections T1, T2 and T3 are shown. The calculation results presented in Figure 6.10(a) are based on the locally measured current velocity, whereas in Figures 6.10(b) and 6.10(c) are based on the numerically simulated velocity. The latter comprises calculation using equilibrium transport formulae and the solution of advection-diffusion equations. Only 9 (out of 15) balance calculations can be observed from the field measurement. This includes 2 calculations from the cross section T1 (data sets 1 and 4), 4 calculations from the cross section T2 (data sets 1, 3, 4 and 5) and 3 calculations from the cross section T3 (data sets 1, 3 and 5). The non available balance calculations are due to the incomplete measurement over the entire tidal cycle. Based on this limited available calculation, it can be observed that cross sections T1 and T2 tend to be flood dominated whereas cross sections T3 tend to be ebb dominated.

In case of using empirical equation and based on the locally measured current velocity, Bijker and van Rijn formulae show respectively 6 and 8 (out of 9) balance calculations that demonstrate the same trend with the field measurement. However, in terms of the magnitude of the sediment balance, the predicted values tend to be underestimated. In case of using the equilibrium sand transport formulae and based on numerical flow field simulation results, only 2 (out of 9) balance calculations show the same trend with respect to those shown by the field measurement. Bijker and van Rijn formulae tend to show a comparable performance quality. In case of using the solution of advection-diffusion equations and based on numerical flow field simulation results, Bijker and van Rijn formulae show respectively 7 and 5 (out of 9) balance calculations that agree well with the field measurement.

It is confirmed here that comparable performance of sediment balance calculations is given by the prediction approach using empirical equation and based on the locally measured current velocity, as well as using the solution of advection-diffusion equations and based on numerical flow field simulation results. In the first case, van Rijn formulae are relatively better than Bijker. In the latter case, Bijker formulae perform better agreement with the measurement. In most cases, the predicted sediment balance tends to be underestimated.



(a) Using empirical equation and based on locally measured current velocity

(b) Using equilibrium sand transport formulae and based on numerical flow field simulation results

(c) Using solution of advection-diffusion equations and based on numerical flow field simulation results

**Figure 6.10: Comparison of measured and estimated balance of total transported sediment in cross section over a tidal cycle**

## 6.4 Modelling applications

Results from the validated model are applied here to depict the spatial distribution of depth-integrated concentrations and total load transports over the entire domain of investigation. Several typical conditions are presented. It considers the variability over a temporal series: around slack waters and during maximum ebb or flood phases. The prediction approach based on the numerically simulated velocity and using the solution of advection-diffusion equation combined with Bijker formulae are chosen to illustrate those dynamics.

Figure 6.11 shows the predicted concentration distribution in the spring tide. During low water, background concentration of about  $0.05$  to  $0.1\text{kg/m}^3$  is distributed along the main channels. Higher background concentration of up to  $0.15\text{kg/m}^3$  is observed in the Piep channel. During the flood phase, sediment is entering the bight through the Norderpiep and Suederpiep channels. The sediment concentration increases from the background level up to a factor of 4 (from  $0.05$  to  $0.2\text{kg/m}^3$ ). During the high water background concentration of about  $0.05$  to  $0.1\text{kg/m}^3$  is again distributed along the tidal channels. Higher background concentration of up to  $0.15\text{kg/m}^3$  is also found in the Piep channel. During the ebb phase, sediment is leaving the bight through the Norderpiep and Suederpiep channels. Higher concentration is observed in the Piep channel. With respect to those observed during the flood phase, a tendency of decreasing concentration magnitudes over the entire domain can be observed.

Figure 6.12 shows the predicted concentration dynamics in the neap tide. The distribution of depth-integrated concentrations is found to be similar to those observed in the spring tide. Higher concentration is found mainly in the main channels. Significant reduction of concentration magnitude of up to a factor of 2 is observed. The depth-integrated maximum concentration is only up to  $0.15\text{kg/m}^3$ . The background concentration decreases up to  $0.05\text{kg/m}^3$ .

Figure 6.13 shows the predicted total load transport dynamics during the spring tide. Within this period no transport dynamics during the slack water can be observed. However a relatively high transport of up to  $1.5\text{kg/ms}$  can be observed in the Piep channel during the high water. During the flood phase sediment is entering the bight through the Norderpiep and Suederpiep channels. It can be observed that higher total load transport is moved through the Suederpiep channel. The maximum total load transport can be up to  $4\text{kg/ms}$ . During the ebb phase the sediment is transported seawards and almost equally distributed into the Norderpiep and Suederpiep channels. Higher total load transport is observed in the Piep channel.

Figure 6.14 shows the predicted total load transport dynamics during the neap tide. With respect to those predicted for the spring tide condition, the predicted total load transport during the neap tide experiences a significant reduction of up to a factor of 4. Less material is transported during the neap tide. The maximum total load transport is only up to  $1\text{kg/ms}$ .

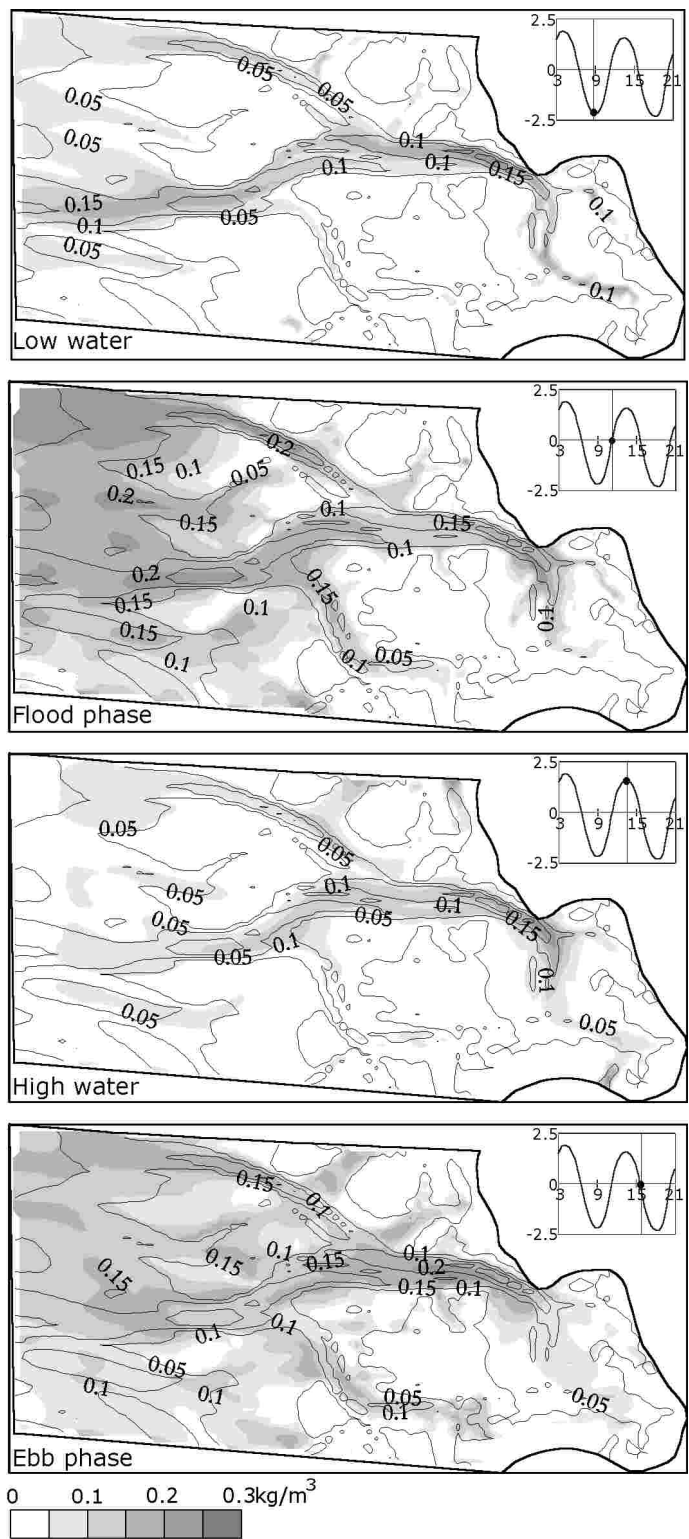


Figure 6.11: Predicted concentration dynamics during a spring tide

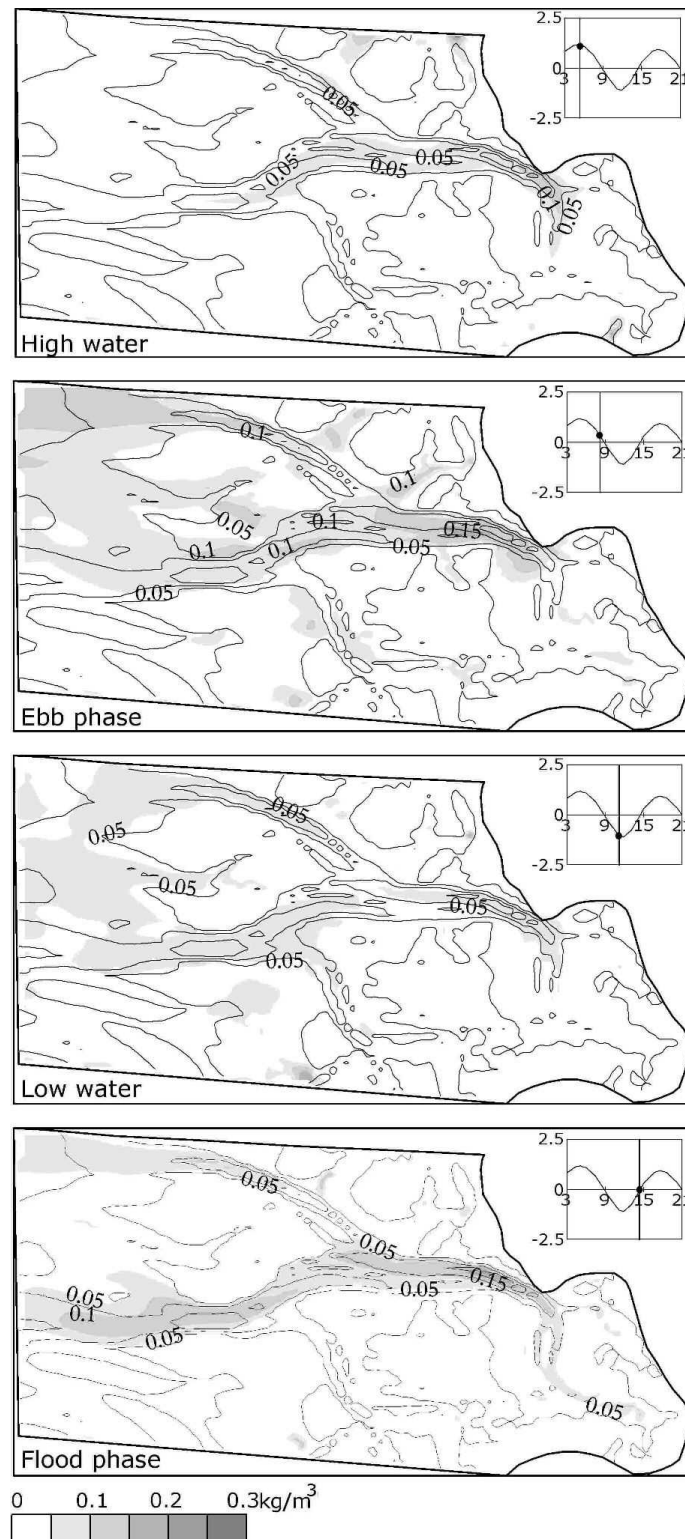


Figure 6.12: Predicted concentration dynamics during a neap tide

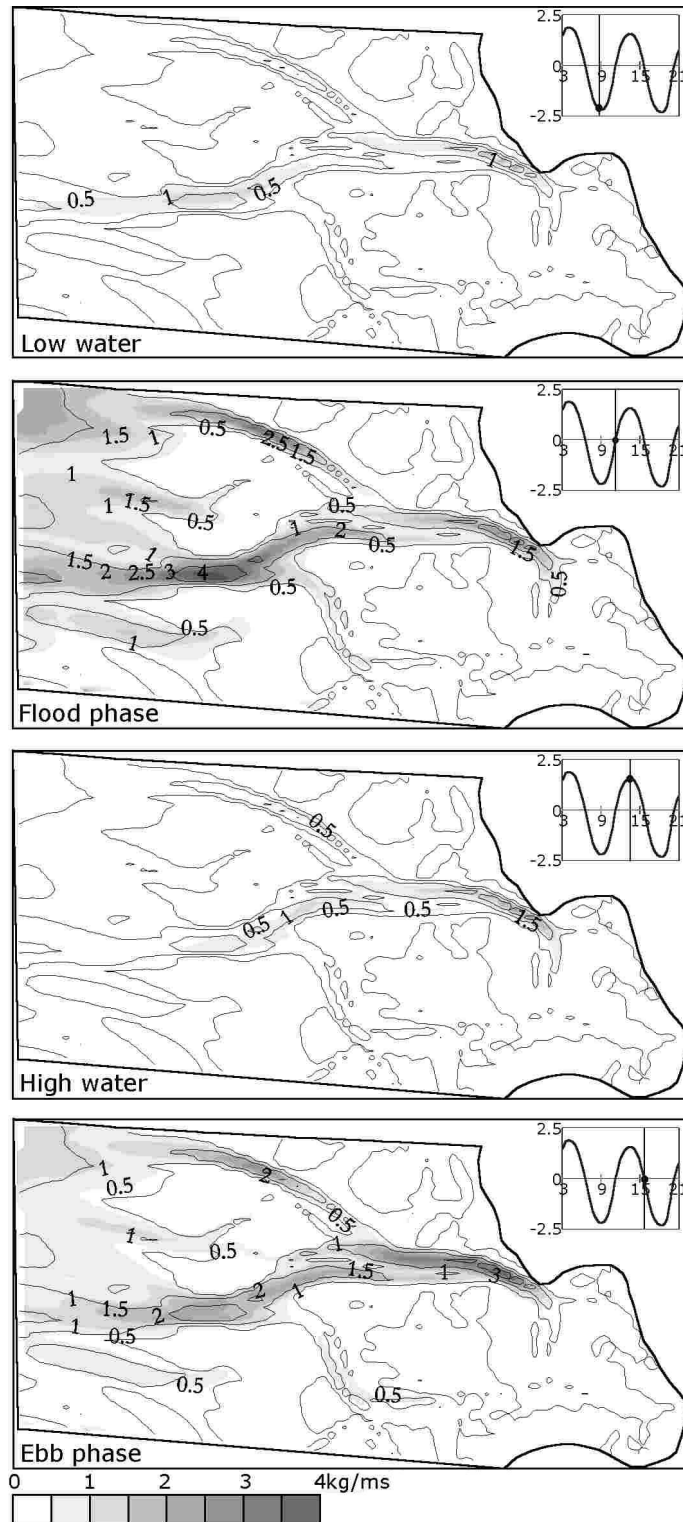


Figure 6.13: Predicted total load transport dynamics during a spring tide

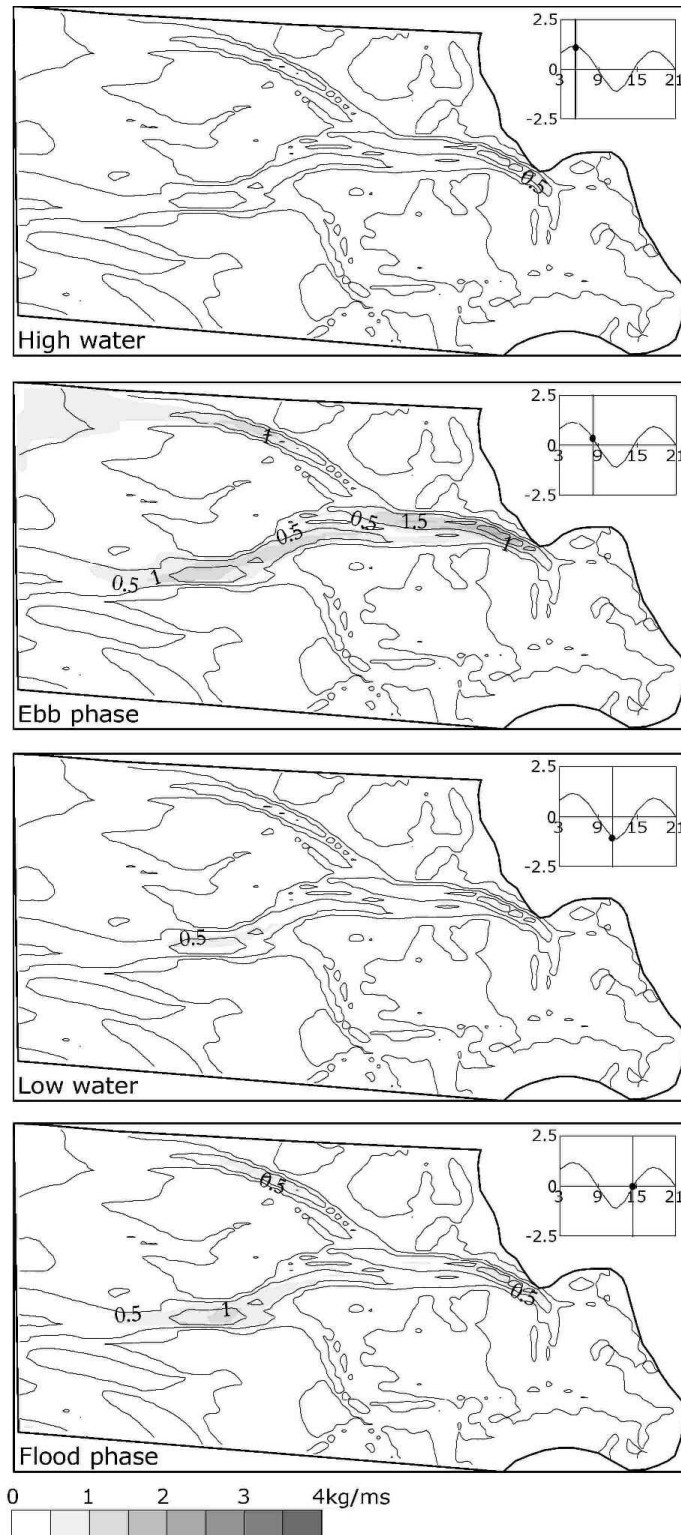


Figure 6.14: Predicted total load transport dynamics during a neap tide



## 6.5 Discussion

The evaluation of the depth-integrated and total load transport prediction has been performed. The results based on the three different prediction approaches were compared and analysed. The ability of the prediction approaches to reproduce the significant features of concentration and transport dynamics as well as the cross sectional and tide-integrated transport is discussed. It has been confirmed that the best prediction result is provided by the simulated velocity and using the solution of advection-diffusion equation. Based on this approach the application of the prediction result was also given. It comprises the dynamics of concentration and total load transport during different periods.

From the prediction results it has been found that the contribution of the bed load transport to the total load transport is less significant. A test is made with the prediction results during the spring tide using Bijker formulae based on the simulated velocity and using the solution of advection-diffusion equation. Figure 6.15 illustrate the contribution of suspended load to the total load transport around maximum flood velocity. The average percentage of bed load transport with respect to the total load transport is only 2%. In the main channel it is found that the contribution of the suspended load transport is equal or higher than 99%. In the tidal flats a value of about 96 to 98% is observed. It confirms the importance of suspended sediment as the primary mode of transport in the investigation area.

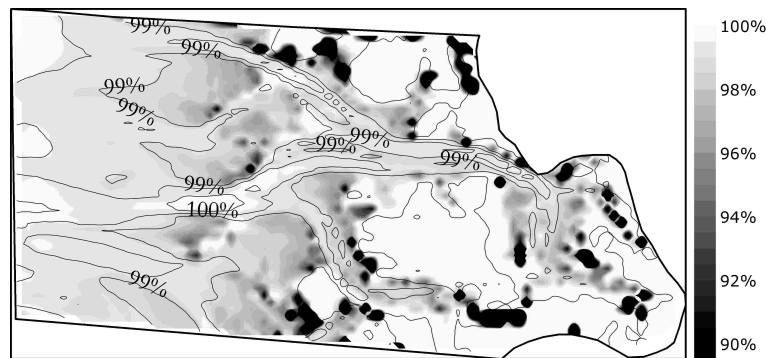


Figure 6.15: Contribution of suspended load to the total load transport



## Chapter 7

# Conclusions

Study of fine sand transport process based on field measurements and numerical modelling has been carried out. The reliability of measuring techniques for capturing site-specific sediment transport dynamics has been investigated and the characterisation of sediment transport dynamics in the investigation area has been described. The use of empirical sand transport formulae for simulating sediment transport dynamics and their incorporation in a numerical model have been evaluated.

### **The reliability of measuring techniques for capturing site specific sediment transport dynamics**

The sediment transport rate is indirectly obtained employing an ADCP for current measurement and an optical beam transmissometer calibrated with filtrated water samples for sediment concentration measurement. For converting the optical transmission measurement to suspended sediment concentration, a calibration curve developed based on around 200 direct sampling concentrations is used. The accuracy of the measuring devices for indirectly measuring the sediment transports is assessed by estimating the uncertainties resulted from the measured data and summarised as follows:

- The uncertainty of ADCP for water current measurement in a tidal channel is estimated based on the study conducted by Jiménez-González et al. [2003] and van Rijn et al. [2002a]. From the studies, an absolute error of ranging from 0.05 to 0.14m/s for point measurement is obtained.
- The uncertainty of the optical beam transmissometer is estimated based on the comparison between direct sample concentrations with the predicted concentrations using the calibration curve. The comparison gives an approximate relative error of 30%.

Based on field measurements, the distribution of sediment concentrations and transports over the water column can be depicted. The variability of depth-integrated concentration and sediment transport in different locations with respect to the neap and spring tides can be described. The total load transport as well as the accumulated material transported in the measuring cross sections during a tidal cycle can also be estimated.

An investigation to the performance of acoustic technology using an ADCP for estimating sediment concentration in the water column was also done. In the investigation, several empirical approaches for converting the acoustic echo intensity to suspended sediment concentration were evaluated. The results confirmed a comparable estimation performance with respect to those given by an independent optical beam transmissometer.

### **The nature of sediment transport dynamics in the investigation area**

Within the limitation of device accuracy and measurement during calm weather period, field measurements show several representative features and principal processes of sediment transport in the investigation area. The variability of sediment transport dynamics over temporal (observation periods) and spatial (observation points) series can be distinctively drawn. Within temporal series, the variability of sediment transport during the ebb and flood phases as well as during the neap and spring tides was described. The dependency of the sediment transport magnitude on the tidal range was indicated. Within spatial series, unique behaviour of sediment transport magnitudes due to the nature of local bed morphology and bed sediment composition is properly captured. The nature of sediment transport dynamics in the investigation area is summarised as follows:

- The composition of the sediments is mainly very fine to fine sands with varying fractions of silt and clay. The bed sediment is mainly well sorted. The sizes of the particles in suspension were found to be much smaller than the ones taken from the bed samples being very fine silt to very fine sand.
- Due to the small sizes of the particles transported in suspension and high turbulence levels, a background concentration level is always present. A clear dependency of the magnitude of the background concentrations with the tidal conditions and measuring locations could not be identified. The vertical distribution of the suspended sediment concentrations and suspended load transports is fairly uniform. As a result most of the sediment is transported in suspension.
- A clear dependency of the amount of suspended sediment concentration and suspended load transport on the tidal range was identified. Higher suspended

sediment concentrations and suspended load transports pertain to higher tidal range.

- Although the balance of sediment material can be estimated from the field measurement, still, no distinct pattern in terms of ebb and flood domination of the transported sediment in the measuring cross sections could be concluded. However, the tendency of flood domination in the Norderpiep and Suederpiep channels are identified, whereas the Piep channel tends to show an ebb domination.
- Suederpiep channel is responsible for most of the suspended sediment entering and leaving the area. In the Norderpiep channel, less sediment materials are transported.

### **Prediction of sediment transport dynamics**

Sand transport formulae selected in this study and their incorporation in a numerical model have been found to be able to handling the condition outside the range of particle size from where they were derived. This confirms the appropriateness of sand transport formulae for modelling fine sand dynamics with presence of mud. Uniform values of median size of bed sediment, bed roughness height and sediment settling velocity were employed. In the prediction of sediment transport dynamics, three different approaches were used. The corresponding results are summarised as follows:

1. Using empirical equations and based on locally measured current velocity (for estimating the bed shear stress):
  - The estimated bed shear stresses from the locally measured current velocities can be reasonably used to predict total load transport dynamics. The predicted results are found to be within the order of magnitude of the measured values.
  - The dynamics of concentration and total load transport over a tidal cycle can be reasonably predicted. Bijker formulae generally show better prediction performance than van Rijn formulae.
  - During slack waters the predicted depth-integrated concentration is always zero and slightly underestimated the total load transport prediction mainly during accelerating and decelerating velocities.

- Most of the trend of ebb or flood domination (negative or positive sediment balance) of total load transports in cross sections can be reasonably reproduced.
2. Using equilibrium sand transport formulae and based on numerical flow field simulation results:
- Equilibrium sand transport formulae can be used to give total load transport predictions that perform a quite good agreement with the measurement. Due to the presence of background concentration during slack waters the concentration dynamics can not be properly reproduced.
  - Bijker formulae generally show better prediction performance than van Rijn formulae. The use of equilibrium sand transport formulae and based on numerical flow field simulation results show a comparable performance with the previously aforementioned approach (i.e. using empirical equations and based on locally measured current velocity for estimating the bed shear stress).
  - The predicted total load transports in cross sections tend to be underestimated mainly during the accelerating and decelerating velocities. Most of the trend of ebb or flood domination of the predicted total load transports in cross sections can not be properly followed.
3. Using solution of advection-diffusion equations and also based on numerical flow field simulation results:
- The concentration dynamics can be reasonably reproduced. However, underestimation and overestimation during respectively slack water and peak velocity periods can still be observed. The total load transport predictions agree quite well with the measurement.
  - Most of the trend of ebb or flood domination (negative or positive sediment balance) of total load transports in cross sections can be reasonably reproduced.
  - With respect to those given by van Rijn formulae, Bijker formulae perform a better agreement with the measurement in predicting concentration and sediment transport dynamics.

A better insight into the understanding of the dynamics of fine sediment transport is gained through the combined application of field measurement and modelling. The best results are performed by modelling using the solution of advection-diffusion equations. For obtaining better prediction results, the use of non-uniform setting parameters are recommended. This should consider mainly the representative size of bed sediment ( $d_{50}$  and  $d_{90}$ ) and effective bed roughness height ( $k_s$ ).





# References

- Aberle, J. & Smart, G. M. (2003). *The Influence of Roughness Structure on Flow Resistance on Steep Slopes*. *Journal of Hydraulic Research*, 41(3):259–269.
- Abott, J. E. & Francis, J. R. D. (1977). *Saltation and Suspension Trajectories of Solid Grains in a Water Stream*. *Proc. Royal Soc.*, 284(A 1321).
- Bagnold, R. A. (1956). *The Flow of Cohesionless Grains in Fluids*. *Proc. Royal. Soc. Philos. Trans. London*, 249.
- Bagnold, R. A. (1973). *The Nature of Saltation and of Bed-Load Transport in Water*. *Proc. Royal Soc.*, (A 332).
- Bayram, A., Larson, M., Miller, H. C., & Kraus, N. C. (2001). *Cross-shore Distribution of Longshore Sediment Transport: Comparison between Predictive Formulas and Field Measurements*. *Coastal Engineering*, 44:79–99.
- Bijker, E. W. (1971). *Longshore Transport Computations*. *Journal of the Waterways, Harbors and Coastal Engineering Division*, 97(WW4):687–701.
- Black, K. S. (1997). *Microbial Factors Contributing the Erosion Resistance in Natural Cohesive Sediments*. In: Burt, N., Parker, R., & Watts, J., (Editors), *Cohesive Sediments*, pages 231–244. John Wiley and Sons, Ltd., Chichester, England.
- Bonnefille, R. (1963). *Essais de Synthèse des Lois de Début d'entraînement des Sédiments sous l'action d'un Courant en Régime Uniforme*. *Bull. du CERC*, (5). Chatou.
- Campbell, D. E. & Spinrad, R. W. (1987). *The Relationship Between Light Attenuation and Particle Characteristics in a Turbid Estuary*. *Estuarine, Coastal and Shelf Science*, 25: 53–65.
- Cheng, R. T., Ling, C. H., & Gartner, J. W. (1999). *Estimates of Bottom Roughness Length and Bottom Shear Stress in South San Fransisco Bay, California*. *Journal of Geophysical Research*, 104(C4):7715–7728.
- Cowell, P. J. & Thom, B. G. (1997). *Morphodynamics of Coastal Evolution*. In: Carter, R. W. G. & Woodroffe, C. D., (Editors), *Coastal Evolution. Late Quaternary Shoreline Morphodynamics*. Cambridge University Press, Cambridge, UK.

- Damgaard, J. S., van Rijn, L. C., Hall, L. J., & Soulsby, R. L. (2001). *Intercomparison of Engineering Methods for Sand Transport*. In: van Rijn, L. C., Davies, A. G., van de Graaf, J., & Ribberink, J. S., (Editors), *Sediment Transport Modelling in Marine Coastal Environments*, pages CJ1–CJ12. Aqua Publications, Amsterdam, The Netherlands.
- Davies, A. G., van Rijn, L. C., Damgaard, J. S., van de Graaff, J., & Ribberink, J. S. (2002). *Intercomparison of Research and Practical Sand Transport Models*. *Coastal Engineering*, (46):1–23.
- Deines, K. L. (1999). *Backscatter Estimation Using Broadband Acoustic Doppler Current Profilers*. In: Anderson, S. P., Terry, E. A., White, J. A. R., & William, A. J., (Editors), *Proceedings of the IEEE 6th Working Conference on Current Measurement Technology*, pages 249–253.
- Dyer, K. R. (1986). *Coastal and Estuarine Sediment Dynamics*. Wiley and Sons, Chichester, England, 2nd edition.
- Efron, B. & Tibshirani, R. J. (1993). *An Introduction to the Bootstrap*. Chapman and Hall, New York, USA.
- Einstein, H. A. (1950). *The Bed-load Function for Sediment Transportation in Open Channel Flow*. Technical Bulletin, US Dept. of Agriculture, (1026).
- Einstein, H. A. & Krone, R. B. (1962). *Experiments to Determine Modes of Cohesive Sediment Transport in Salt Water*. *Journal of Geophysical Research*, 67(4).
- Fedderson, F., Gallagher, E. L., Guza, R. T., & Elgar, S. (2003). *The Drag Coefficient, Bottom Roughness, and Wave-breaking in the Nearshore*. *Coastal Engineering*, 48:189–195.
- Flagg, C. N. & Smith, S. L. (1989). *On the Use of the Acoustic Doppler Current Profiler to Measure Zooplankton Abundance*. *Deep-Sea Research*, 36(3):455–474.
- Francis, J. R. D. (1973). *Experiments on the Motion of Solitary Grains along the Bed of a Water Stream*. *Proc. Royal Soc.*, (A 332).
- Fredsøe, J. & Deigaard, R. (1992). *Mechanics of Coastal Sediment Transport*. World Scientific, Singapore.
- Freitag, P., McPhaden, M., Meinig, C., & Plimpton, P. (2003). *Mooring Motion Bias of Point-Doppler Current Meter Measurement*. In: Rizoli, J. A., (Editor), *Proceedings of the IEEE 7th Working Conference on Current Measurement Technology*. San Diego, USA.
- Frijlink, H. C. (1952). *Discussion des formules de débit solide de Kalinske, Einstein et Meyer-Peter et Mueller compte tenue des mesures récentes de transport des rivières Néerlandaises*. 2me Journal Hydraulique, pages 98–103. Société Hydraulique de France, Grenoble, France.

- Galappatti, R. (1983). *A Depth-integrated Model for Suspended Sediment Transport*. Communications in Hydraulics, pages 83–7. Delft University of Technology.
- Garabato, A. C. N., McDonagh, E. L., Steven, D. P., Heywood, K. J., & Sanders, R. J. (2002). *On the Export of Antarctic Bottom Water from the Weddell Sea*. Deep-Sea Research, II(49):4715–4742.
- Gartner, J. W. (2002). *Estimation of Suspended Solids Concentrations Based on Acoustic Backscatter Intensity: Theoretical Background*. Turbidity and Other Sediment Surrogates Workshop.
- Gordon, R. L. (1996). *Acoustic Doppler Current Profiler: Principles of Operation*. RD Instruments, San Diego, USA, 2nd edition.
- Green, M. O. & Black, K. P. (1999). *Suspended Sediment Reference Concentration under Waves: Field Observations and Critical Analysis of Two Predictive Models*. Coastal Engineering, 38:115–141.
- Griffin, M. S. & Mueller, D. S. (1998). *Three-dimensional Velocity Measurements from a Moving Boat*. Kentucky Water Resources Annual Symposium Proceedings.
- Gross, T. F. & Nowell, A. R. M. (1983). *Mean flow and Turbulence Scaling in a Tidal Boundary Layer*. Continental Shelf Research, (2):109–126.
- Hanes, D. M., Vincent, C. E., Huntley, D. A., & Clarke, T. L. (1988). *Acoustic Measurements of Suspended Sand Concentration in the C<sup>2</sup>S<sup>2</sup> Experiment at Stanhope Lane, Prince Edward Island*. Marine Geology, (81):185–196.
- Heywood, K. J., Scrope-Howe, S., & Barton, E. D. (1991). *Estimation of Zooplankton Abundance from Shipborne ADCP*. Deep-Sea Research, 38(6):677–691.
- Holdaway, G. P., Thorne, P. D., Flatt, D., Jones, S. E., & Prandle, D. (1999). *Comparison between ADCP and Transmissometer Measurements of Suspended Sediment Concentration*. Continental Shelf Research, (19):421–441.
- Huhta, C. & Ward, C. (2003). *Flow Measurement using an Upward-looking Argonaut-SW Doppler Current Meter*. In: Rizoli, J. A., (Editor), *Proceedings of the IEEE 7th Working Conference on Current Measurement Technology*. San Diego, USA.
- Jantschik, R., Nyffeler, F., & Donard, O. F. X. (1992). *Marine Particle Size Measurement with a Stream-scanning Laser System*. Marine Geology, (106):239–250.
- Jiménez-González, S., Mayerle, R., & Egozcue, J. J. (2003). *On the Accuracy of Acoustic Doppler Current Profilers for In-situ Measurements. A Proposed Approach and Estimations for Measurements in Tidal Channels*. In: Rizoli, J. A., (Editor), *Proceedings of the IEEE 7th Working Conference on Current Measurement Technology*. San Diego, USA.

- Ke, X., Collins, M. B., & Poulos, S. E. (1994). *Velocity Structure and Sea Bed Roughness Associated with Intertidal (Sea and Mud) Flats and Saltmarshes of the Wash U. K.* *Journal of Coastal Research*, 10(3):702–715.
- Kesper, J. (1992). *Sedimentdynamik ausgewälter Außensände vor der Schleswig-Holsteinischen Westküste*. PhD thesis, Christian Albrechts Universität, Kiel, Germany.
- King, C. A. M. (1959). *Beaches and Coasts*. Edward Arnold, London, UK.
- Komar, P. D. (1998). *Beach Process and Sedimentation*. Prentice Hall, New Jersey, USA, 2nd edition.
- Krishnappan, B. G. & Engel, P. (1997). *Critical Shear Stresses for Erosion and Deposition of Fine Suspended Sediments of the Fraser River*. In: Burt, N., Parker, R., & Watts, J., (Editors), *Cohesive Sediments*, pages 279–288. John Wiley and Sons, Ltd., Chichester, England.
- Krone, R. B. (1986). *The Significance of Aggregates Properties to Transport Process*. In: Mehta, A. J., (Editor), *Estuarine Cohesive Sediment Dynamics*, pages 66–84. Springer-Verlag, Heidelberg, Germany.
- Lane, A., Knight, P. J., & Player, R. J. (1999). *Current Measurement Technology for Near-shore Waters*. *Coastal Engineering*, (37):343–368.
- Le Hir, P., Bassoullet, P., & L'Yavanc, J. (1993). *Application of a Multivariate Transport Model for Understanding Cohesive Sediment Dynamics*. In: Mehta, A. J., (Editor), *Nearshore and Estuarine Cohesive Sediment Transport*, pages 467–485. American Geophysical Union, Washington, USA.
- Libicki, C., Bedford, K. W., & Lynch, J. F. (1989). *The Interpretation and Evaluation of a 3-MHz Acoustic Backscatter Device for Measuring Benthic Boundary Layer Sediment Dynamics*. *Journal of the Acoustical Society of America*, (85).
- Lick, W. & Huang, H. (1993). *Flocculation and the Physical Properties of Flocs*. In: Mehta, A. J., (Editor), *Nearshore and Estuarine Cohesive Sediment Transport*, pages 21–29. American Geophysical Union, Washington, USA.
- Liu, H. K. (1957). *Mechanics of Sediment-Ripple Formation*. *Journal of Hydraulic Division ASCE*, 83(HY2):1–21.
- Lu, Q. X. (2003). *Evaluation of Empirical Approaches for Converting Acoustic Backscatter to Suspended Sediment Concentration*. MSc thesis, Christian Albrechts Universität, Kiel, Germany.
- Mayerle, R. & Palacio, C. (2002). *Open Boundary Condition Approaches for Near Coastal Area Models*. In: *13th Congress of the Asia and Pacific Division of IAHR*. Singapore.

- Mayerle, R., Razakafoniaina, N., Palacio, C., & Pramono, G. H. (2002). *Bedforms and Equivalent Roughness Sizes in Tidal Channels*. River Flow 2002, IAHR. Louvain-la-Neuve, Belgium.
- Moody, J. A., Butman, B., & Bothner, M. H. (1987). *Near-bottom Suspended Matter Concentration on the Continental Shelf During Storms: Estimates Based on 'In-situ' Observations of Light Transmission and a Particle Size Dependent Transmissometer Calibration*. *Continental Shelf Research*, 7(6):609–628.
- Nichols, M. M. (1986). *Effects of Fine Sediment Resuspensions in Estuaries*. In: Mehta, A. J., (Editor), *Estuarine Cohesive Sediment Dynamics*, pages 5–42. Springer-Verlag, Heidelberg, Germany.
- Nikuradse, J. (1932). *Gesetzmäßigkeiten der Turbulente Strömung in Glatten Röhren*. Ver. Deut. Ing. Forschungsheft, (356).
- Palacio, C. (2001). *Meldorf Bight Flow Model: Calibration and Validation of the Flow Model using Extensive Field Measurement Data*. Technical Report 15-01, Coastal Research Laboratory - Christian Albrechts University, Kiel, Germany.
- Palacio, C., Winter, C., & Mayerle, R. (2001). *Set-Up of a Hydrodynamic Model for the Meldorf Bight*. In: *World Water and Environmental Resources Congress (ASCE/EWRI)*. Orlando, USA.
- Parchure, T. M. & Mehta, A. J. (1985). *Erosion of Soft Cohesive Sediment Deposits*. *Journal of Hydraulic Engineering, ASCE*, 111(10).
- Partheniades, E. (1965). *Erosion and Deposition of Cohesive Soils*. *Journal of the Hydraulic Division, ASCE*, 91(HY1).
- Partheniades, E. (1986). *A Fundamental Framework for Cohesive Sediment Dynamics*. In: Mehta, A. J., (Editor), *Estuarine Cohesive Sediment Dynamics*, pages 219–250. Springer-Verlag, Heidelberg, Germany.
- Partheniades, E. (1993). *Turbulence, Flocculation and Cohesive Sediment Dynamics*. In: Mehta, A. J., (Editor), *Nearshore and Estuarine Cohesive Sediment Transport*, pages 40–59. American Geophysical Union, Washington, USA.
- Patino, E. & Byrne, M. J. (2001). *Use of Acoustic Instruments for Estimating Total Suspended Solids Concentration in Streams. The South Florida Experience*.
- Poerbandono & Mayerle, R. (2003). *Effectiveness of Acoustical Backscatter Measurements from Acoustical Profilers for Estimation of Suspended Sediment Concentration*. In: Rizoli, J. A., (Editor), *Proceedings of the IEEE 7th Working Conference on Current Measurement Technology*. San Diego, USA.

- Poerbandono, Winter, C., & Mayerle, R. (2003). *Field Measurements of Sediment Dynamics in Tidal Channels: Preliminary Results*. In: *Proceedings of the 5th International Symposium on Coastal Engineering and Science of Coastal Sediment Process*. Florida, USA.
- Postma, H. (1967). *Sediment Transport and Sedimentation in the Estuarine Environment*. In: Lauff, G. H., (Editor), *Estuaries*, volume Publication No. 83, pages 158–179. American Association for the Advancement of Science, Washington, USA.
- PROMORPH (2003). *Prognose mittelfristiger Küstenmorphologieänderungen*. Christian-Albrechts-Universität zu Kiel. Schlussbericht.
- Razakafoniaina (2001). *Assessment of the Equivalent Bed Roughness Size in Tidal Channels on the Basis of Numerical Model Simulation and Side Scan Sonar Observations*. MSc thesis, Christian Albrechts Universität, Kiel, Germany.
- Roelvink, J. A. & van Banning, G. K. F. M (1994). *Design and Development of DELFT3D and Application to Coastal Morphodynamics*. In: Verwey, A., Minns, A. W., Babovic, V., & Maksimovic, C., (Editors), *Hydroinformatics '94*, pages 451–456. A. A. Balkema, Rotterdam, The Netherlands.
- Rouse, H. (1937). *Modern Conceptions of the Mechanics of Fluid Turbulence*. Trans. ASCE, 102:461–543.
- Schott, F. & Johns, W. (1987). *Half-year-long Measurements with a Buoy-mounted Acoustic Doppler Current Profiler in the Somali Current*. Journal of Geophysical Research, 92 (C5):5169–5176.
- Shields, A. (1936). *Anwendung der Ähnlichkeits-Mechanik und der Turbulenz-forschung auf die Geschiebebewegung*. Preussische Versuchsanstalt für Wasserbau und Schiffbau, Berlin.
- Simons, D. B. & Richardson, E. V. (1966). *Resistance to Flow in Alluvial Channels*. Geological Survey Prof. Paper, Washington, USA, (422-I).
- Simpson, M. R. (2001). *Discharge Measurements using a Broad-Band Acoustic Doppler Current Profiler*. Open File Report 01-1. USGS, California, USA.
- SonTek, Inc. (2002). *ADP Versatility in San Felipe, Mexico Deployment*. <http://www.sontek.com/apps/profiler/adp-sf/adp-sf.htm> (May 27th, 2002).
- Soulsby, R. L. (1997). *Dynamics of Marine Sands*. Thomas Telford Publications, London, UK.
- Störtenbecker, M. (1992). *Sedimentologische Bearbeitung von Profilen im Watt vor dem Hedwigenkoog/Büsum über Lasergranulometrie*. Diplomarbeit. Christian Albrechts Universität zu Kiel. Kiel, Germany.

- Teeter, A. M., Johnson, B. H., Berger, C., Stelling, G., Scheffner, N. W., Garcia, M. H., & Parchure, T. M. (2001). *Hydrodynamic and Sediment Transport Modeling with Emphasis on Shallow-water, Vegetated Areas (Lakes, Reservoirs, Estuaries and Lagoons)*. *Hydrobiologia*, 444:1–23.
- Thorne, P. D. & Hardcastle, P. J. (1991). *Application of Acoustic Backscattering to Measuring Suspended Sediment Concentration*. In: Soulsby, R. L. & Bettess, R., (Editors), *Euromech 262 - Sand Transport in Rivers, Estuaries and the Sea*. Balkema, Rotterdam, The Netherlands.
- Thorne, P. D., Vincent, C. E., Hardcastle, P. J., Rehman, S., & Pearson, N. (1991). *Measuring Suspended Sediment Concentrations using Acoustic Backscatter Devices*. *Marine Geology*, (98):7–16.
- Toorman, E. A. & Berlamont, J. E. (1993). *Mathematical Modeling of Cohesive Sediment Settling and Consolidation*. In: Mehta, A. J., (Editor), *Nearshore and Estuarine Cohesive Sediment Transport*, pages 167–183. American Geophysical Union, Washington, USA.
- Torfs, H. (1997). *Erosion of Mixed Cohesive/Non-cohesive Sediments in Uniform Flow*. In: Burt, N., Parker, R., & Watts, J., (Editors), *Cohesive Sediments*, pages 245–252. John Wiley and Sons, Ltd., Chichester, England.
- U. S. Army, Corps of Engineer (1986). *Engineering and Design Laboratory Soils Testing*. Department of the Army, U. S. A. Engineering Manual 1110-2-1906.
- Urlick, R. J. (1948). *The Absorption of Sound in Irregular Particles*. *Journal of the Acoustical Society of America*, 20(3):283–289.
- van den Berg, J. H. & van Gelder, A. (1989). *Scour and Fill Sequences in Flows over Very Fine Sand and Silt*. Proc. 4th Int. Conf. on Fluvial Sedimentology, Barcelona, Spain.
- van der Lee, W. T. B. (1998). *The Impact of Fluid Shear and the Suspended Sediment Concentration on the Mud Floc Size Variation in the Dollard Estuary, the Netherlands*. In: Black, K. S., Paterson, D. M., & Cramp, A., (Editors), *Sedimentary Process in the Intertidal Zone*, volume 139, pages 187–198. Geological Society, London.
- van der Linde, D. W. (1998). *Protocol for the Determination of Total Suspended Matter in Oceans and Coastal Zones*. Space Applications Institute, Marine Environment. EC Joint Research Centre, Ispra, Italy. Technical Note No. I.98.182.
- van Leussen, W. V. (1997). *The Kolmogorov Microscale as a Limiting Value for the Floc Sizes of Suspended Fine-grained Sediments in Estuary*. In: Burt, N., Parker, R., & Watts, J., (Editors), *Cohesive Sediments*, pages 45–62. John Wiley and Sons, Ltd., Chichester, England.
- van Rijn, L. C. (1984a). *Sediment Transport, Part I: Bed Load Transport*. *Journal of Hydraulic Engineering*, 110(10):1431–1456.

- van Rijn, L. C. (1984b). *Sediment Transport, Part II: Suspended Load Transport*. Journal of Hydraulic Engineering, 110(11):1613–1641.
- van Rijn, L. C. (1984c). *Sediment Transport, Part III: Alluvial Roughness*. Journal of Hydraulic Engineering, 110(12).
- van Rijn, L. C. (1993). *Principles of Sediment Transport in Rivers, Estuaries and Coastal Seas*. Aqua Publications, Amsterdam, The Netherlands.
- van Rijn, L. C., Davies, A. G., van de Graaf, J., & Ribberink, J. S. (2001). *Sediment Transport Modelling in Marine Coastal Environment*. EC MAST Project, MAS3-CT97-0115. Aqua Publications, The Netherlands.
- van Rijn, L. C., Grassmeijer, B. T., & Ruessink, B. G. (2002a). *Accuracy of Measurement Instruments*. In: van Rijn, L. C., Ruessink, B. G., & Mulder, J. P. M., (Editors), *The Behaviour of a Straight Sandy Coast on the Time Scale of Storms and Seasons: Process Knowledge and Guidelines for Coastal Management*, pages E1–E21. Aqua Publications, Amsterdam, The Netherlands.
- van Rijn, L. C., Walstra, D. J. R., Grasmeijer, B., Sutherland, J., Pan, S., & Sierra, J. P. (2002b). *Simulation of Nearshore Hydrodynamics and Morphodynamics on the Time Scale of Storms and Seasons using Process-based Profile Models*. In: van Rijn, L. C., Ruessink, B. G., & Mulder, J. P. M., (Editors), *The Behaviour of a Straight Sandy Coast on the Time Scale of Storms and Seasons: Process Knowledge and Guidelines for Coastal Management*, pages S1–S33. Aqua Publications, Amsterdam, The Netherlands.
- Vela-Diez, S. (2001). *Sediment Mapping of the Tidal Flat Channels off Büsum*. MSc thesis, Christian Albrechts Universität, Kiel, Germany.
- Vermeyen, T. B. (2003). *Acoustic Doppler Velocity Measurements Collected Near a Municipal Water Intake, Lake Mead, Nevada-Arizona*. In: Rizoli, J. A., (Editor), *Proceedings of the IEEE 7th Working Conference on Current Measurement Technology*. San Diego, USA.
- Villes, H. & Spencer, T. (1999). *Coastal Problems. Geomorphology, Ecology and Society at the Coast*. Edward Arnold, London, UK.
- Vincent, C. E., Hanes, D. M., Tamura, T., & Clarke, T. L. (1986). *The Acoustic Measurement of Suspended Sand in the Surf-zone*. In: *Int. Conf. Measuring Techniques of Hydraulic Phenomena in Offshore, Coastal and Inland Waters*, pages 443–451. Br. Hydraul. Res. Assoc., London, UK.
- White, B. R. & Schultz, J. C. (1977). *Magnus Effect in Saltation*. Journal of Fluid Mechanics, 81.
- Whitehouse, R. J. S., Bassoullet, P., Dyer, K. R., Mitchener, H. J., & Roberts, W. (2000). *The Influence of Bedforms on Flow and Sediment Transport over Intertidal Mudflats*. Continental Shelf Research, (20):1099–1124.



- Willis, D. H. & Crookshank, N. L. (1997). *Modelling Multiphase Sediment Transport in Estuaries*. In: Burt, N., Parker, R., & Watts, J., (Editors), *Cohesive Sediments*, pages 383–394. John Wiley and Sons, Ltd., Chichester, England.
- Winter, C. & Mayerle, R. (2003). *Calibration and Validation of a Sediment Transport Model with Extensive Data-sets for a Tidal Channel System in the German Wadden Sea*. In: *Proceedings of the 5th International Symposium on Coastal Engineering and Science of Coastal Sediment Process*. Florida, USA.
- Wren, D. G., Barkdoll, B. D., Kuhnle, R. A., & Derrow, R. W. (2000). *Field Techniques for Suspended Sediment Measurement*. *Journal of Hydraulic Engineering*, 126(2):97–104.
- Yalin, M. S. (1972). *Mechanics of Sediment Transport*. Pergamon Press, Oxford, UK.
- Yalin, M. S. (1977). *Mechanics of Sediment Transport*. Pergamon Press, New York, USA, 2nd edition.
- Yalin, M. S. (1985). *On the Determination of Ripple Geometry*. *Journal of Hydraulic Engineering*, 3(8).
- Young, R. A., Merrill, J., Proni, J. R., & Clarke, T. L. (1982). *Acoustic Profiling of Suspended Sediments in the Marine Boundary Layer*. *Geophysical Research Letter*, 9(3): 175–178.
- Zielke, W., Gross, G., Hoyme, H., Mayerle, R., Ricklefs, K., Winter, C., Eppel, D., & Witte, G. (2000). *Predictions of Medium-scale Morphodynamics (Promorph)*. In: *Proceedings of the 27th Conference on Coastal Engineering*. Sydney, Australia.



# Acknowledgement

I would like to express my gratitude to Prof. Dr. Roberto Mayerle for his trust in giving me the opportunity and supports to do this research. Without his supervision this work would not be in its best state. I also thank Prof. Dr. Franciscus Colijn for accepting to be the *Korreferent* of my dissertation. I gratefully thank Late Prof. Dr. Chandra Nalluri for those scientific discussions during his visits in Kiel. Research facilities and materials as well as supports from the directors and staffs of the Research and Technology Centre (*Forschungs- und Technologiezentrum* - FTZ) in Büsum are acknowledged.

I thank Dr. Klaus Ricklefs for his help at the beginning of my research work in Büsum and for introducing me to various measuring devices and field measuring techniques. I appreciate the generous helps provided by Mr. Burkhard Meier and Mr. Uwe Becker during the field measuring campaigns. I also appreciate the works carried out by my working colleagues at the Coastal Research Laboratory: for providing the data post processing system to Dr. Fernando Toro and for preparing the basis of the flow and sediment transport modelling environment respectively to Dr. Carlos Palacio and Dr. Christian Winter. That nice working atmosphere will not work well without the nice friendship of my working colleagues: Nils Asp, MSc for all his unpretentious helps, to ir. Jort Wilkens for the tricks and tips in handling the Delft3D model as well as to Gatot H. Pramono, MSc and to the visiting scientist Prof. Carlos Mejia for the tricks and tips in using MATLAB. I also thank Dipl.-Ing. Dirk Schulz for the translation of my abstract.

Financial supports for most of the research period in Germany and at the end of promotional phase respectively from the German Academic Exchange Service (*Deutsche Akademische Austauschdienst* - DAAD) and from the FTZ are acknowledged.

Finally, I have to thank my wife and son, Lia and Rian, for their patience, understanding and for loosing most of their rights to be with me, as well as to our parents for their never ending praise and pray. This work is dedicated to them and I will always wish them the best.

Kiel, November 2003

Poerbandono



# Erklärung

Hiermit erkläre ich, dass die Abhandlung -abgesehen von der Beratung durch meine akademischen Lehrer- nach Inhalt und Form meine eigene Arbeit ist. Diese Arbeit hat an keiner anderen Stelle im Rahmen eines Prüfungsverfahrens vorgelegen. Außerdem erkläre ich, dass diese mein erster Promotionsversuch ist.

Kiel, den 3. November 2003

Poerbandono



# Curriculum vitae

## Personal data

|                  |   |
|------------------|---|
| Name             | Poerbandono                             |
| Place of birth   | Jember, Indonesia                       |
| Date of birth    | 25 January 1970                         |
| Nationality, sex | Indonesian, male                        |
| Marital status   | Married, 1 child                        |
| Address          | Schwefelstrasse 14, 24118 Kiel, Germany |
| Telephone        | +49(0)431 570 8402                      |
| E-mail           | poerbandono@corelab.uni-kiel.de         |

## Educational background

|           |  |
|-----------|--|
| 1975-1977 | TK Pertiwi, Mataram, Indonesia   |
| 1977-1983 | SDN Jember Lor IV, Jember, Indonesia                                   |
| 1983-1986 | SMPN II, Jember, Indonesia   |
| 1986-1989 | SMAN I, Jember, Indonesia  |
| 1989-1995 | Bachelor of Engineering<br>Institute of Technology, Bandung, Indonesia |
| 1995-1996 | Master of Management<br>Institute of Technology, Bandung, Indonesia    |

## Working experiences

|           |   |
|-----------|---|
| 1996-1999 | Instructor at the Hydrography Working Group<br>Department of Geodetic Engineering<br>Faculty of Civil Engineering and Planning<br>Institute of Technology, Bandung, Indonesia |
| 1999-2003 | Research co-worker at the Coastal Research Laboratory<br>Christian Albrechts University of Kiel, Germany  |